THE FINITE ELEMENT ANALYSIS OF IRRADIATION INDUCED STRESSES IN GRAPHITE CORE COMPONENTS OF A NUCLEAR REACTOR

A thesis submitted for the award of the degree Doctor of Philosophy in the Faculty of Engineering, University of London

by

Anton Jezernik
Dipl.Mech.Eng. (University of Ljubljana)
DIC, M.Sc. (University of London)

Nuclear Power Section,
Mechanical Engineering Department,
Imperial College of Science and Technology,
London, S.W.7.

June 1971.

ABSTRACT

A review of work on irradiation induced stresses in graphite components of a nuclear reactor is given and the mechanism of generation of stresses described. A choice of a suitable finite element matrix displacement method is discussed. The finite element model for graphite under multiaxial stress is developed and equations governing the stresses, strains and deformations of graphite components/time are presented for plane strain and axi-symmetric cases. Computer programs are described which solve the equations, stepwise in time, advancing in suitable time steps and using always the stresses from previous time interval to calculate the current creep strain increments.

Two versions of the finite element program have been developed. One version is based on Gaussian elimination (direct-band program) the other on the Gauss-Seidel iterative procedure (iterative program) to solve the system of equilibrium equations for the whole structure. For graphite components in a reactor in general, temperature and neutron dose distribution and material properties all vary in space and time. With particular reference to these changes, the solution techniques (programs) were compared. Other influences on the stability of results, such as the choice of time step, mesh size and pattern were also studied. Some conclusions regarding the relative suitability of both solution techniques are drawn.

The stress analysis of three more complex graphite components has been attempted: a hollow rod fuel pin under temperature tilt, a teledial fuel pin and a multichannel graphite block. The results are presented and some conclusions are drawn regarding the stress levels and suitability of the particular graphite components. Also desirable techniques of providing mesh data and temperature, neutron dose and material properties changes with time when solving complex large size problems are described. Finally some suggestions for further work on reactor graphite and other time dependent problems are given.

ACKNOWLEDGEMENTS

I wish first to express my sincere gratitude to the Dragon Project, Winfrith, England which financially enabled my research work at Imperial College and to several Members of the Project, Mr.M.R. Everett, Mr. E. Smith and Mr. A.N. Kinkead for many useful discussions and for providing the informations and data used in the analyses.

Special thanks are due to Dr.J.L Head. I will not forgett his valuable guidance, assistance and advice throughout the course of this work. Many thanks also to Profesor P.J. Grant and Members of Nuclear Power Section for all help I occasionally needed.

Finally, I wish to thank my wife, Ida, for patiently and expediently typing this thesis.

CONTENTS

1. INTRODUCTION

In the past twenty years graphite moderated and gas cooled reactors of different types have been developed, designed and built in a number of countries. Most of early graphite reactors have been built in United Kingdom and France and use carbon dioxide as coolant and graphite moderator blocks fueled with natural uranium metal clad in magnesium/aluminium alloy, called Magnox. In the United Kingdom a second generation of Advanced Gas-cooled Reactors (AGR), fueled with slightly enriched uranium oxide, clad in stainless steel and also cooled with carbon dioxide is at present being built.

The current efforts in the development of graphite reactors, in Europe and America are however focused on High Temperature Gas Cooled Reactors (HTR) using graphite moderator and ceramic fuel and cooled by helium. High Temperature reactors were designed with the aim of the developing an advanced converter reactor with a high thermal efficiency and good conversion ratio, which should be at reasonable costs suitable for commercial power stations. As far as the family of graphite power reactors is concerned HTR's are also to some extent an extension of work done on Magnox and AGR power reactors and much previous experience can be utilizied eventhough the work has been actually in part carried out simultaneously. One of the key advantages of HTR's is the use of improved graphites as moderator and core structural material in the absence of any metallic canning or structure within the core. Thus the outlet coolant temperature is not strictly limited and it is possible to raise it to 900°C or more making possible also the direct cycle application using gas turbines.

The HTR has been developed since the late fifties in the USA and Europe and some prototype reactors have been built. In Europe most of work has been done or sponsored by the Dragon Project, established in 1959, in which 12 European countries take part: Austria, Denmark, Euratom-countries, Norway, Sweden, Switzerland and the United Kingdom in cooperation with the USA

designer of the HTR, Gulf-GA. The Dragon Project is centred at the Atomic Energy Establishment Winfrith, England, where the 20MW prototype HTR, Dragon, has been in operation since August 1964. At present, further studies and the design of a full scale commercial HTR are being carried out by the Dragon Project and also by some large design consortia in the UK (British Nuclear Design and Construction Ltd., The Nuclear Power Group Ltd) and elsewhere (e.g. Brown Boveri Cie, Baden, Switzerland).

At Imperial College in the Nuclear Power Section, the research work on the stresses in the reactor graphite has been going on, for a number of years under supervision of Dr.J.L.Head and supported by the Dragon Project, starting with the stress analysis of Magnox and AGR graphite blocks and analysing at present different graphite components of HTR.

The irradiation of graphite by high energy neutrons causes the carbon atoms to be displaced from crystal lattice sites. This damage to the crystal structure causes changes of the physical properties of the graphite and also causes dimensional changes (growth or shrinkage), termed usually as Wigner strains. The magnitude of dimensional changes depends on several factors including the graphite temperature, the neutron dose and energy spectrum. Also, due to the elevated temperature of the graphite, the material will expand causing the thermal strains. In the reactor the graphite components will be subject to temperature gradients and dose variations and therefore spatial variations of Wigner and thermal strains. Stresses will develop, analogous to thermal stresses in a body which is not at a uniform temperature. The stresses in the graphite components will be modified by an irradiation activated creep mechanism.

If the reactor is shut-down during the operation and the core is cooled to the uniform temperature the effect of differential thermal strains vanishes and a new stress distribution is established. The stresses with the reactor shut-down (cold) are termed in this thesis as residual stresses to distinguish them

from the stresses with the reactor at power (hot) called operating stresses.

The calculation of stresses in a number of graphite components of different reactors have been performed at Imperial College by various authors [1,2,3,4,5,6,7,8,9] over a number of years, however all of the analyses have been one-dimensional and use numerical integration computer codes.

This work is an attempt to develop and apply the method used in these one-dimensional stress analyses, to analyse the time dependent stresses and strains in arbitrary two-dimensional graphite core components using the finite element matrix displacement methods. Next, the aim is also to develop the corresponding computer programs and demonstrate the validity of the finite element model.

In Chapter 2 of the thesis a short description of the core of High Temperature Reactors is given together with basic reactor data. Different forms of graphite core components: fuel pins and multichannel graphite blocks, currently under consideration for commercial HTR's are described and shown in Fig's 2,3,4 in order to define the stress problems in the graphite core.

In Chapter 3 the basic equations of the problem are established and corresponding finite element model developed for two-dimensional plane strain and axisymmetric cases. The inclusion of plane stress option and changes of equations if the material is only transversely isotropic are given in detailed form in App.I. A 3-dimensional form of creep law proposed by Head [2] is adopted on the basis of theoretical considerations and limited data from uniaxial creep tests. This chapter also includes a review of previous work in the field.

The next step in the development of the finite element model for graphite core components was to compare the results of the finite element stress analysis with earlier results from one dimensional analysis of the hollow rod fuel pin using the basic operational data of Dragon reactor (Ch.6.1.1). When the results of these analysis were found to be in reasonable agreement,

a comparative analysis was performed, examining the accuracy of results, stability of solutions and required computer time and memory of two finite element computer programs developed for this purpose. One program uses Gauss-Seidel iteration the other Gaussian elemination to solve the system of algebraic equations. The iterative version of the program was found to be faster for the same accuracy and more suitable for further development. Both computer programs are discused at some length in Chapter 4.

In Chapter 5 the initial calculations required by the finite element program for mesh generation, temperature and equivalent dose calculation and input of materials data are described. These initial calculations, and the input of materials data have been performed by subroutines or independent programs written for this purpose and information supplied to the main program.

The stress analysis of some complex HTR core components has been performed using the iterative version and results are presented in Ch.6. The finite element model has been demonstrated by analysing three different reactor components: a hollow rod fuel pin under temperature tilt (Ch.6.2.2), a teledial fuel pin (Ch.6.3) and a multichannel graphite block (Ch.6.4) under arbitrary temperature and equivalent dose distribution.

In Chapter 7, conclusions are drawn, relating to the validity of the chosen creep law, the comparison of matrix displacement methods and on the particular graphite components analysed. An attempt is made to outline the possible future lines of development. Only the graphite components of HTR's have been analysed but the finite element model and computer programs can be used in the analysis of graphite components of other graphite moderated gas cooled reactors.

The finite element codes developed should in general enable analysis of most of the stress problems in graphite core components of graphite gas cooled reactors, especially the HTR. The codes should enable in particular the solution of the complex stress

cases at radial and axial core reflector boundaries with temperature and equivalent dose gradients and perturbations (Fig.4) not possible by earlier one-dimensional models.

Finally it seems that some of the results of comparative analysis (Ch.6.2.1) using the finite element model can be utilizied in the stress analysis of some other time dependent problems, such as time-dependent creep of concrete. Also some of the peripheral programs and subroutines written for example to generate the mesh data for complex structures can possibly be utilizied in the finite element analysis of some other nuclear or non-nuclear structures.

2. THE GRAPHITE CORE OF HIGH TEMPERATURE REACTORS

2.1 The core and graphite components

The Dragon Reactor is a graphite moderated and helium cooled system using enriched uranium as fuel (see for example Shepherd [10]). The size of the Dragon Reactor was chosen to be the smallest which would adequately demonstrate the principles on which any HTR would depend. The reactor has a small core with an equivalent diameter of 107 cm and height of 160 cm and consists of 37 fuel elements on a hexagonal lattice, each being a cluster of 7 geometrically identical fuel rods. The fuel, enriched uranium in the form of coated particles is placed in graphite cartridges, filled inside with graphite filler pieces and surrounded outside by graphite fuel tubes in the form of hexagons (Fig.2). The 20MW of heat produced is removed by helium which enters at the bottom of the core at 350°C and emerges at 750°C, cooling the fuel elements by passing through the core along trefoil coolant channels.

Many types of fuel elements have been constructed and tested in the Dragon core and series of data were obtained about core materials, operational conditions and reactor performances. One of the question of primary importance is the choice of a suitable graphite. The earlier reactor graphites with low permeability - to prevent the escape of fission products into coolant channels - show a high rate of dimensional change (shrinkage or growth) and anisotropic behaviour under irradiation, undesirable for strain/stress buildup. A major change in development occured in 1961 when the concept of coated particle fuel was adopted and considered to be more suitable than previously examined fuel, emitting fission products and coupled with an expensive fission product purge system (see for example Smith [12]). As a consequence new types of reactor graphites with higher permeability were developed - which proved to undergo more moderate dimensional changes under irradiation and had a higher degree of isotropy. One of the improved graphites

is pressed Gilsocarbon graphite used as material for all the graphite components analysed in this thesis. A detailed account of reactor graphites analysing their crystalline structure, the process of manufacture and their behaviour in reactor environments is given by Head [2].

After completion of the design and construction of the Dragon reactor, the Dragon Project turned its attention to large scale power reactor applications (see Lockett & Hosegood [11]). Different fuel-cycles and core configurations for a full scale commercial power HTR have been studied. Low - enrichment uranium cycles were found to be attractive for the HTR, preliminary design studies for this fuel cycle involved strongly heterogeneous core arrangments in which the fuel was concentrated in channels of about 30 cm diameter in a fixed graphite structure. However, subsequent studies of the low - enriched uranium version related to a more homogeneous core arrangment which appears in most respects to be superior to the heterogeneous arrangement. The core of the homogeneous reactor (Fig.1) has the moderator built in block form with the fuel carried within the blocks in a number of fuel pins placed in individual coolant channels about 6-7 cm in diameter to form robust fuel element assemblies. The multichannel graphite blocks are changed when fuel is changed and the problem of the long term dimensional behaviour of graphite does not arise. This form is capable of a high thermal power density with relatively modest fuel and graphite temperatures.

Three proposed types of fuel pins: a hollow rod fuel pin, a tubular interacting fuel pin and a teledial fuel pin are shown in Fig.2. Next, two proposed types of multichannel graphite blocks in the form of pentagon and hexagon are shown in Fig.3. These fuel pins and graphite blocks are being now considered for commercial high temperature reactors.

In Fig.4 typical shrinkage, temperature and neutron dose data at the end of fuel life in the core of a commercial HTR are shown. The attention of the stress analysts is centred

especially at the core - reflector boundary regions with substantial temperature and equivalent dose gradients.

Some basic reactor data of a commercial homogeneous HTR are given in Ch.2.2.

2.2 Basic reactor data

2.2.1 Dragon reactor

Thermal power of the reactor	20 MW (4)
Core dimensions	107 cm dia.x 160 cm high
Lattice pitch	6.35 cm
Radial power averaging factor	1.3
Axial power averaging factor	1.16
Average heat rating of rod	482,6 W/cm
Helium inlet temperature	350°C
Helium outlet temperature	750°C
Number of fuel elements	37
Number of fuel rods per elements	7

Assumed basic parameters in the calculations of stresses of a Dragon reactor fuel pin (Fig.2):

Inner radius of fuel tube	2.22 cm
Outer radius of equivalent cylinder (calculated)	3.12 cm

2.2.2 A typical homogeneous core of a commercial HTR

Thermal Power	1500 MW
Mean core power density	6 MW/m^3
Mean fuel rating	60 MW/tonne U
Mean burn-up	72000 MWd/tonne U
Fuel lifetime	1200 days
Peak fast neutron dose in fuel	$4 \times 10^{21} n/cm^2$ (Dido-Nickel Eq.)
Mean outlet coolant temperature	800°C
Peak systematic fuel temperature	1300°C

FUEL PINS

Hollow rod fuel pin

Inner radius	2.22 cm
Outer radius (without considering the ribs)	3.12 cm

Teledial fuel pin

Inner radius of fuel pin (coolant channel)	0.9335 cm
Outer radius of fuel pin (without considering the ribs)	2.9365 cm
Outer radius of fuel pin across the ribs	3.3465 cm
Radius of fuel holes	1.935 cm
Diameter of fuel holes	1.203 cm
Number of fuel holes	8

GRAPHITE BLOCKS

Pentagon graphite block

Approximate dimensions	
one side of pentagon	28 CM
maximum dimensions	43 CM
no of coolant channels	16-19
diameter of coolant channels	6-7 cm

Hexagon graphite block

Approximate dimensions	20-3o cm
one side of hexagon	30 cm
no of holes	20-30
dia of holes	6-7 cm

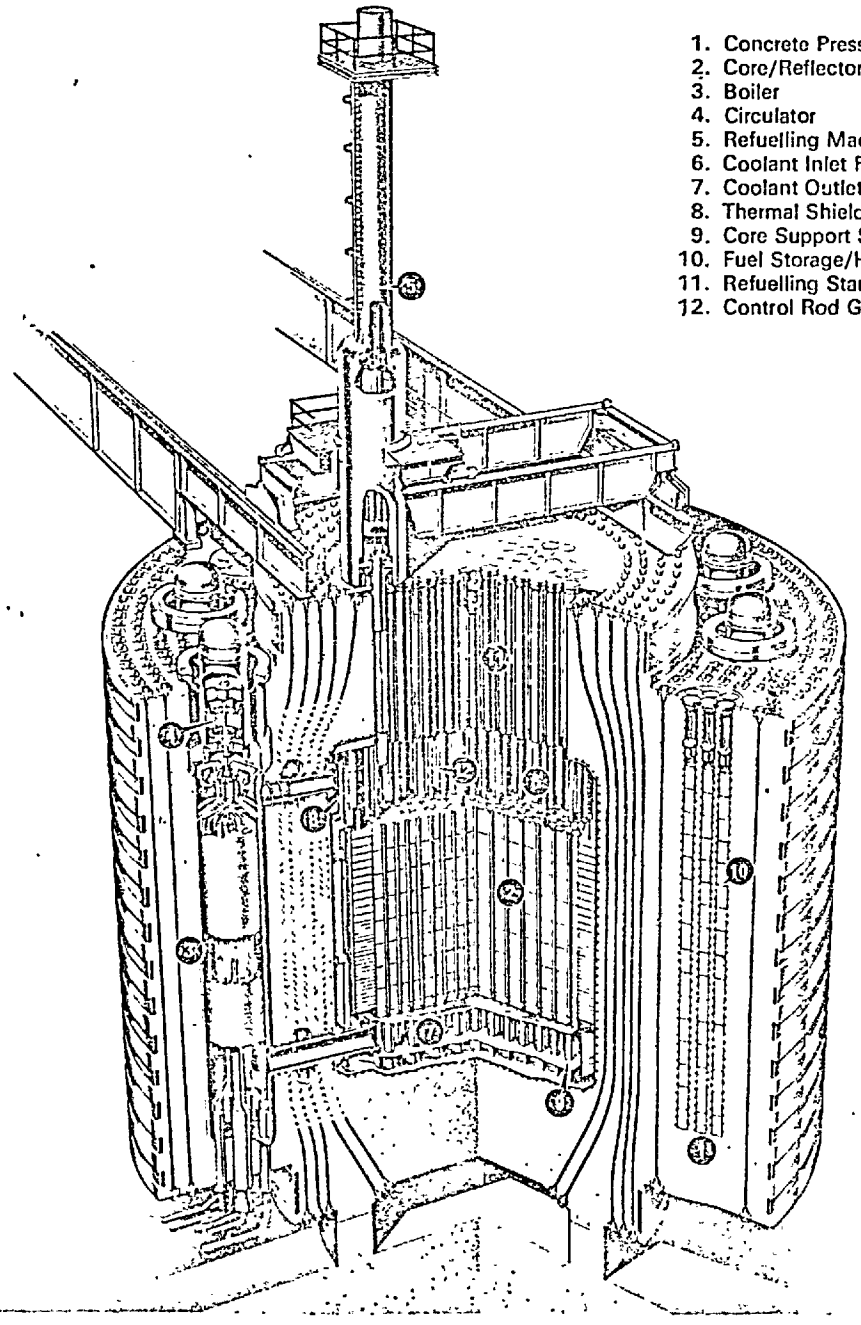

Fig. 1

630 MW(e) HOMOGENEOUS HTR

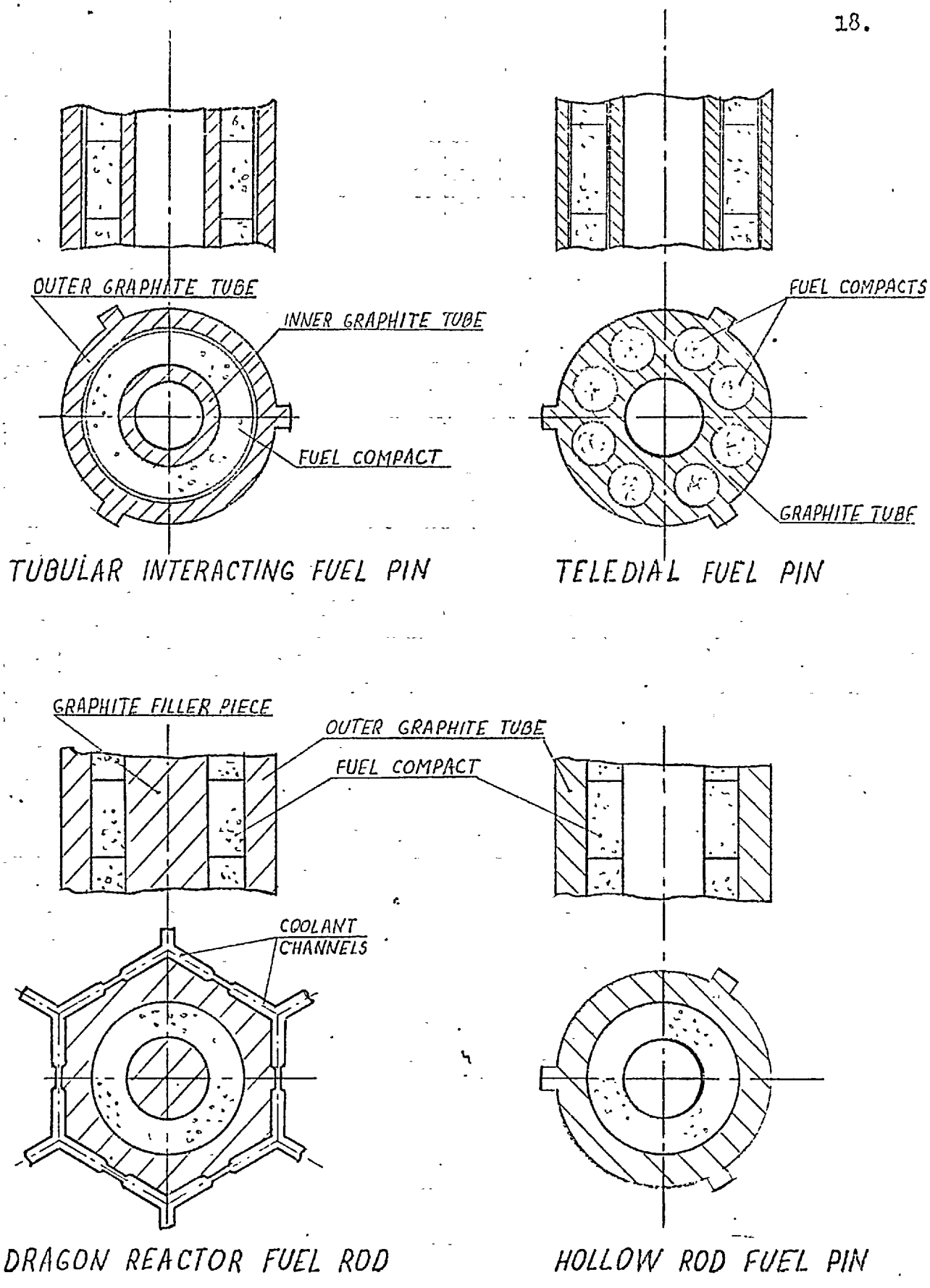

Fig. 2

DIFFERENT TYPES OF GRAPHITE FUEL PINS

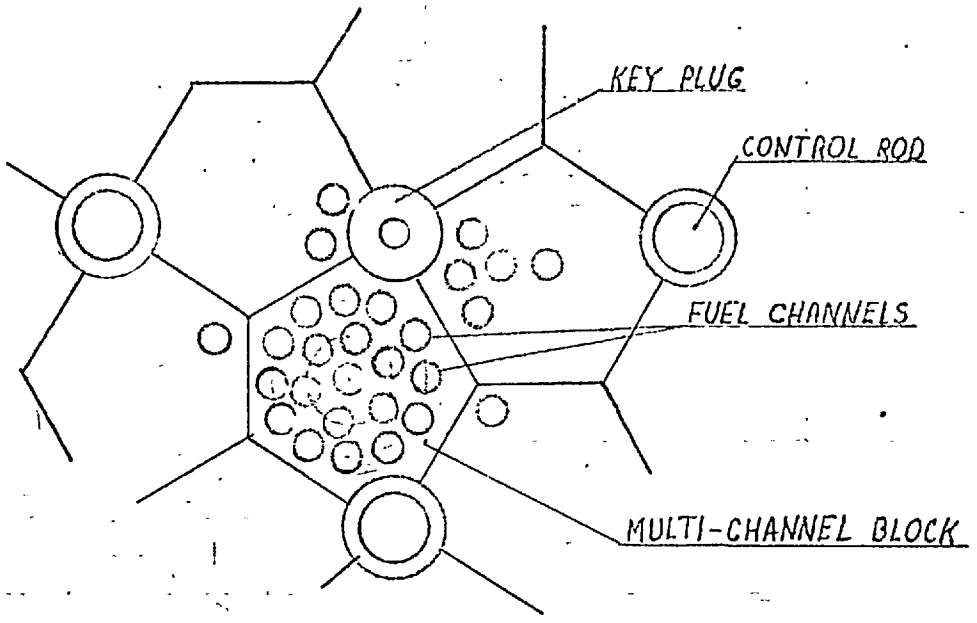

PART PLAN OF HTR CORE

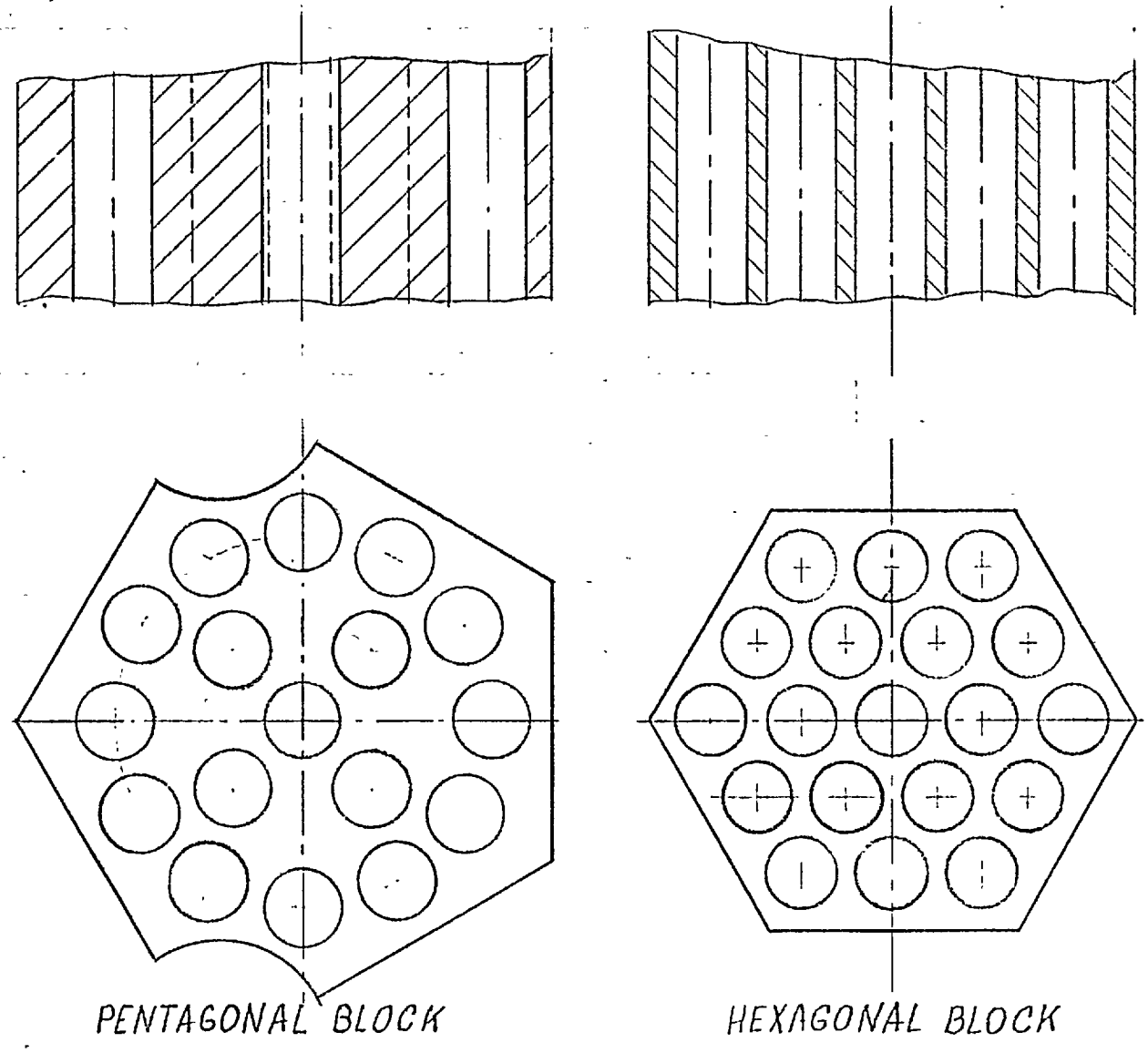

Fig. 3

MULTICHANNEL GRAPHITE BLOCKS AND

PART PLAN OF A HTR CORE

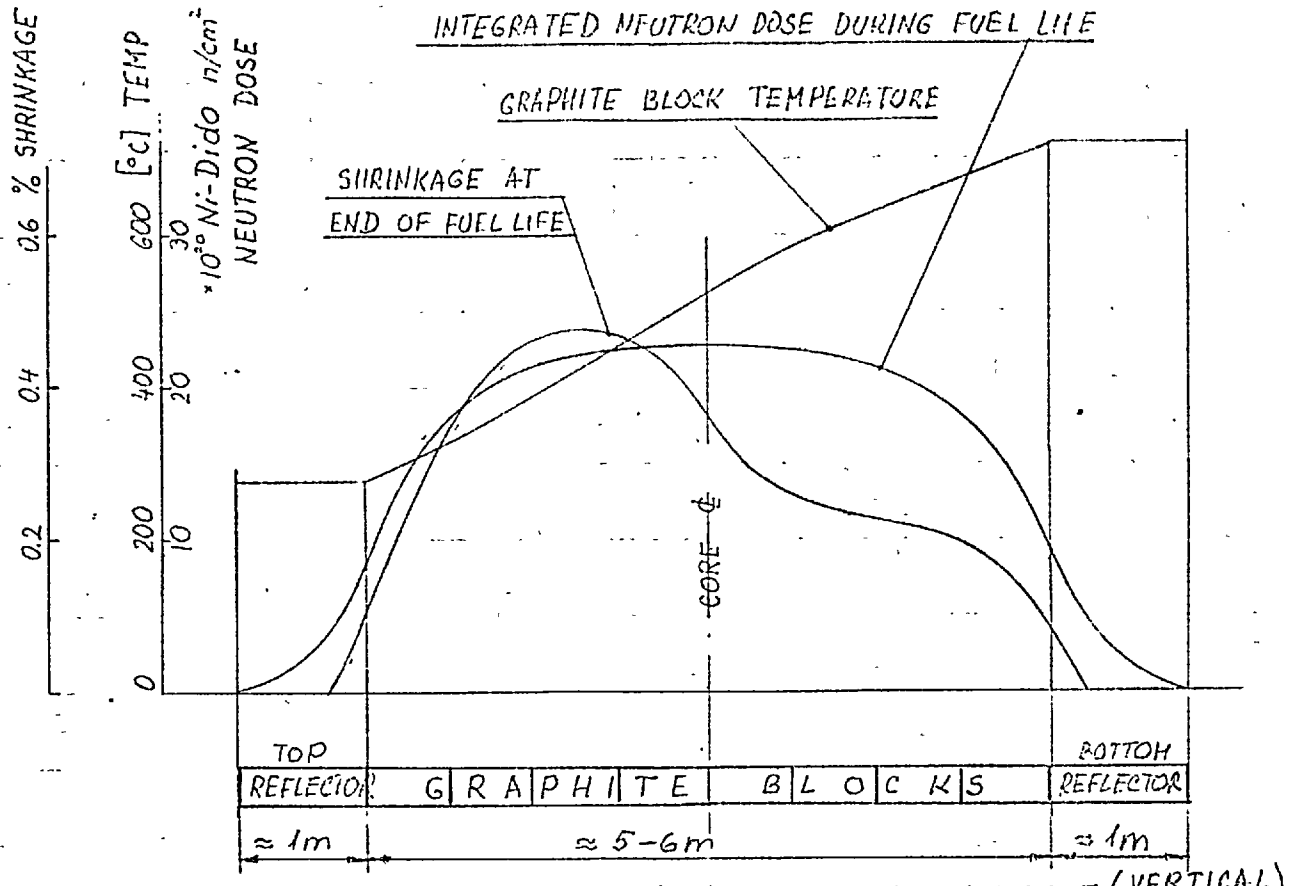

GRAPHITE BLOCK SHRINKAGE, TEMPERATURE AND NEUTRON DOSE (VERTICAL AXIS) AT END OF FUEL LIFE

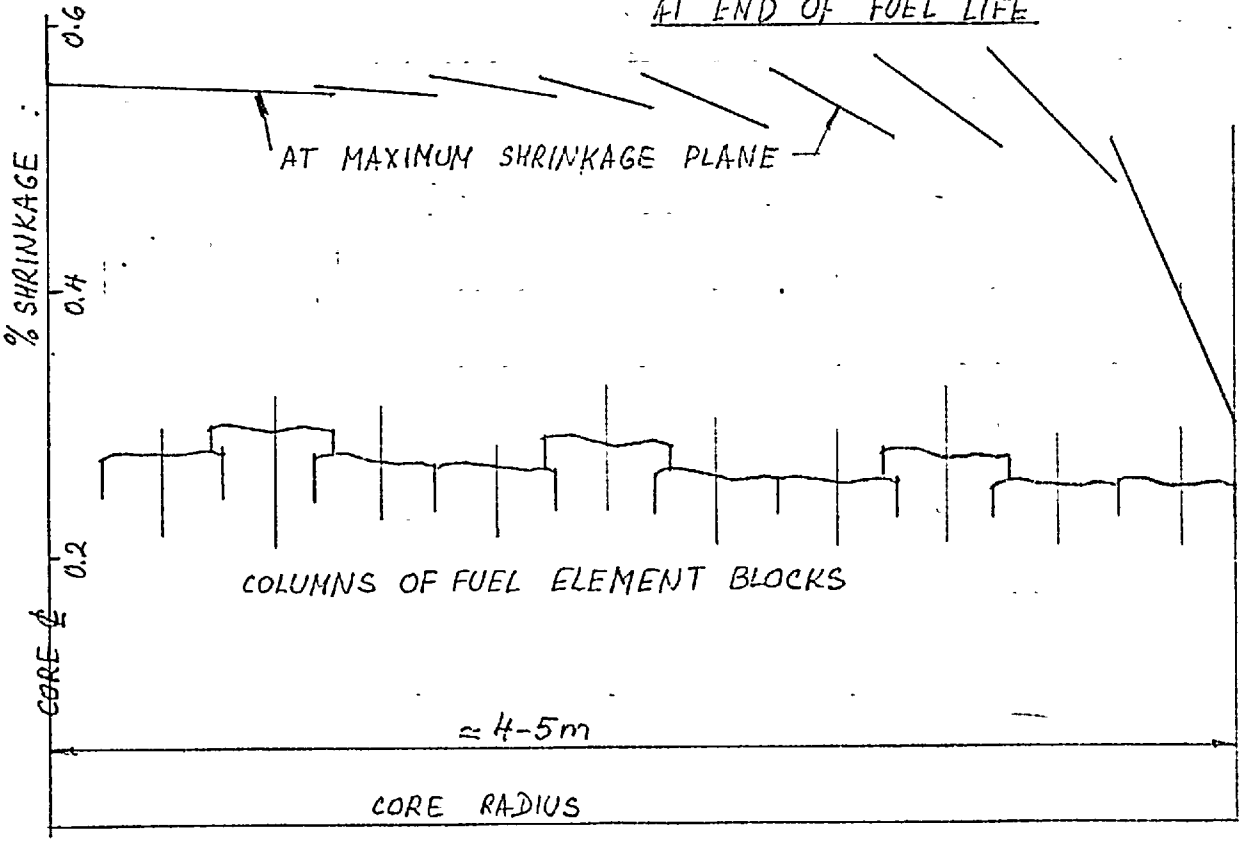

GRAPHITE BLOCK SHRINKAGE AT END OF FUEL LIFE (ACROSS CORE)

Fig. 4

TYPICAL SHRINKAGE, TEMPERATURE AND NEUTRON DOSE DATA AT END OF FUEL LIFE IN THE CORE OF A HTR

3. THEORETICAL ANALYSIS

3.1 Introduction and review of previous work

The early work at Imperial College on the analysis of the stresses in the moderator graphite of a nuclear reactor was concerned with the so-called one-dimensional stress model. The stresses and strains were calculated for a state of generalised plane strain assuming axial symmetry for graphite components of cylindrical shape. The mentioned one-dimensional analyses of stresses are all based on a step by step method of solution similar to that proposed by Mendelson, Hrischberg & Manson [13] and since used by many authors for solution of problems involving thermal creep (see for example Smith [14]). This method of solution was adapted by Head [2] to analysis of graphite stresses and is given in more detail in Ch.3.3. The main assumption in this approach is that the graphite behaviour in reactor environments is equivalent to the response of a Maxwell viscoelastic model, with space and time dependent properties. It is assumed that the strain tensor can be separated into an elastic strain tensor related to the stress tensor by the Hooke's law and a nonelastic strain tensor consisting of thermal, Wigner and creep strains (Ch.3.3.2.3). The basic equations of equilibrium, compatibility and stress-strain relationship are derived and solved for stresses in terms of the non-elastic strains and elastic constants in an integral formulation. These equations are then solved at suitable time intervals. The thermal and Wigner strains are estimated at each time interval directly from experimental data. The incremental creep strains at the current time interval are always found from a relationship between the creep strain rate tensor and the general stress tensor (a flow rule) by iteration. The total creep strains at each time interval are found by summation of incremental creep strains over the previous and current time intervals.

On this basis, the first computer programs, named later as Nessan I and II, were developed by Sockalingam [7] for the

calculation of stresses in the Magnox reactor moderator blocks and by Barnes [8] for the AGR moderator blocks. These programs were followed later by Nessan III, developed by Jezernik [3] and Hassan developed by Alujevič [9] for the calculation respectively of the stresses in the hollow rod and tubular interacting fuel pins (Fig.2) proposed for the HTR.

The early programs Nessan I and II calculate the stresses with the reactor at power (hot) at a particular position in core. In Nessan III the calculation of stresses at any position along a particular channel and calculation of stresses with reactor shut-down (cold) was made possible in a single run. Additionally the effects of temperature and neutron dose on thermal conductivity, the temperature dependence of the creep rate and the influence of fuel rating changes on the temperature distribution during the lifetime of the reactor core were considered. The same features were adopted later in Hassan. Thus with Nessan III, a study of the spatial variation of the stresses in the reactor core became possible, giving an indication of the areas where the highest stresses occur. The stresses with the reactor shut down are usually more severe than stresses with the reactor at power. All three Nessan programs and Hassan code have built-in temperature routines i.e. the temperature distribution is calculated successively for each dose interval.

The value and validity of Nessan programs is limited, by the assumptions of plane strain and axial symmetry, to the central region of a reactor core with flat radial flux and temperature distribution and only low axial gradients of flux and temperature. On the other hand Nessan programs are comparatively fast, so far as computer time is concerned, and results relatively accurate. If used together with more elaborate computer codes, Nessan programs could be valuable in the first estimations of the regions with highest stresses and for comparison of the behaviour of different types of graphite, especially on account of the computer time economy.

The aim of the analysis described in this thesis was to develope a mathematical model and write a computer program for a general two-dimensional case (plane stress/strain and

axi-symmetric geometry) with, for example, non-symmetric flux and temperature distribution and for complex geometrical shapes like a multi-channel block or the teledial fuel pin (Figs.2,3). This program should enable a more detailed analysis of the stresses in graphite moderator cores, in particularl- at radial and axial core boundaries where temperature and flux tilts usually have the highest values. The finite element approach was chosen as a method of solution as the method offers many advantages as discussed later. Finally some assessments, conclusions and proposals for futher work are made.

3.2 The finite element method

3.2.1 A brief review of work on the finite element method

It is well known that by the use of classical mathematical formulation of a problem only a limited number of engineering field problems can be explicitly solved. Attempts to formulate and solve explicitly complex problems often either fail or lead to sophisticated mathematics and/or trivial solutions.

The finite element method can be regarded as a suitable answer and a practical engineering approach to the solution of complex field problems. One of the main advantages of the method is the piecewise continuous field definition enabling irregular boundaries to be simply fitted. The credit of approximating a continum by a number of elements with multiple connecting points goes to Turner at al [15] in 1956, Clough [16] in 1960 and Argyris [17], 1955.

It will be beyond the scope of this work to give a detailed account of the development of the finite element method since it was introduced. It is possible however to state that most of the problems to which it has been applied are of the structural solid mechanics type and that major advances occured in the formulation of the approach the introduction of different elements and the developments of various computer techniques for solving the system of equations for the whole structure.

In the early sixties, the basic two-dimensional finite element programs using for example Gaussian elemination or the Gauss-Seidel iterative procedure to solve for nodal displacement have been applied extensively to elastic problems (see for example Zienkiewicz [18] and Wilson [19]). Thus today the elasticity problems seem to be covered in considerable detail. The observation that if the total number of degrees of freedom associated with an element is increased, then equal accuracy can be obtained with fewer degrees of freedom for the complete structure leads to the introduction of more complex (isoparametric) elements. Triangles and tetrahedra with nodes placed at midsides were introduced by Veubeke [20] and Argyris [21], respectively. Next, the isoparametric curved type elements were introduced (see for example Ergatoudis, Irons & Zienkiewicz [22]) enabling a close boundary representation with a smaller number of finite elements. In the recent past and at present the use of finite element method is rapidly being extended into the nonstructural fields of fluid mechanics, heat transfer etc, and to some more complex structural problems of creep, plasticity and dynamics. One of these extensions is the development of the finite element model for reactor graphite components.

A discusion of work on nonlinear problems of creep and plasticity and a review of work on irradition induced creep of reactor graphite is given in Ch.3.3.1.

3.2.2 The basic principles

The finite element method is a general method of structural analysis in which a continuous structure is replaced by a finite number of elements interconnected at finite number of nodal points (Fig.s 9,10,11). Approximations are made concerning the behaviour of the elements in an attempt to approximate to the behaviour of the continuous structure. To obtain a complete solution the conditions of displacement compatibility and equilibrium have to be satisfied throughout. The equilibrium

condition has to be satisfied within an element and over all the elements of the structure.

Assuming elastic behaviour of the structure (material) the system of equations for overall equilibrium of the structure will be of the form:

$$[K] \quad \{\delta\} = \{R\} \qquad (3.1a)$$

or

$$\{\delta\} = [K]^{-1} \quad \{R\} \qquad (3.1b)$$

where K is termed the stiffness of the complete structure and can be found by systematic addition of the stiffnesses of all elements in the system. The stiffness of a typical element is an expression for the corner forces resulting from unit corner displacement.

$$\{\delta\} = \begin{Bmatrix} \delta_1 \\ \cdot \\ \cdot \\ \delta_n \end{Bmatrix}$$

is the system of nodal displacement of the structure and

$$\{R\} = \begin{Bmatrix} R_1 \\ \cdot \\ \cdot \\ R_n \end{Bmatrix}$$

are the external forces by which the structure is loaded

The system of equations (3.1) can be solved once the prescribed support displacements have been substituted to prevent rigid body movements of the structure. Without a minimum number of prescribed displacement it is impossible to solve this system, because the displacement cannot be uniquely determined by the forces in such a situation.

Once the system of algebraic equations (3.1b) is solved and the displacements of all nodal points of the structure calculated, using the strain/displacement relationship and stress/strain relationship within each element, the stresses in each particular element can be calculated.

The basic principles of the finite element method are well established (see for example Zienkiewicz [18] and Przemienicky [23]), however, in this thesis the basic formulation of the method is re-stated, with the modification necessary when applying the method to the solution of (time dependent) problems of graphite core component analysis.

3.3 Finite element model for the time dependent stress analysis of graphite core components

3.3.1 Introduction

When graphite is irradiated with high energy neutrons, carbon atoms are displaced from lattice sites. This damage to the crystal structure causes changes of the physical properties of the graphite and also causes dimensional changes (growth or shrinkage). The magnitude of the dimensional changes depends on several factors including the graphite temperature and neutron dose and energy spectrum. In recent years, considerable progress has been made towards understanding the mechanism of radiation damage in graphite. A large volume of experimental data has been accumulated on the effects of neutron irradiation on the bulk dimensions and properties of various polycrystalline graphites (see for example Netley & Martin [24] , Everett Graham [25] and Blackstone et al. [26]). Due to the elevated temperature of the graphite the material will also expand causing therefore thermal strains. The magnitude of thermal expansion coefficient depends on temperature and neutron dose.

In a nuclear reactor core, the graphite components will be subject to temperature gradients and to spatial variations of neutron energy spectrum. There will therefore be spatial variations of the dimensional changes and thermal strains. Stresses will develop, analogous to thermal stresses in a body which is not at a uniform temperature. The stresses in the graphite components will be modified by an irradiation - induced

creep of the graphite.

With the further development of graphite moderated reactors the irradiation induced stresses in the graphite components become a subject of increased attention. Most of the stress analyses of graphite components up to the present day used numerical integration methods of solution or finite difference approximations. One of more significant contributions and also the earliest published analysis to take account of radiation creep was that of Cornwall & Jobson [27] . In this analysis the graphite block was regarded as a long thick-walled cylinder with axi-symmetric damage flux and temperature distributions and with negligible axial gradients. The transient creep was neglected (the graphite was regarded as a Maxwell material) but the steady creep was taken into account by the use of hereditary integral. The use of the hereditary integral means that this method of analysis cannot take into account the temperature dependence of the material properties. Witt & Greenstreet [28] analysed the stresses in multichannel graphite blocks of the American Experimental Gas Cooled Reactor (EGCR), which are not axi-symmetric, using a finite difference method. This analysis also assumed that the blocks are long and axial gradients of damage flux are negligible. The temperature variation in the block and the effect of radiation creep were however neglected.

Very recently Chang & Rashid [29] developed a finite element viscoelastic model for graphite materials in irradiation enviromments. In their approach, the field equations are derived by the aid of Laplace transform using a constitutive equation in hereditary integral form for each element where the neutron flux and temperature fields are assumed to be locally uniform. This follows the classical approach to the solution of viscoelastic problems in which the material elastic moduli in the elastic solution are replaced by the appropriate viscoelastic moduli (corespondence principle).

Finally the development of finite element methods for the

solution of the problems of thermal creep and plasticity should also be mentioned since these problems have some similarities with finite element analysis of reactor graphite. One method which emerged in recent years for the solution of elastic-plastic and thermal creep problems is the so-called method of initial strain. This method is based on the idea of modifying the equations of equilibrium so that the elastic equations can be used throughout on the left hand side of the equations (3.1a). The development of the matrix equations has been attributed to Padlog et al, Argyris et al, and Jensen et al, by Marcal [30]. Using this approach Greenbaum and Rubinstein [31] developed a direct finite element program for creep analysis of some axisymmetric bodies. In their work the elastic solution is first obtained (at the beginning of the calculation). Using these stresses the creep strains for a small time interval are computed. These are then regarded as initial strains for the next time interval and are included in the evaluation of the nodal displacements and element stresses and strains. The solution for the next time increment proceeds in the same manner. The basic assumption used in this approach is that the change in stress during any time increment is small compared to the stress at the beginning of that increment.

The finite element analysis described in this thesis is a development of the initial strain method for the analysis of stresses in graphite core components. The step-by-step approach used in early one-dimensional calculations of the stresses in reactor graphite at Imperial College, as mentioned in Ch.3.1. has been adopted in the analysis.

It may be concluded, from behaviour of graphite under irradiation, that when subjected to uni-axial stress in a reactor environment, its response exhibits the characteristics of a 4-parameter linear viscoelastic model consisting of Maxwell and Kelvin elements in series Fig.5 (see for example Cornwall & Jobson [27] and Head [2]). The dashpot forces are proportional to the rate of change of strain with respect to neutron dose. The 4-parameter model under step function loading exhibits an

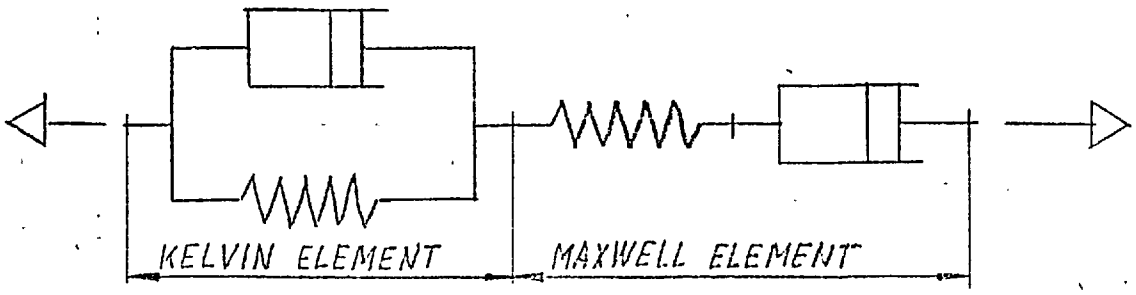

4 PARAMETER MODEL

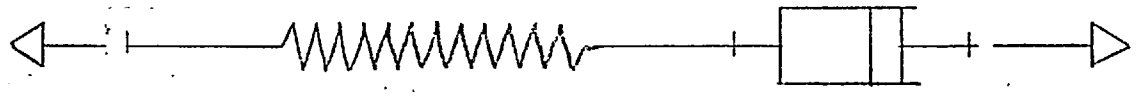

MAXWELL MODEL

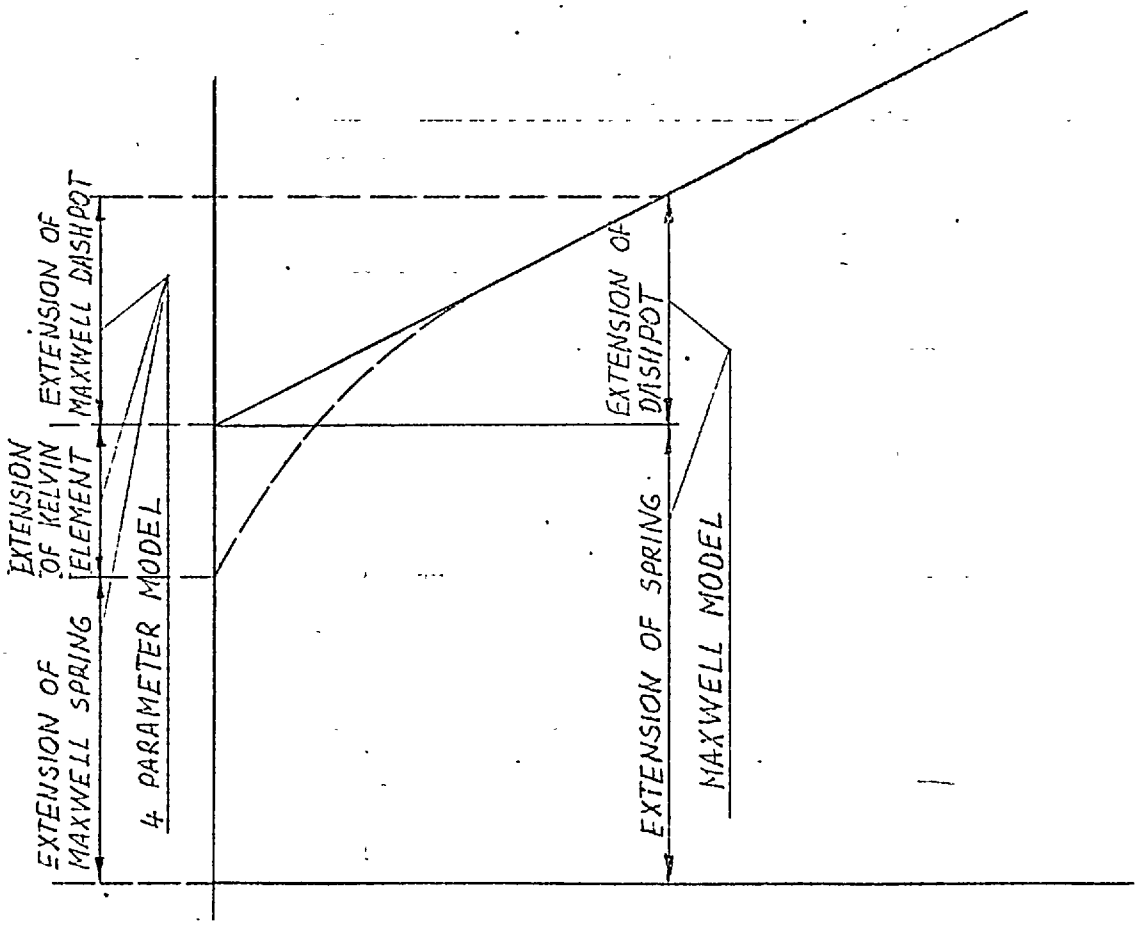

Fig.5

4-PARAMETER AND MAXWELL MODEL

AND RESPONSE TO STEP FUNCTION LOADING.

initial elastic response, plus transient and steady creep. For graphite, the experimental evidence (see for example Perks & Simmons [32]) showed that the transient creep increment represented in Fig.5 by the Kelvin element is proportional to the stress increment, is recoverable and occurs nearly instantaneously. Therefore the transient creep can be taken into account by the use of modified elastic constants. This is equivalent to the use of a Maxwell model as shown in Fig.5, with the spring constant modified to allow for transient creep. The Maxwell viscoelastic model was chosen to represent the behaviour of graphite in three dimensions also, but the possible choices of three-dimensional model are discused later in this thesis.

Similarly as in the one-dimensional programs (see Ch.3.1) the solution is again advanced by short time step during which the temperature distribution in the graphite component, and therefore material properties may, be assumed to be constant. The strain tensor is separated as discused in Ch.3.1. In early programs (Nessan etc) the creep strains at each time step were found by iteration. In this analysis the creep iteration proved to be an uneconomic proposition since it requires, due to the features of finite element solution techniques, an excessive amount of computer time (see discussion in Ch.4). The time step has been therefore suitably adjusted (decreased) and stresses from the previous time interval used to calculate the creep strain increments during the current time interval*. The total strains are obtained by summation of the incremental creep strains for the proceding and current intervals.

With choice of initial strain method and Maxwell viscoelastic model to analyse stresses in reactor graphite the remaining task is to modify the finite element equations, examine the suitability of various finite element solution techniques

---

*A partial creep iteration at each time step involving only 2-3 iterations may well be a suitable alternative, since it will not excessively increase the computer time but will improve the approximations for creep strain increments (see Ch.4). This partial iteration will probably be especially suitable for analysis of components where the stresses change rapidly with time.

and analyse in parallel also the possible choices of three-dimensional viscoelastic model. The problem is complicated by the spatial variation of temperature, due to the generation of heat within the graphite components and the variation with time of the temperature distribution resulting from the radiation induced changes of thermal conductivity and changes in fuel burn-up. The viscoelastic parameters of graphite are temperature dependent (see Ch.5) and therefore vary both spatially and with time.

In the following Chapters, the step-by-step finite element model for time dependent stress analysis of reactor graphite is given for plain strain and axisymmetric geometry.

3.3.2 Plane strain

3.3.2.1 Basic assumptions

The basic equations are derived for plane strain* (ε_z=const) and transversely isotropic material. It is assumed that the z-coordinate direction coincides with the direction in which the graphite is pressed or extruded and that the material is isotropic in the transverse plane. Changes required in the equations to analyse plane stress problems or fully isotropic materials are discused or given in App.I. It is further assumed that creep occurs at constant volume. However the derivations can be used also if creep does not occur at constant volume and modifications required are discused in App.I. Triangular elements with a linear displacement field are used throughout in the analysis.

---

*In plane strain case $\varepsilon_z = 0$ or ε_z = const. depending on conditions - the structure is either restrained or free to move in the axial direction. The conditions with ε_z = const. are usually called the generalized plane strain case. In general, the graphite components in HTR are free to move in axial direction, therefore the equations for generalized plane strain conditions apply in this analysis.

3.3.2.2 Strain/displacement relationship

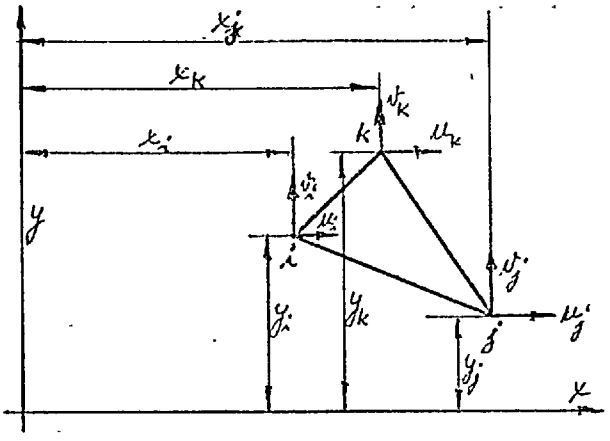

Fig.6 Triangular element

To calculate the stiffness of a typical element the three components of strain within each element have to be expressed in terms of six corner displacement. The displacement within an element with a linear displacement field are uniquely defined by six corner displacements:

$$u = u_i + C_1 (x - x_i) + C_2 (y - y_i) \qquad (3.2a)$$

$$v = v_i + C_3 (x - x_i) + C_4 (y - y_i) \qquad (3.2b)$$

where the matrix

$$\begin{bmatrix} C_1 \\ \cdot \\ \cdot \\ C_4 \end{bmatrix} \qquad (3.3)$$

is defined in App.I.

From the assumed displacement field the strains within the element can be obtained:

$$\varepsilon_x = \frac{\partial u}{\partial x} = C_1 \qquad (3.4a)$$

$$\varepsilon_y = \frac{\partial v}{\partial y} = C_4 \qquad (3.4b)$$

$$\gamma_{xy} = \frac{\partial u}{\partial y} + \frac{\partial v}{\partial x} = C_2 + C_3 \qquad (3.4c)$$

The strain displacement relationship can be written in the form:

$$\begin{Bmatrix} \varepsilon_x \\ \varepsilon_y \\ \gamma_{xy} \end{Bmatrix} = [B] \quad \{\delta\} \qquad (3.5)$$

where matrix $\{\delta\}$ represents six nodal displacements of nodes i,j,k

$$\{\delta\} = \begin{Bmatrix} u_i \\ v_i \\ u_j \\ v_j \\ u_k \\ v_k \end{Bmatrix} \qquad (3.6)$$

and matrix $[B]$ is given in App.I.

3.3.2.3 Stress/Strain Relationship

3.3.2.3.1 The Strain Tensor

The strain tensor can be separated into an elastic strain tensor ε^e_{ij} related to the stress tensor by Hooke's law and a nonelastic strain tensor ε^n_{ij} (see Mendelson et al [13]):

$$\varepsilon_{ij} = \varepsilon^e_{ij} + \varepsilon^n_{ij} \qquad (3.7)$$

It is further assumed that the non-elastic strain can be separated into a thermal strain tensor ε^t_{ij}, a Wigner strain tensor ε^W_{ij} and a creep strain tensor ε^c_{ij} and that these tensors may be calculated separately:

$$\varepsilon^n_{ij} = \varepsilon^t_{ij} + \varepsilon^W_{ij} + \varepsilon^c_{ij} \qquad (3.8)$$

The total strain matrix for plane strain and transversely isotropic material is then as follows:

$$\{\varepsilon\} = \begin{Bmatrix} \varepsilon_x^e \\ \varepsilon_y^e \\ \varepsilon_z^e \\ \gamma_{xy}^e \end{Bmatrix} + \begin{Bmatrix} \varepsilon_x^t \\ \varepsilon_y^x \\ \varepsilon_z^t \\ 0 \end{Bmatrix} + \begin{Bmatrix} \varepsilon_x^W \\ \varepsilon_y^W \\ \varepsilon_z^W \\ 0 \end{Bmatrix} + \begin{Bmatrix} \varepsilon_x^c \\ \varepsilon_y^c \\ \varepsilon_z^c \\ \gamma_{xy}^c \end{Bmatrix} \qquad (3.9)$$

3.3.2.3.2 Stress/Elastic Strain Tensor Relationship

The stress tensor is related to the elastic strain tensor with the equation of the form:

$$\{\sigma\} = [D] \quad \{\varepsilon^e\} \qquad (3.10)$$

where $[D]$ is a 4 x 4 matrix and $\{\varepsilon^e\}$ and $\{\sigma\}$ 4 x 1 column matrices. The matrix $[D]$ varies for isotropic, transversely isotropic and fully anisotropic materials. In general, the matrix $[D]$ for each particular case can be derived from the 6 x 6 compliance matrix of three-dimensional elasticity.

3.3.2.3.3 Thermal Strain Tensor

If the material is transversely isotropic the thermal expansion tensor ε_{ij}^t must be invariant with any rotation about z axis.

The thermal strains are related to the thermal expansion tensor and temperature by the matrix equation:

$$\{\varepsilon^t\} = T \quad \begin{Bmatrix} \alpha_\perp \\ \alpha_\perp \\ \alpha_{\parallel} \\ 0 \end{Bmatrix} \qquad (3.11)$$

3.3.2.3.4 Wigner Strain Tensor

Similarly as for thermal strains the Wigner strain tensor ε^{W}_{ij} must be invariant with any rotation about z axis and the matrix equation for Wigner strains is of the form:

$$\left\{\varepsilon^{W}\right\} = \begin{Bmatrix} \varepsilon^{W}_{\perp} \\ \varepsilon^{W}_{\perp} \\ \varepsilon^{W}_{\parallel} \\ 0 \end{Bmatrix} \tag{3.12}$$

The Wigner strains $\left\{\varepsilon^{W}\right\}$ as a function of dose and temperature are obtained (Ch.5) directly from experimental data.

3.3.2.3.5 The creep strain tensor and flow rule for graphite

At present time, there is no experimentally established flow rule for graphite, therefore the form it might take must be considered in the light of the existing experimental data on the creep of graphite, all of which has been obtained from uniaxial tests. A relationship is required between the creep strain rate tensor and the general stress tensor (a flow rule).

A flow rule for reactor graphite in 3 dimensions has been derived by Head [2] . This flow rule takes account of the transverse isotropy of the graphite and incorporates the assumptions that hydrostatic (normal) stress causes no permanent disortion of an element and that there is no permanent volume change.

Due to transverse isotropy, the creep compliance tensor must be invariant with respect to rotation about z-axis. The following matrix equation for incremental creep strains is obtained:

$$\begin{Bmatrix} \delta\varepsilon^{c}_{x} \\ \delta\varepsilon^{c}_{y} \\ \delta\varepsilon^{c}_{z} \\ \delta\gamma^{c}_{xy} \end{Bmatrix} = \delta\,(De) \begin{bmatrix} (U+V), & -U, & -V, & 0 \\ -U, & (U+V), & -V, & 0 \\ -V, & -V, & 2V, & 0 \\ 0, & 0, & 0, & (4U+2V) \end{bmatrix} \begin{Bmatrix} \sigma_{x} \\ \sigma_{y} \\ \sigma_{z} \\ \tau_{xy} \end{Bmatrix} \tag{3.13}$$

Where the compliances U and V are temperature dependent. The above 4 x 4 creep compliance matrix is derived in App.I from a general 4 x 4 creep compliance matrix (for 2 dimensions) which can be used for conditions where creep does not occur at constant volume*, provided the experimental data are available.

3.3.2.4 Stress resultants and element stiffness

The next step is to replace the uniform stresses acting on the edges of the element with stress-resultants acting at the corners of the element. The relationship is well known and the corner forces** expressed in terms of components of stress as given by Wilson [19] are:

$$\{S\} = \Delta \quad [B]^T \quad \{\sigma\} \qquad (3.14)$$

where the matrices $\{S\}$, $[B]^T$ and $\{\sigma\}$ for plane stress/strain are derived in App.I.

---

*At a recent UK/Euraton Conference on Stresses in Graphite Structures related to HTR Design at Berkeley Nuclear Laboratories (17-19/5/1971), England, Dr.B.T.Kelly mentioned in general discusion the recent experimental evidence which indicates that irradiation induced creep of graphite does not occur at constant volume. In this analysis it was assumed that creep occurs at constant volume since no experimental data have been available indicating volume changes (see also App.I).

**It should be noted that throughout the calculation when deriving the expression for stress resultants and element stiffness (Ch.3.3.2.4) and equilibrium equations for complete structure (Ch.3.3.2.5) the matrix [D] is a 3 x 3 matrix and $\{\varepsilon\}$, $\{\varepsilon^t\}$, $\{\varepsilon^w\}$, $\{\varepsilon^c\}$ are 3 x 1 matrices since the stresses in plane x-y are evaluated first and longitudiual stress σ_z afterwards as given in Ch. 3.3.2.6. The 3 x 1 $\{\varepsilon\}$ matrices and 3 x 3 [D] matrix are obtained from original 4 x 1 and 4 x 4 matrices if the third row (and for matrix [D] also third column) are ommited. The detailed equations (Ch.3.3.2.4) are derived in App.I in appropriate form.

Element stresses can be expressed in terms of corner displacement by substituting eq. (3.5) into eq. (3.10), but $[D]$ is a 3 x 3 matrix (see footnote previous page):

$$\{\sigma\} = [D]\,[B]\,\{\delta\} \tag{3.15}$$

Substituting (3.15) into (3.14)

$$\{S\} = [B]^T\,[D]\,[B]\,\{\delta\}\,\Delta \tag{3.16}$$

which is an expression for corner forces in terms of corner displacement and can be rewritten in the following form:

$$\{S\} = [k]\,\{\delta\} \tag{3.17}$$

where $[k]$ is the 6 x 6 stiffness matrix for one element given by:

$$[k] = [B]^T\,[D][B]\,\Delta \tag{3.18}$$

The detailed derivations are again given in App.I.

3.3.2.5 Equilibrium Equations for Complete structure

The equilibrium of the system of elements in plane xy for the complete structure is an expression for nodal point loads in terms of nodal point displacements. For elastic case it is given by the following force/displacement matrix equation, as defined in Ch.3.2:

$$\{R\} = [K]\,\{\delta\} \tag{3.1a}$$

or

$$\{\delta\} = [K]^{-1}\,\{R\} \tag{3.1b}$$

where $[K]$, the stiffness matrix for the complete assembly is formed by superposition of the element stiffness matrices and $\{\delta\}$ is here the displacement column matrix for the whole structure.

In the particular case of reactor graphite the system of equilibrium equations for the complete structure can be written in the form:

$$[K]\ \{\delta\} = \{R\} - \{R^n\} \qquad (3.1c)$$

or

$$\{\delta\} = [K]^{-1}\{\{R\} - \{R^n\}\} \qquad (3.1d)$$

where

$$\{R^n\} = \{R^t\} + \{R^W\} + \{R^c\} \qquad (3.19)$$

are nodal loads required to balance the nodal displacements due to thermal, Wigner and creep strains $\{\varepsilon^t\}$, $\{\varepsilon^W\}$ and $\{\varepsilon^c\}$.

3.3.2.6 The calculation of stresses in plane and longitudinal stress

When solving the system of equations (3.1d) the non-elastic strains in plane x-y are evaluated first. From the known non-elastic strains the nodal forces required to suppress the non-elastic strains in plane x-y can be calculated using equations (3.10) and (3.14). Thus when the system of equations (3.1d) is solved the total displacements are obtained for the complete structure. Finally the total strains are obtained from (3.5) the non-elastic strains are subtracted and the stresses are obtained for each element from the equation (3.10) i.e:

$$\{\sigma\} = [D]\{\{\varepsilon\} - \{\varepsilon^n\}\} \qquad (3.20)$$

where $\{\varepsilon\}$ is the total strain matrix defined in eq.(3.9) and $\{\varepsilon^n\}$ is the non-elastic strain matrix.

It should be noted that the stresses σ_x , σ_y and τ_{xy} in plane x-y are evaluated first and axial stress is calculated separately afterwards as follows.

In the case of plane strain the axial stress on the n-th element necessary to suppress the strain in the axial (z) direction is:

$$(\sigma_z)_n = \gamma_{\perp\parallel}(\sigma_x + \sigma_y)_n - E_{\parallel}(\varepsilon_z^t + \varepsilon_z^W + \varepsilon_z^c)_n \qquad (3.21)$$

The total restraining force in the axial direction is given by:

$$P = \sum_n \left\{\left[\gamma_{\perp\parallel}(\sigma_x + \sigma_y)_n - E_{\parallel}(\varepsilon_z^t + \varepsilon_z^W + \varepsilon_z^c)_n\right] A_n \right. \qquad (3.22)$$

In the present analysis, it is assumed that the graphite component is free of axial restraint, the axial stress on the n-th element is given therefore by:

$$(\sigma_z)_n = -\frac{1}{A_{total}} \sum_n \left\{\left[\gamma_{\perp\parallel}(\sigma_x + \sigma_y)_n - E_{\parallel}(\varepsilon_z^t + \varepsilon_z^W + \varepsilon_z^c)_n\right] A_n\right\}$$

$$+ \gamma_{\perp\parallel}(\sigma_x + \sigma_y)_n - E_{\parallel}(\varepsilon_z^t + \varepsilon_z^W + \varepsilon_z^c)_n \qquad (3.23)$$

3.3.3 Axi-symmetric stress analysis

The same basic assumptions apply as for plane strain case in Ch.3.3.2.

3.3.3.1 Strain/displacements relationship

The crossection of a typical triangular ring element is shown in Fig.6. In order to obtain the required axi-symmetric geometry we have to replace in Fig.6 coordinate x with r and coordinate y with z, considering also that the element is a body of revolution. The displacement in the r-z plane within the

element are assumed to be of the following form:

$$u(r,z) = u_i + C_1(r - r_i) + C_2(z - z_i)$$
$$v(r,z) = v_i + C_3(r - r_i) + C_4(z - z_i) \qquad (3.24)$$

The constants C_1, C_2, C_3 and C_4 are of the same form as for plane strain case (eq.3.3) but considering the change of coordinates above.

The strains can be obtained from the assumed displacement field:

$$\varepsilon_z = \frac{\partial v}{\partial z} = C_4$$
$$\varepsilon_r = \frac{\partial u}{\partial r} = C_1 \qquad (3.25)$$
$$\varepsilon_\theta = \frac{u}{r} = \frac{u_i}{r} + C_1 + C_2 \frac{z}{r} = C_1 \frac{r_i}{r} - C_2 \frac{z_i}{r}$$
$$\gamma_{rz} = \frac{\partial u}{\partial z} + \frac{\partial v}{\partial r} = C_2 + C_3$$

Similarly as in the plane strain case:

$$\begin{Bmatrix} \varepsilon_z \\ \varepsilon_r \\ \varepsilon_\theta \\ \gamma_{rz} \end{Bmatrix} = [B] \{\delta\} \qquad (3.26)$$

the matrix $\{\varepsilon\}$ is defined later and matrix $[B]$ in App.I.

3.3.3.2 Stress/strain relationship

3.3.3.2.1 The strain tensor

The total strain matrix is:

$$\{\varepsilon\} = \begin{Bmatrix} \varepsilon_z^e \\ \varepsilon_r^e \\ \varepsilon_\theta^e \\ \gamma_{rz}^e \end{Bmatrix} + \begin{Bmatrix} \varepsilon_z^t \\ \varepsilon_r^t \\ \varepsilon_\theta^t \\ 0 \end{Bmatrix} + \begin{Bmatrix} \varepsilon_z^W \\ \varepsilon_r^W \\ \varepsilon_\theta^W \\ 0 \end{Bmatrix} + \begin{Bmatrix} \varepsilon_z^c \\ \varepsilon_r^c \\ \varepsilon_\theta^c \\ \gamma_{rz}^c \end{Bmatrix} \qquad (3.27)$$

3.3.3.2.2 Stress/elastic strain tensor relationship

The stress tensor is related to the elastic strain tensor with the equation of the form:

$$\{\sigma\} = \begin{Bmatrix} \sigma_z \\ \sigma_r \\ \sigma_\theta \\ \tau_{rz} \end{Bmatrix} = [D]\{\varepsilon^e\} \qquad (3.28)$$

$[D]$ is a 4 x 4 matrix and $\{\varepsilon^e\}$ a 4 x 1 column matrix. Similar relationship apply for axi-symmetric case as derived in Ch.3.3.2.3 for plane strain. Detailed form of equations are given or can be derived from App.I.

3.3.3.3 Stress resultants and element stiffness

Following the derivations in Ch.3.3.2.4, similarly:

$$\{S\} = [B]^T\{\sigma\} \qquad (3.29)$$

In the axi-symmetric case the volume integral has to be taken over the whole ring of material and:

$$k = 2\pi \int [B]^T [D][B]\, r \; dr \; dz \tag{3.30}$$

In solving eq. (3.30) the simplest approximate procedure is to evaluate $[B]$ for a centroidal point $\bar{r}$ and $\bar{z}$ in this case as a first approximation:

$$[k] = -2\pi \Delta [\bar{B}]^T [D][\bar{B}]\, \bar{r} \tag{3.31}$$

Finally, considering eq. (3.26 and 3.27):

$$\{S\} = -2\pi \Delta [\bar{B}]^T \bar{r} [D] \{\varepsilon\} = -2\pi [\bar{B}]^T \bar{r} [D][\bar{B}]\{\delta\}$$

or

$$\{S\} = [k]\{\delta\} \tag{3.32}$$

Similarly as in the plane stress/strain case the system of equilibrium eq. (3.1d) have to be solved considering the above derivations. Finally the stresses are calculated in a similar way as for plane strain (but of course the longitudinal stress σ_z is calculated directly form the matrix equation (3.27)). The matrices $[\bar{B}]$ and $[\bar{B}]^T$ are given in detailed form in App.I.

4. COMPUTER PROGRAMS

4.1 Introduction

In the stress analysis of graphite components by the finite element displacement method the system of simultaneous linear equations:

$$[K]\{\delta\} = \{R\} - \{\{R^t\} + \{R^W\} + \{R^c\}\} \qquad (3.1c)$$

or

$$\{\delta\} = [K]^{-1}\{\{R\} - \{R^t\} - \{R^W\} - \{R^c\}\} \qquad (3.1d)$$

have to be solved for the displacements in terms of the nodal forces for each time step.

The matrix displacement methods use mainly two approaches for solving the system of equations (3.1d). One referred to as the direct approach uses Gaussian elemination technique, the other called iterative approach uses the Gauss-Seidel iterative procedure. The development of two-dimensional finite element programs based on both techniques has been influenced by various factors: the size of the problem (number of elements), the type of element, the required central memory and computing time.

In the early sixties a computer program based on a modified Gauss-Seidel iterative technique and a direct so called triple-band code based on Gaussian elemination have been developed (see Wilson [19] and Zienkiewicz [18] respectively). It was soon concluded that the iterative program is in general faster but uses in comparison with the triple-band code more central memory, especially for medium and large-size problems. The direct triple-band program uses less central memory since magnetic discs are used to store the large stiffness matrices and the method is therefore suitable for large-size problems. On the other hand the program is more complex to run. Elastic versions of both programs have been taken as the starting point in the

development of the time-dependent finite element stress program for reactor graphite. The iterative and direct-triple-band program are described in Ch.4.2 and Ch.4.3.

In the recent past another direct program has been developed using the front-solution technique (see for example Irons [33]). This program has certain advantages over direct-triple-band approach and it seems that its solution technique is especially suitable for two-dimensional problems using higher order elements and for three-dimensional calculations.

The first step in developing a finite element code for stress analysis of reactor graphite was to examine basic two-dimensional constant stress triangle finite element programs, using iterative and direct techniques of solution for stress analysis of elasticity problems. Then both elasticity versions have been modified and developed into time-dependent programs, for plane stress/strain analysis of stresses in graphite core components. The results of both versions for graphite have been compared analysing first simple structures and then the iterative version chosen for the further analysis since it was considered to be faster and more suitable for stress analysis of particular graphite components. The program was named STAG (Stress two-dimensional analysis of graphite).

At present, different versions of STAG analyse different graphite core components: a hollow rod fuel pin, a teledial fuel pin and a multichannel graphite block. The possibility exsists to assemble the versions into one single program and include in addition an axisymmetric option which is now in its final phase of development.

In the program are incorporated some parts of the subroutines developed in Nessan III. New subroutines (programs) have been written especially to generate automatically the mesh data for complex reactor core geometries. The subroutines are described in Chapter 5.

In the following Chapters the flowcharts of both versions of STAG are presented and techniques discused and compared.

4.2 Iterative program

4.2.1 The basic theory

The iterative method used is a modification of the Gauss-Seidel iterative technique which in solving the system of equations (3.1d) involves the repeated calculation of new displacements from the equation:

$$\delta_n^{(s+1)} = K_{nn}^{-1} \left[R_n - \sum_{i=1,n-1} K_{ni}\, \delta_i^{(s+1)} - \sum_{i=n+1,N} K_{ni}\, \delta_i^{(s)} \right] \qquad (4.1)$$

bearing in mind that (see eq. (3.19), Ch.3.3.2.5)

$$R_n = R_n^{tot} - \left\{ R_n^t + R_n^W + R_n^c \right\} \qquad (4.2)$$

where n is the number of the unknown and s is the cycle of iteration.

The equation (4.1) is simultaneously applied to both components of displacement at each nodal point. Therefore δ_n and R_n become vectors with x and y components and the stiffness coefficients may be expressed in the 2 x 2 submatrix form:

$$k_{lm}^{(q)} = \begin{bmatrix} k_{xx} & k_{xy} \\ k_{xy} & k_{yy} \end{bmatrix}_{lm}^{(q)} \qquad (4.3)$$

and the term $k_{lm}^{(q)}$ represents the forces developed on element q at nodal point l due to unit displacements at nodal point m.

By calculating the change in the displacement of the nodal point n between the cycles of iteration:

$$\delta_n^{(s)} = \delta_n^{(s+1)} - \delta_n^{(s)} \qquad (4.4)$$

the rate of convergence of the iterative technique can be increased by the use of an over-relaxation factor β.
The new displacement of nodal point n is then determined by:

$$\delta_n^{(s+1)} = \delta_n^{(s)} + \beta \cdot \Delta\delta_n^{(s)} \qquad (4.5a)$$

or by substitution of eq. (4.1) into eq's(4.4)and then eq's(4.4) into eq.(4.5a):

$$\delta_n^{(s+1)} = \delta_n^{(s)} + \beta \cdot K_{nn}^{-1} \cdot \left[R_n - \sum_{i=1,n-1} K_{ni}\, \delta^{(s+1)} - \sum_{i=n,N} K_{ni}\, \delta_i^{(s)} \right] \qquad (4.5b)$$

The optimum value of the factor β depends on the characteristics of the particular problem and it is usually 1.85 approximately.

4.2.2 The program layout

A generalized flow chart of iterative version of STAG for plane stress/strain problems is given in Fig.7.

In the initial part of program the basic data are read in or calculated in subroutines. The main DO LOOP(700)enables the calculations to be performed at prescribed number of axial positions in the reactor and for each crossection at a prescribed number of time intervals. Inside the inner DO LOOP(700)the equivalent dose and temperature distributions are calculated or read in. Then the dimensional changes (Wigner strains) creep strains and thermal strains are calculated.

In principle the nonelastic strains (thermal, Wigner and creep) are calculated at the beginning of time interval and nodal point loads are then evaluated considering also other external loads (e.g. surface pressures) if any. The gravity forces have been neglected in the calculation. The total stiffness arrays are calculated and inversion of nodal point stiffnesses (2x2) performed at each time interval. Before proceeding with the solution of the equation (3.1d) the prescribed displacements have to be considered.

Next, the system of equations (3.1d) is solved by iteration for nodal point displacement using equation (4.5b) on a given tolerance. After iteration of nodal point displacements the stresses and strainsin the xy plane with the reactor at power are calculated. Assuming that axial strain ε_z = const,.the axial stress σ_z is calculated (see Ch.3.3.2.6) with the structure not being allowed to bend. The stresses with the reactor at power are stored to calculate the creep strain increments in the next dose interval.

The procedure is repeated at the next and successive time intervals.

The total stiffness array, inversion of nodal stiffness and modification of boundary flexibilities are evaluated only once if the elastic constants (E,γ) do not vary with neutron dose (time).

At prescribed time intervals the thermal strains are set to zero and residual stresses (reactor shut down) calculated. In this case also the total stiffness array, inversion of nodal stiffnesses and modification of boundary flexilibities need not be revaluated. Only nodal forces at the right hand side in the system of equations (3.1c) have to be modified and the system solved again.

The total creep strainsat each time interval are obtained by summation of the incremental creep strains over the previous and current time intervals. In the early Nessan programs (see Ch.3.1) the incremental creep strains occuring during a time interval are obtained from a relationship between the creep strain rate tensor and the general stress tensor by iteration. The finite element method however requires a considerable amount of central processor time and the creep strain iteration will prolong the required time to an untolerable value. If creep strain iteration is performed it means that the iteration of nodal point displacements will have to be performed after each creep strain approximation and the number of iterations of nodal point displacements will be higher by a factor equal to the number of creep iterations. Thus the creep strain increments have

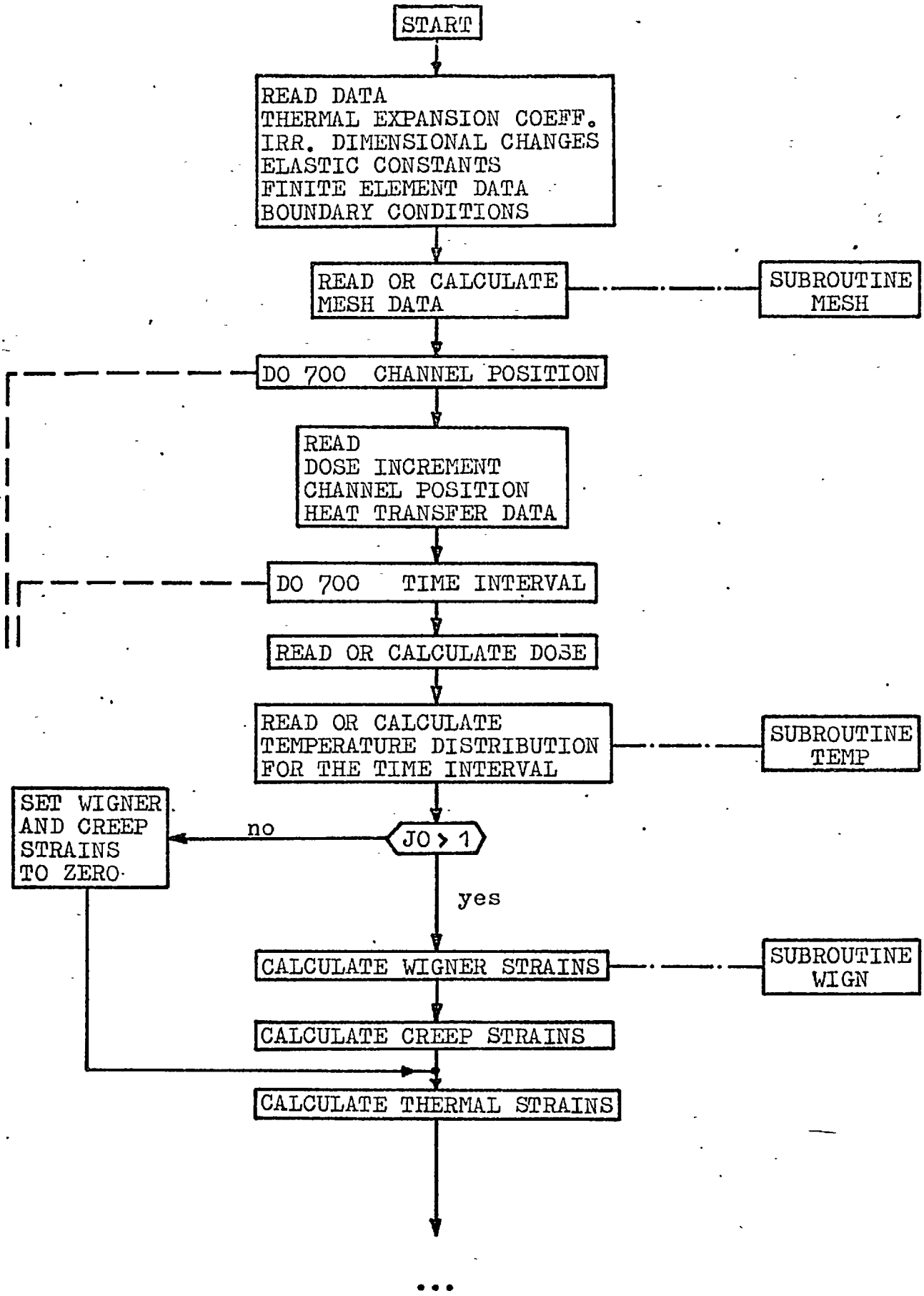
START
READ DATA
THERMAL EXPANSION COEFF.
IRR. DIMENSIONAL CHANGES
ELASTIC CONSTANTS
FINITE ELEMENT DATA
BOUNDARY CONDITIONS
READ OR CALCULATE MESH DATA
SUBROUTINE MESH
DO 700 CHANNEL POSITION
READ
DOSE INCREMENT
CHANNEL POSITION
HEAT TRANSFER DATA
DO 700 TIME INTERVAL
READ OR CALCULATE DOSE
READ OR CALCULATE TEMPERATURE DISTRIBUTION FOR THE TIME INTERVAL
SUBROUTINE TEMP
SET WIGNER AND CREEP STRAINS TO ZERO
no
JO > 1
yes
CALCULATE WIGNER STRAINS
SUBROUTINE WIGN
CALCULATE CREEP STRAINS
CALCULATE THERMAL STRAINS
...

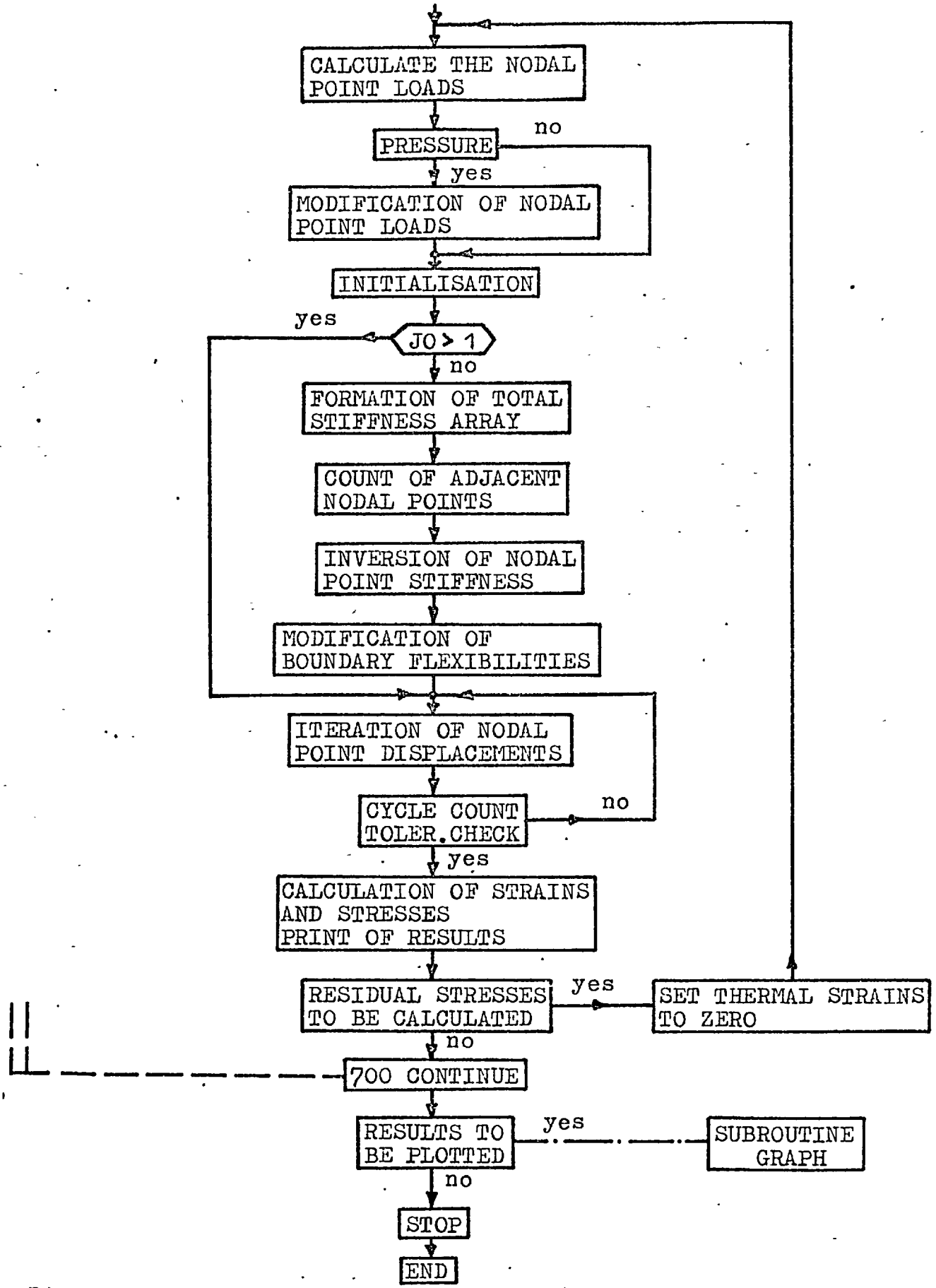

Fig.7

FLOW DIAGRAM 'STAG' ITERATIVE VERSION.

been calculated without iteration using the stresses from previous interval and chosing a short dose step. Thus for example a dose step equal to a half of dose step used in Nessan III calculations gave an adequate accuracy, without iteration (see also Ch.6).

Since a non-elastic time-dependent calculation requires substantially more computer storage than elastic analysis, the central memory requirements of the program have been reduced, by rewriting also the basic elastic version. Some variables, for example thermal strains and differences between x and y coordinates of triangles, normally calculated once and stored in the form of arrays have been changed to a single constant form and values are calculated 3 times in the program when required. This increases marginally the computer time but reduces the central memory requirements. For problems with large number of elements it is of advantage to read from tape or cards the mesh data (once) and temperature and equivalent dose distribution at each time interval and to prepare the mentioned input data by separate programs. If mesh, temperature and dose distribution data are read in from tapes or cards the capacity of program to analyse the problems with a larger number of finite elements is substantially increased.

4.3 Direct program

4.3.1 The basic principles

The direct methods of solution differ from iterative techniques in solving the system of equations (3.1d):

$$\{\delta\} = [K]^{-1}\left\{\{R\} - \{R^t\} - \{R^W\} - \{R^c\}\right\} \qquad (3.1d)$$

The system of equations (3.1d) can be solved also by calculating the stiffness matrix $[K]$ and its inverse for the complete structure. However the size of matrix $[K]$ and its inverse

depends on the number of elements and nodal numbers of the structure and $[K]$ and $[K]^{-1}$ have to be stored in central memory. Therefore the number of elements of the analysed structure is limited by the available computer central memory and further the inversion of large size matrices consumes considerable computer time. To overcome the limitations imposed by the size of the available central memory, the direct approach has to be suitably modified. Therefore the principle of solving the system of equations (3.1d) by a direct method is to proceed with solving the system in sections, considering always the coupling effects between the two adjacent parts of the structure. The matrix $[K]$ and its inverse $[K]^{-1}$ for the complete structure need not to be built and stored in the central memory and structures with much larger number of elements can be considered.

In one of the direct displacement methods considered in this analysis and sometimes referred as tri-band method, the complete structure is divided into a number of elemental regions (Fig.9) called partitions. The matrix K and its inverse are calculated for each region and stored on magnetic disc. The calculation proceeds from one elemental region to the other and the coupling effects between adjacent partitions are always considered and stored in central memory. Except for the matrices $[K]$ in the first and last partitions, every matrix is connected to two other matrices only. This partitioning is known therefore as tridiagonal i.e. partitions are connected in series.

It can be seen that if the elements of a structure are numbered in a suitable order all non-zero elements will lie close to the matrix diagonal or the matrix will have a narrover band. For the same number of equation this will require less solution time and central storage.

The system of matrix equations (3.1c) can be written in a triadiagonalized form as follows:

$$\begin{bmatrix} K_I & C_I & 0 & 0 & \cdot & \cdot & 0 & 0 \\ C_I^T & K_{II} & C_{II} & 0 & \cdot & \cdot & 0 & 0 \\ 0 & C_{II}^T & K_{III} & C_{III} & \cdot & \cdot & 0 & 0 \\ \cdot & \cdot & \cdot & \cdot & \cdot & \cdot & \cdot & \cdot \\ \cdot & \cdot & \cdot & \cdot & \cdot & \cdot & \cdot & \cdot \\ 0 & 0 & 0 & 0 & \cdot & \cdot & K_{N-1} & C_{N-1} \\ 0 & 0 & 0 & 0 & \cdot & \cdot & C_{N-1}^T & K_N \end{bmatrix} \begin{Bmatrix} \delta_I \\ \delta_{II} \\ \delta_{III} \\ \cdot \\ \cdot \\ \delta_{N-1} \\ \delta_N \end{Bmatrix} = \begin{Bmatrix} R_I \\ R_{II} \\ R_{III} \\ \cdot \\ \cdot \\ R_{N-1} \\ R_N \end{Bmatrix}^* \tag{4.6}$$

The first two matrix equations are:

$$\left[K_I\right]\left\{\delta_I\right\} + \left[C_I\right]\left\{\delta_{II}\right\} = \left\{R_I\right\} \tag{4.7}$$

$$\left[C_I^T\right]\left\{\delta_I\right\} + \left[K_{II}\right]\left\{\delta_{II}\right\} + \left[C_{II}\right]\left\{\delta_{III}\right\} = \left\{R_{II}\right\} \tag{4.8}$$

From the first equation:

$$\left\{\delta_I\right\} = \left[K_I\right]^{-1}\left\{R_I\right\} - \left[K_I\right]^{-1}\left[C_I\right]\left\{\delta_{II}\right\} \tag{4.9}$$

and substituting in the second gives:

$$\left(\left[K_{II}\right] - \left[C_I^T\right]\left[K_I\right]^{-1}\left[C_I\right]\right)\left\{\delta_{II}\right\} + \left[C_{II}\right]\left\{\delta_{III}\right\} = \left\{R_{II}\right\} - \left[C_I^T\right]\left[K_I\right]^{-1}\left\{R_I\right\} \tag{4.10}$$

By defining new symbols:

$$\left[\bar{K}_{II}\right] = \left(\left[K_{II}\right] - \left[C_I^T\right]\left[K_I\right]^{-1}\left[C_I\right]\right. \tag{4.11}$$

$$\left\{\bar{R}_{II}\right\} = \left\{R_{II}\right\} - \left[C_I^T\right]\left[K_I\right]^{-1}\left\{R_I\right\} \tag{4.12}$$

---

* $R_I, R_{II}, R_{III} \ldots R_N$ are the nodal forces at the right hand side of eq. (3.1d).

equation (4.10) may be written:

$$\left[\bar{K}_{II}\right]\left\{\delta_{II}\right\} + \left[C_{II}\right]\left\{\delta_{III}\right\} = \left\{\bar{R}_{II}\right\} \tag{4.13}$$

The process of substitution and elemination goes on until the last row equation is reached. The displacements in the last partitions are then found from the equation:

$$\left\{\delta_N\right\} = \left[\bar{K}_N\right]^{-1} \left\{\bar{R}_N\right\} \tag{4.14}$$

Using the equations of the form (4.9) the displacements for the whole structure are found by the process of back-substitution. For the N-1 partition thus:

$$\left\{\delta_{N-1}\right\} = \left[\bar{K}_{N-1}\right]^{-1} \left\{\bar{R}_{N-1}\right\} - \left[\bar{K}_{N-1}\right]^{-1} \left[C_{N-1}\right] \left\{\delta_N\right\} \tag{4.15}$$

and similarly in sequence the displacements for other partitions are obtained.

4.3.2 The program layout

A generalized flow chart of the direct version of STAG for plane stress/strain problems is given in Fig.8.

The initial part of the program is to some extent similar to the corresponding part of iterative version. Additional input data are required to divide the structure of elements into partitions. The essential difference in comparison with the iterative version is in assembling and storing the total stiffness matrix for the complete structure and in solving the system of equations (3.1c,d).

After the calculation of nodal point loads the stiffness matrices of partitions are formed, the prescribed displacements introduced and matrices stored on magnetic disc. The system of equations (3.1d) is solved in subroutine SOLVE for displacements

by Gaussian climination. Finally the strains and stresses are calculated in the main program with the residual stresses as an option.

The flow chart given in Fig.8 includes the creep iteration option which could be included into the iterative version also. However in the present analyses of the structures with a large number of elements (teledial, graphite block) creep iteration has not been used since it has been considered to be too time consuming. Similarly as in the iterative version a dose step equal to a half of dose step used in Nessan III calculations gave an adequate accuracy (see Ch.6).

If the elastic constants (E, ν) do not vary with neutron dose (time) only the nodal forces at the right hand side of the equation (3.1c) have to be modified at each time step and the stiffness matrices of partitions need to be calculated assembled and stored on disc only once. Also in subroutine SOLVE the forward elimination is performed only once and the triangulated form and the necessary multipliers are stored so that for each new time interval, with a new set of nodal loads, the backsubstitution can be carried out to obtain the displacements. Since the process of inverting a large size matrix of a partition is prticularly time consuming a considerable amount of computer time is saved in the calculation if the above criteria is satisfied.

If the residual stresses are calculated at prescribed time intervals or creep iteration is performed similarly only the nodal forces at the right hand side of the equation (3.1c) have to be modified and the already known stiffness matrices for the particular time interval can be utilizied. Next in subroutine SOLVE again, only backsubstitution ca be carried out to obtain the displacements.

The problem of computer storage is less critical using the direct version since the magnetic discs are used to store the stiffness matrices of the partitions. However, the central memory requirements of the direct version have been reduced by rewriting the basic elastic version which was developed into

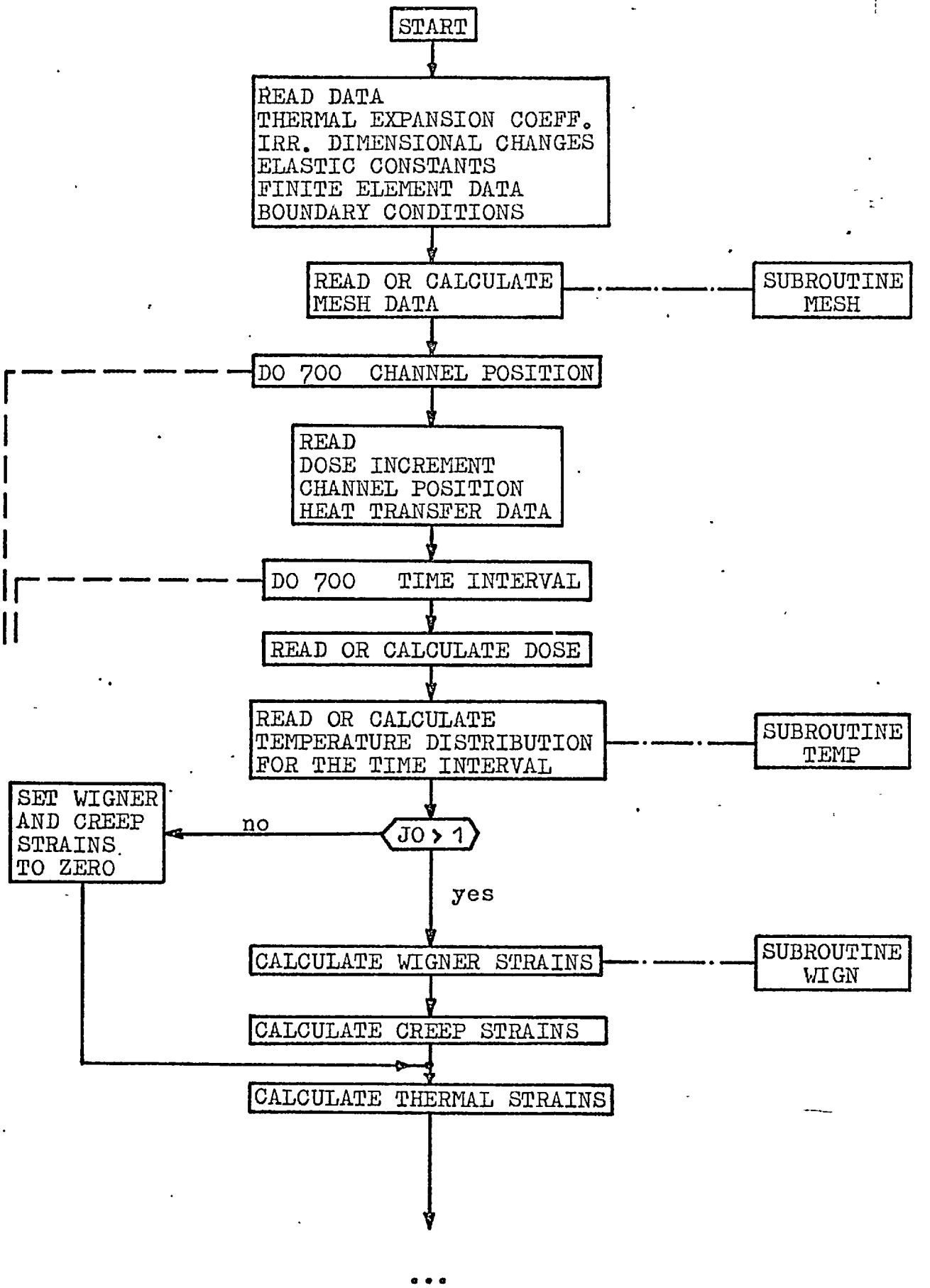
START
READ DATA
THERMAL EXPANSION COEFF.
IRR. DIMENSIONAL CHANGES
ELASTIC CONSTANTS
FINITE ELEMENT DATA
BOUNDARY CONDITIONS
READ OR CALCULATE MESH DATA
SUBROUTINE MESH
DO 700 CHANNEL POSITION
READ
DOSE INCREMENT
CHANNEL POSITION
HEAT TRANSFER DATA
DO 700 TIME INTERVAL
READ OR CALCULATE DOSE
READ OR CALCULATE TEMPERATURE DISTRIBUTION FOR THE TIME INTERVAL
SUBROUTINE TEMP
SET WIGNER AND CREEP STRAINS TO ZERO
no
JO > 1
yes
CALCULATE WIGNER STRAINS
SUBROUTINE WIGN
CALCULATE CREEP STRAINS
CALCULATE THERMAL STRAINS
...

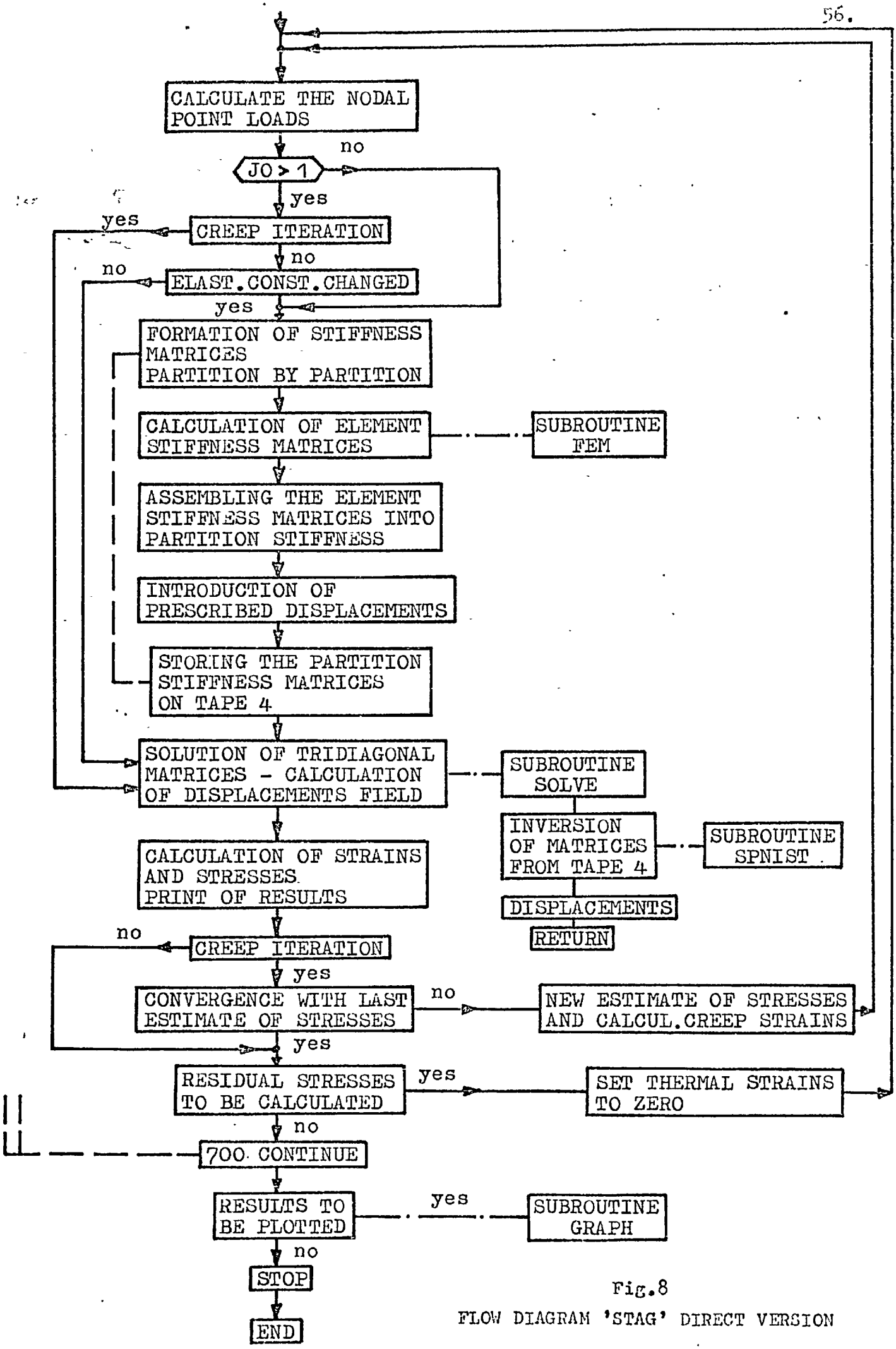

Fig.8

FLOW DIAGRAM 'STAG' DIRECT VERSION

STAG similarly as the iterative version. Further, for example, the use of 2 magnetic disc have been dropped to simplify the program, but because of this the central memory requirements have been increased slightly.

4.4 Axi-symmetric program

The layout and calculation procedure of the iterative elastic axi-symmetric program is similar to the plane stress/strain code.

A program could be developed which will include plane stress/strain and axi-symmetric geometry and in which most of the program can be utilizied by both options. The required central memory will remain approximately the same.

If the axi-symmetric calculation is included into the existing STAG the following main changes have to be added as options for axial geometry:

(1) The calculations of creep strain using a 4 x 4 compliance matrix (see App.I).

(2) The calculation of nodal point loads at the beginning of computation as discused in App.I.

(3) The appropriate coordinates have to be considered for axial symmetry, thus r replaces x and z replaces y.

(4) The matrix $[D]$ has to be defined, also some terms of matrix $[B]$ and $[B]^T$ and multipliers to give the appropriate element stiffness matrix $[k]$ (see App.I.).

Considering the r-z coordinate system for axi-symmetric geometry some mesh generation programs and some subroutines for calculation of dimensional changes used in the plane stress/strain version of STAG can be utilized. The temperature and equivalent dose distribution have to be provided by separate programs. Most of equations required to include axi-symmetric option into STAG are derived in Ch.3.3.3 and in App.I.

4.5 Comparison of different solution techniques and conclusions

In the calculation of stresses in reactor graphite, in the most general case the temperature and equivalent dose distribution and material properties all vary in space and time. Also, the external loads (if any) may be time dependent. Because of these changes with time the right hand side of eq.(3.1c) must be modified at each time step. The stiffness matrix $[K]$ for the whole structure is a function of geometrical dimensions and elastic constants (E, ν). Since Young's modulus E of graphite normally changes with time (dose) the stiffness matrix $[K]$ has to be recalculated repeatedly and its inverse found, at each time step. The stiffness matrix $[K]$ has to be recalculated also if the geometrical dimensions due to nonelastic strains with time are large and thus the basic dimensions change considerably.

If the equations (3.1d) are solved with direct triple-band approach the formulation of stiffness matrix $[K]$ and especially its inversion is the most time consuming process since the inversion of large size matrices (e.g. 40x40) is required (see Ch.4.3). If the iterative procedure is used only small size matrices of the order 2 x 2 are inverted (Ch.4.2) and the formation and inversion of total stiffness matrix requires considerable less time, however the iteration of nodal point displacements may well be time-consuming (depends on the changes of stresses/time). As seen in TABLE I the iterative procedure is in general faster than direct triple-band approach for the problems where the stiffness matrix $[K]$ and nodal point forces have to be recalculated at each time step.

If the elastic constants and material dimensions do not vary with time, the stiffness matrix $[K]$ and its inverse have to be calculated only once, nodal point forces modified and the system of equations (3.1d) re-solved at each time step. In the direct procedure only the backward - substitution process using modified loads is performed when solving the

equations (3.1d) since the values of matrix $[K]$ and $[K]^{-1}$ are stored for subregions (partitions) and read from disc. For this particular case the direct approach may well use a comparable amount of time as iterative procedure.

If the required central memory is compared between iterative and direct versions of STAG the difference is less marked for small and medium size problems but increases with the number of elements and nodes. Thus for example for the 605 elements (see Table I) the difference in required central memory is appr. 10.000 words but it is still possible slightly to reduce the required memory of the direct program for simple structures by introducing a larger number of small partitions. For complex problems for example a multichannel graphite block the partitions have to be relatively large and it is almost impossible to use very small partitions. With the increased number of elements and nodes the central memory requirement of the iterative version of STAG increases faster than that of the direct one. A conclusion can be reached, that since the size of available computers has increased considerably since the early sixties, the central memory requirements do not represent any more a major obstacle for use of the iterative technique for most 2-D engineering problems if constant-stress triangles are used. For example with appr. 100.000 words of central memory available, graphite structures with up to approximately 1500 elements and 1000 nodal points can be analysed by the iterative version, and up to appr. 3000-4000 elements by direct tri-ple band version. Thus only very complex - large size problems can not be dealt with the iterative program. For problems with many thousand elements the very large computing time required may well become an uneconomic proposition.

A futher factor in using either of the versions is the amount of input data required. The direct version requires considerably more effort to prepare the input data. A carefull numbering of the structure has to be performed due to the requirements of partitioning and the partitions defined separately

by specifying in the input data first and last nodes and first and last elements in each partition. For large complex problems this is a tedious and time-consuming task. The iterative method has in this respect definite advantages since the structure can be arbitrarily numbered and partitions are not required.

It was not possible to compare fully the accuracy of results and stability of solutions obtained by both methods. The results obtained by both version compare favourably. It is thought that regarding accuracy and stability of solution one solution has no definite advantages over the other for most general engineering problems particularly since the accuracy of results can be always improved by using for example double precision arithmetic for $[K]$ in the direct method or smaller tolerance in iterative procedure. A comparative analysis of both procedures may well be valuable since it will point out the means of improving the quality of results.

TABLE I

Sample comparison of iterative and direct STAG code

Capacity of the programs	Iterative version	Direct version
No of elements	610	610
No of nodes	380	380
Program requirements		
Central memory	40,000 wds	30,000 wds
Computing time required	100	250*

An example - teledial fuel pin	
No of elements	605
No of nodes	379
No of time intervals	41
No of calculations of residual stresses	4
Computing time** required (Central processor)	appr.1200 secs (CDC 6600)

*Values obtained on an example with 108 elements and 76 nodes (Fig.20). The time for direct program could be slightly reduced by a better choice of partitions.

**Elastic constants (E, ν) are changing in time and space. Iterative version used.

5. INITIAL CALCULATIONS AND INPUT OF DATA

5.1 Calculations of the finite element mesh

5.1.1 General

In the analysis of a structure by finite elements, the structure is considered to be divided into a large number of small elemental regions. In this thesis triangular elements are considered. A substantial amount of the data required in the analysis consists of the co-ordinates of the corner points (nodes) and nodal and element numbers that are associated with each element. The manual preparation and checking of this input mesh data is lengthy and tedious.

In recent years extensive use has been made of a coordinate digitising table, the so called D-mac table, linked to a card punch. In principle the mesh data are generated by placing a drawing of the proposed mesh on the table and by pointing the D-mac pencil at the nodes of the structure. The coordinates of each node are then automatically recorded and punched on card in the required format. Frederik et al. [34] proposed a method where the D-mac facility is used together with a computer program to generate the complete mesh data in a form suitable for use in direct - tri-band program. They claim that coordinates can be recorded to an accuracy of±0.03 cm. If the D-mac facility is used some manual effort is still required but complex meshes with difficult topological restriction can be generated.

An alternative way is to write a mesh generation program, to generate, correlate and check the mesh data required by the particular finitc element stress program. This approach will be especially suitable for structures with large numbers of elements.

In one technique for automatic generation of triangular meshes, presented by Zienkiewicz [18] , it is sugested that the

structure should be divided by a number of straight lines and/or arcs of circles and each line should be divided further to give the node data. To generate the nodal coordinates it is necessary to define the coordinates at the end of each row of nodes and the spaces between nodes in each row. If unequal spacing of nodes is required, weighting factors are introduced. The calculations have to follow a definite sequence i.e. row after row. Finally the nodes on the lines are interconnected into triangles in a way that gives optimum triangles for finite element analysis.

Lewis and Fullard [35] have described a similar 2 dimensional mesh generation program FEMG.

Different automatic mesh subroutines have been written to generate the mesh data for graphite core components. The subroutines are written to some extent in general form and can be used as separate programs for preparation and storing of mesh data on tapes or cards. An approach to be used in mesh generation programs for some complex two-dimensional structures is suggested in Ch.5.1.4.

5.1.2 The mesh data input requirements

The graphite core of future commercial HTR will be built from multichannel graphite blocks filled with fuelled graphite tubes or fuel pins. At present different types of fuel pins and multichannel graphite blocks are studied.

In this thesis the mesh data for two types of fuel pin, a hollow rod and a teledial fuel pin, and one form of multichannel graphite block are required. The element and node numbering should also satisfy the partioning scheme of the direct (tri-band) version of the program. The mesh routines should be capable of producing input data for different designs of fuel pins and graphite blocks without major modifications.

5.1.3 The choice of approach and mesh generation programs

In the ideal case an automatic mesh program should generate the required data if the origin of coordinate system, the geometrical boundaries and the type and size of the element are specified previously.

In writing the mesh generation programs the desire to specify a minimum of basic information about the structure to generate the required mesh data has been given the priority. It is thought that if lengthy preparation of input data for the mesh generation program is needed, the required man-hours may well diminish the potential value of the program and some other technique like the use of a D-mac table becomes a more attractive alternative.

In the mesh generation programs developed for this work, the basic geometrical boundaries and the type and size of element are specified. The program then calculates automatically all mesh data. In the case of large or complex structures, for example the multichannel graphite block, the mesh is built from basic structural units and only the distance of the unit centre from the coordinate origin has to be specified additionally. Exceptions can be programmed separately, following again the same principles and calculating and defining exception areas in similar units as far as possible.

The graphite tube (Fig.9) represents the simplest example. By defining the inner radius, the thickness of the tube and the origin of the coordinate system the subroutine needs only one further piece of information, namely the element size (or the number of elements across the tube thickness) to calculate the complete set of mesh data. The mesh pattern and element type is however predefined. Fig's 9,10. show the type of mesh generated by this program .

Similarly, a triangular mesh for a 45° sector of a teledial fuel pin has been calculated (Fig.11). Most of the nodes lie at intersections between radial lines and arcs of concentric

circles, or at intersections between the radial lines or the arcs with the geometrical boundaries of the pin. Some exceptions are calculated separately. Mesh data for more complex geometries, for example a multi-channel block, have been generated using as a basic unit a prespecified hexagon*(Fig.12). Again, some exceptional areas have been programmed separately, but as far as possible these exceptional areas have been built up from similar units. With all of these programmes, the mesh can be partially or completely refined (Fig.13) by introducing some modifications.

5.1.4 Some conclusions about mesh generation

It is possible to conclude from the work of Zienkiewicz [18], Frederik et al. [34] and Lewis and Fullard [35] as well as from the work described in this thesis that the writing of automatic mesh generation programs for various types of structure is a practical possibility. It seems that complexity of geometrical shape is one of the main difficulties and that it will be indeed very difficult if not practically impossible to write a mesh generation program suitable for any arbitrary two or three dimensional structure. Therefore, for the time being it seems that a parallel use of automatic mesh generation programs and the D-mac facility will be a suitable answer. It appears that the D-mac facility is especially suitable for very complex geometries, however automatic mesh generation is attractive for very large and moderately complex structures.

In nuclear power and in mechanical engineering in general a number of structures exibits a certain degree of similarity. For the analysis of certain types of structure by finite element methods, a general automatic mesh generation program which requires a minimum of basic input data may well be a suitable solution.

---

*Another example is shown in Fig.13, which is a mesh generated for the analysis of the top cap of a prestressed concrete pressure vessel.

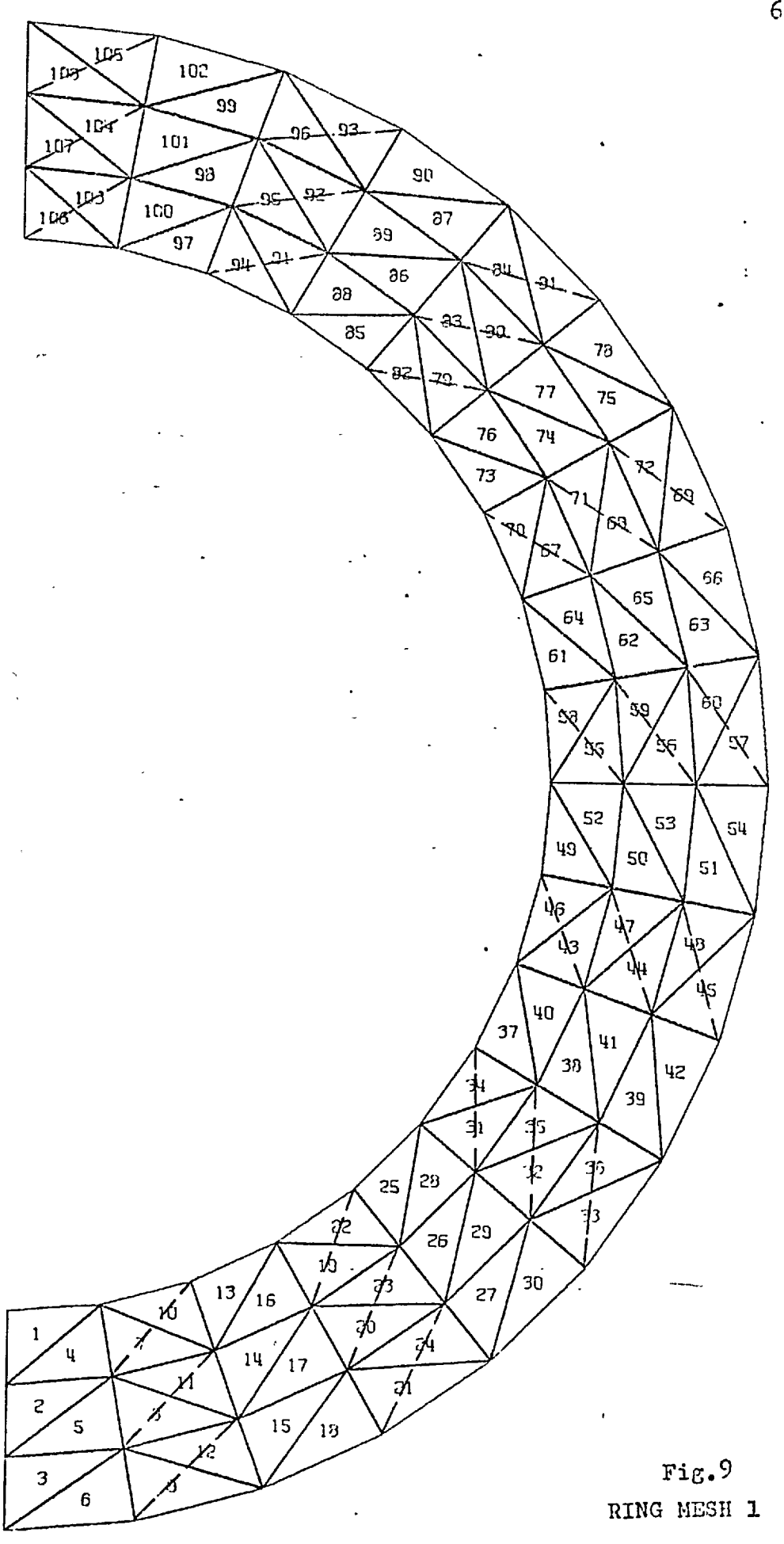

Fig.9
RING MESH 1

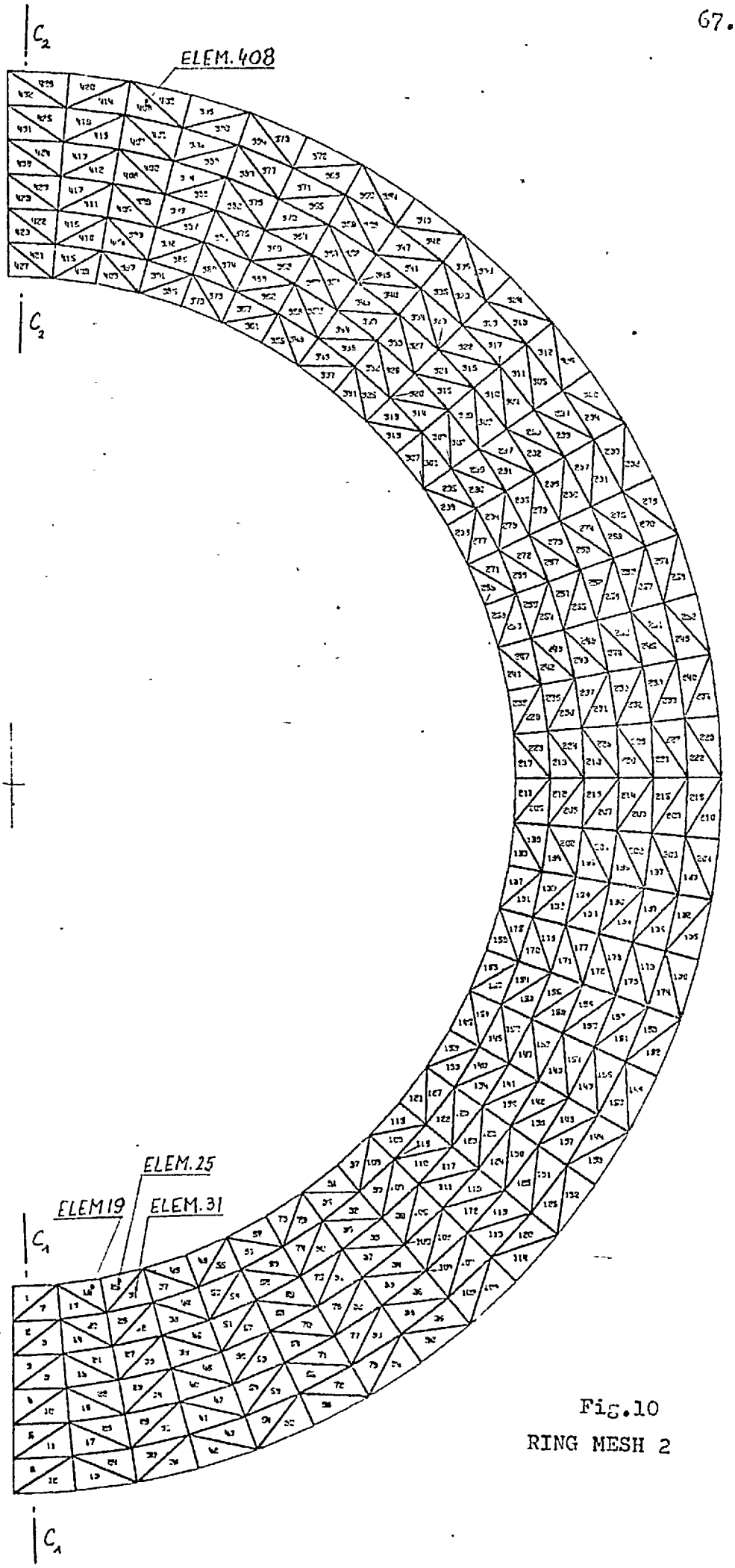

Fig.10
RING MESH 2

Fig.11
TELEDIAL MESH

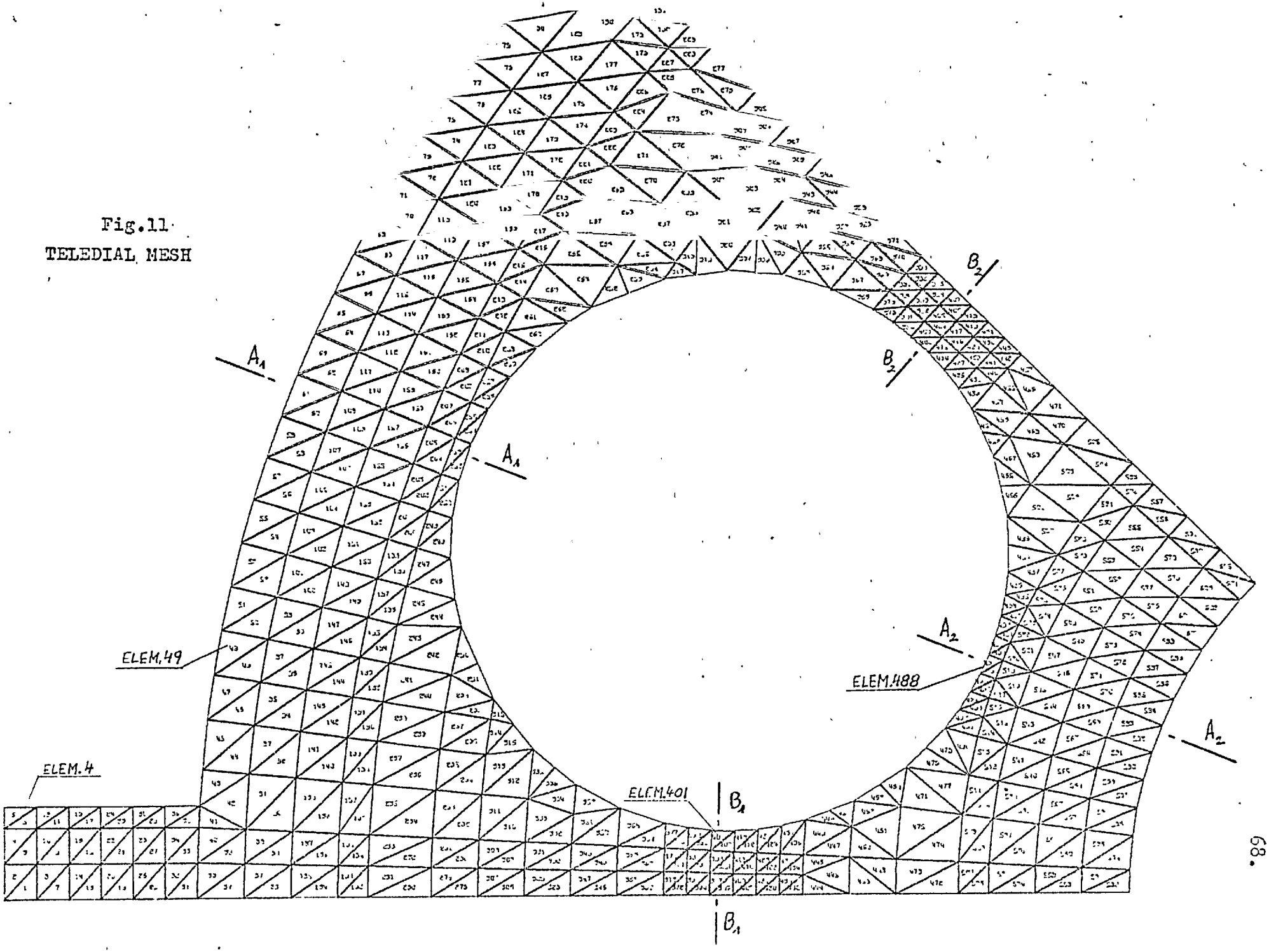

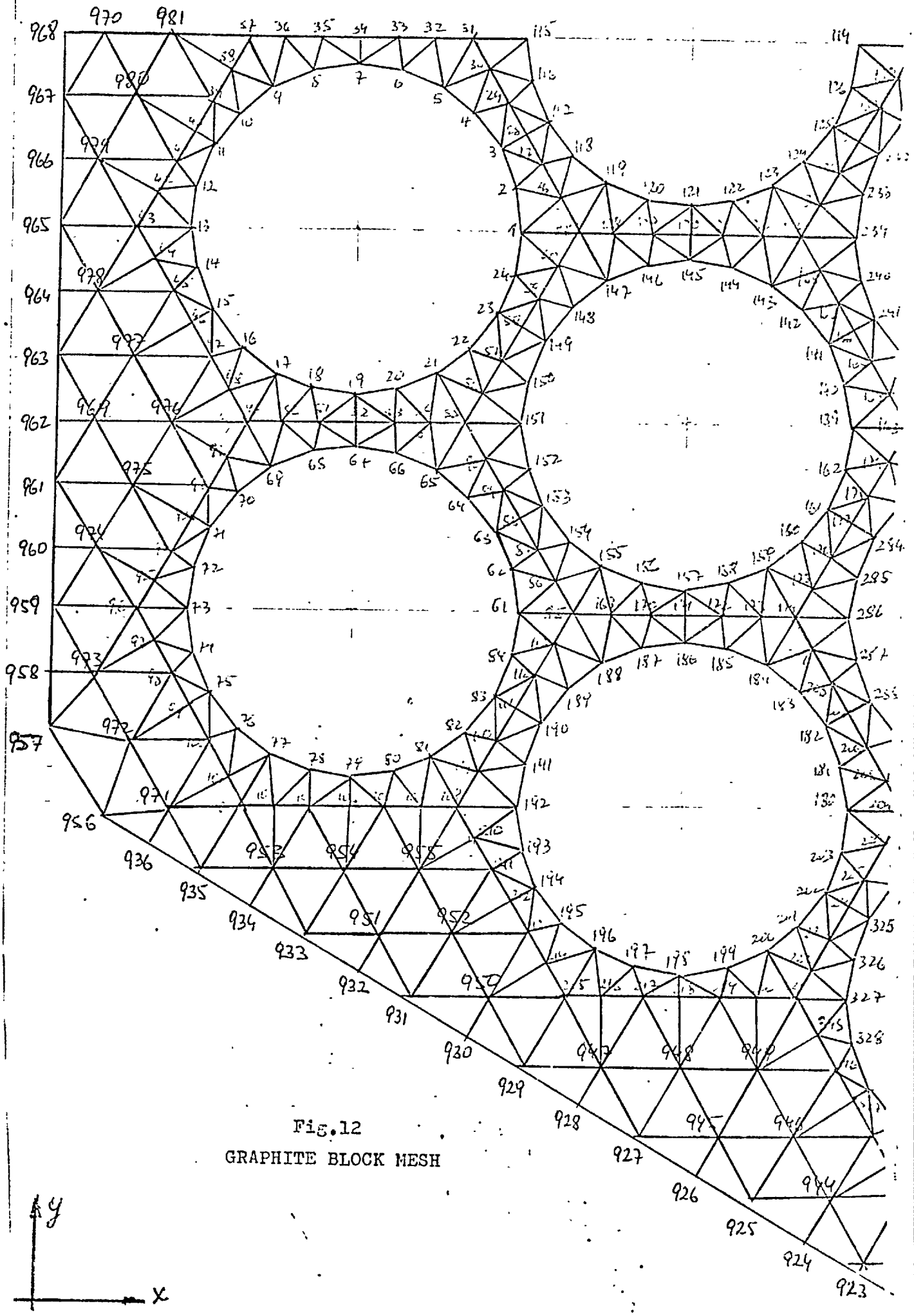

Fig.12
GRAPHITE BLOCK MESH

Fig.13

AN EXAMPLE OF MULTIHOLE MESH

(TOP CAP OF A PRESTRESSED PRESSURE VESSEL)

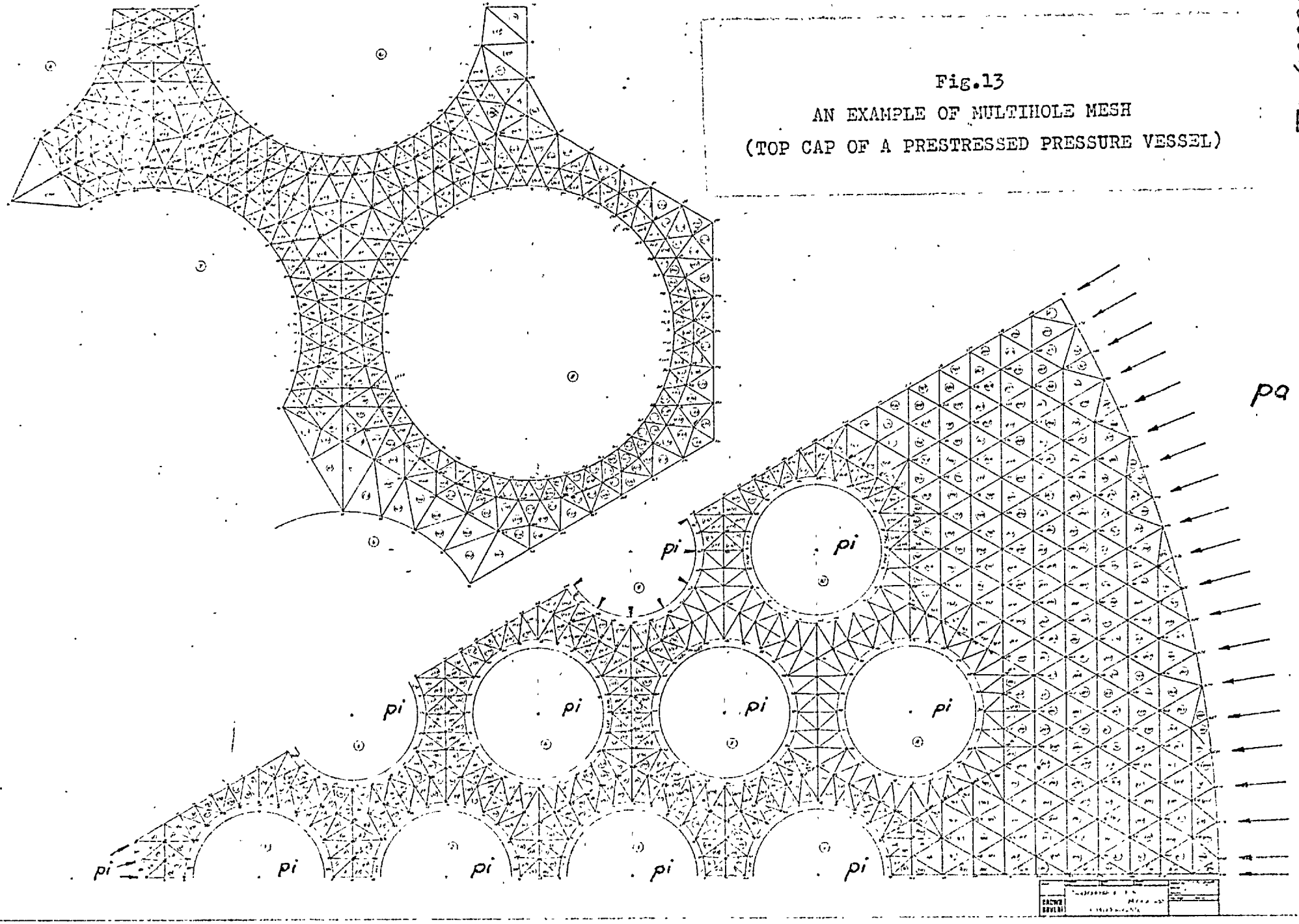

In the particular example of the multichannel graphite block, the mesh program will generate the mesh data for dimensionally different but similar in pattern multihole structures. Only a few basic data such as the outside dimensions of the structure, the origin of the coordinate system the coordinates and diameter of holes need be given.

The program could be used in the analysis of a number of other multi-hole two dimensional structures used in nuclear power and in mechanical engineering generally. For example, calandria ends, heat exchanger and condensor tube plates.

5.2 Temperature calculations

In the earlier one-dimensional analysis using the program Nessan III the calculations of temperature have been performed by subroutines incorporated in the program.

One way to provide the temperature distribution data for each time interval in the finite element stress analysis will be to include in the program a two-dimensional finite element code for the calculation of temperature distribution. The coupled program could take account of changes of graphite conductivity and changes of boundary conditions and could also consider long-term changes in power of fuel pins due to fuel burn-up during the life of the pin. The set-up of a combined program was however not attempted on account of the very long computing time and storage required by such a code. Thus the temperature distribution were calculated separately and read in as input data.

The temperature distribution for the teledial pin shown in Fig.11 was provided by Kinkead [36] and was calculated for the time in the life of the fuel pin when the maximum fuel temperature occurs. In the analysis described in this thesis, this temperature distribution was assumed to remain unchanged troughout the life of the fuel pin although the program permits the element temperatures to be re-read as frequently as required.

The graphite block was assumed to be under an arbitrary temperature tilt. This arbitrary temperature distribution has been

determined by considering a temeprature distribution provided by P.J., Allen [47] and used in a design study on a typical HTR block. Thus the results presented (see Ch.6) should provide some indications about stresses in graphite blocks under real conditions in a HTR. The temperature distribution in the graphite block also, was assumed to remain unchanged.

For the purpose of comparing STAG and NESSAN III results for a hollow rod fuel pin with axi-symmetric temperature distribution, the temperature routine TEMPR written for Nessan III, was also incorporated in STAG. This did not involve too great an increase of computing time and storage as in this case the temperature calculation is one-dimensional. For testing STAG under conditions of temperature tilt, a subroutine was written which generates an arbitrary temperature distribution varying sinusoidally around the fuel pin.

5.3 Equivalent dose

The equivalent* dose distribution has to be calculated within the program or read in similarly.

The stresses in both types of fuel pin, the hollow rod and the teledial, have been calculated up to a maximum equivalent dose of 4×10^{21} n/cm^2 Ni-Dido. The stresses in the graphite block have been calculated up to an equivalent dose of 1×10^{21} n/cm^2 Ni-Dido.

---

*The production of damage in the graphite of a power reactor is determined largely by the burnup of the adjacent fuel, and by the neutron energy spectrum. Bell et al [37] proposed that allowance should be made for neutron spectrum variations by defining an 'equivalent dose'. The equivalent dose received by the graphite at a point X in a reactor lattice is defined as the burnup of the fuel in a Calder reactor which causes the same number of carbon atom displacements per unit volume of graphite at a standard position in a Calder reactor as occur at the point X. Currently, the equivalent dose is expressed in units megawat - day per adjacent tonne (MWD/Ate) or neutrons/cm^2 Ni-Dido. Bell et al give a conversion factor between these two units of 1000 MWD/Ate $\equiv 1 \times 10^{20}$ n/cm^2 Ni-Dido. In this thesis the terms neutron dose or dose are sometimes used instead of equivalent dose.

It has been assumed that the equivalent dose received by the graphite has a constant value over the cross-section of all graphite components analysed. With modification of the computer program it is however possible to take account of any equivalent dose variation across the fuel pin. The equivalent dose was calculated for each time interval and dose steps in the range 1×10^{20} n/cm^2 to 2×10^{20} n/cm^2 Ni-Dido were used in the calculations*. The dose step 2×10^{20} n/cm^2 was used in earlier Nessan III calculations of Dragon reactor fuel pin.

The calculation of equivalent dose for a Dragon reactor fuel pin has been performed by Reed [38] using Monte-Carlo method. Reed estimated that an equivalent dose of 15×10^{20} n/cm^2 Ni-Dido will correspond to approximately 300 days of fuel pin life in the Dragon reactor at power. In a commercial HTR, maximum integrated fast neutron doses of up to 25×10^{20} to 30×10^{20} n/cm^2 Ni-Dido are expected to be received by the graphite components during their life in the reactor (see Fig.4). Thus the stress calculations in this thesis, which are continued to a dose up to 40×10^{20} n/cm^2 Ni-Dido cover adequately the life of the graphite fuel pins in the reactor. The value 4×10^{21} n/cm^2 Ni-Dido has been chosen because the experimental data for graphite are known up to this equivalent dose. The stresses in the graphite block have been calculated up to lower dose 1×10^{21} n/cm^2 Ni-Dido and therefore only some characteristic results are presented (see Ch.6).

5.4 Graphite data

In this thesis the stresses in graphite components made from a pressed, near - isotropic Gilsocarbon graphite have been analysed. The physical properties and irradiation data for

---

*Since the equivalent dose is assumed to be constant over the cross-section of the fuel pin, we may use the term dose step in place of the time step.

Gilsocarbon graphites have been assembled by Everett and Manzel [39] . All Gilsocarbon graphite data used in this analysis have been taken from this reference.

5.4.1 Thermal conductivity

Data on the irradiation induced changes of the thermal conductivity of a Gilsocarbon graphite, are shown in Fig.14. To introduce these experimental data into the computations of stresses, polynomials were fitted to the data, using a least square curve fitting programme. Non-linear interpolation has been used to determine the values of thermal conductivity for intermediate dose values, as discused in Ch.5.5.

5.4.2 Fuel rating changes

For hollow rod fuel pins it was assumed that the heat rating falls by a factor* 2 during the time which coresponds to 40×10^{20} n/cm^2 Ni-Dido, corresponding to the lifetime of about 2.5 years in the Dragon reactor. For the teledial fuel pin and graphite block it was assumed that the fuel rating remains constant.

5.4.3 The coefficient of thermal expansion

The coefficient of thermal expansion (C.T.E.) of graphite changes with temperature and with neutron dose. The variation of C.T.E with neutron dose for isotropic Gilsocarbon graphite has been given by Everett and Graham [25] . The C.T.E initially increases with dose reaches a maximum value about 14 % higher than the unirradiated value then falls approximately to the initial value. Since the changes of C.T.E with dose are small and transient they have been neglected and the data for the unirradiated graphite used throughout the analysis. The temperature

---

*This information was originally provided by Dragon Project [40] and was used in the analysis of hollow rod fuel pins to examine the influence of fuel rating changes on the strain/stress history

Fig.14
PRESSED GILSOCARBON GRAPHITE.
IRRADIATION INDUCED CHANGES OF
THERMAL CONDUCTIVITY.

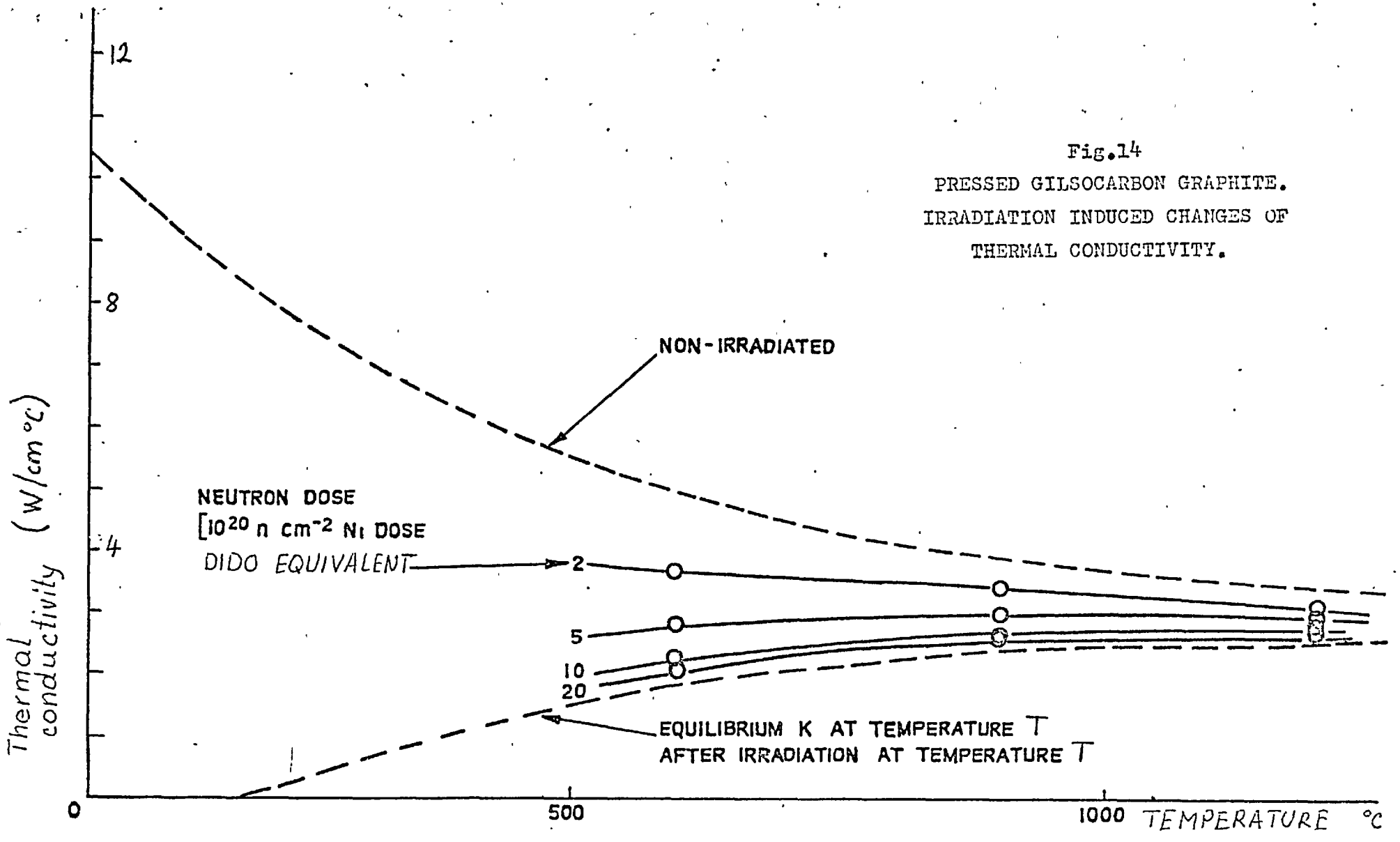

dependence of C.T.E has been taken into account by fitting straight lines to the experimental data for unirradiated graphite. The following expressions were used:

Longitudinal direction:

$$\alpha_{\parallel} = 6.15 \cdot 10^{-6} + 1.92 \cdot 10^{-9} (T - 500)^{\circ}C$$

Transverse direction:

$$\alpha_{\perp} = 6.0 \cdot 10^{-6} + 1.5 \cdot 10^{-9} (T - 500)^{\circ}C$$

5.4.4 Dimensional changes

The dimensional changes are shown graphically in Fig.15 and 16. The Gilsocarbon graphite behaviour is slightly anisotropic but the pattern of dimensional changes in the transverse and longitudinal direction is similar. Polynomials have been fitted to the data and non-linear interpolation used to termine the Wigner strains for intermediate temperatures. as discused in Ch.5.5.

5.4.5 Creep Data

A summary of irradiation creep data for different graphites, including Gilsocarbon graphite, is given in Fig.17. In this analysis, a linear variation of creep constant with temperature was assumed. The lower of the two lines Fig.17 was used, so tending to underestimate the creep and overestimate operating stresses. All information about irradiation creep has been obtained from uniaxial tests. The choice of a three-dimensional creep law for use in the analyses is discussed in detail in Ch.3 and App.I.

5.4.6 Elastic constants and strength of material

Young s modulus of graphite is increased by neutron irradiation. Data given by Everett and Manzel show a rapid initial increase

(Fig.18), the modulus change then temporarily saturating at a value which depends on the irradiation temperature.

The values of Young's modulus saturate at equivalent doses between 2 and 6×10^{20} n/cm^2 Ni-Dido. Further substantial changes occur for higher doses at temperatures between 900°C and 1200°C.

In this analysis constant values of Young's modulus were used for hollow rod fuel pins and graphite block, equal to the irradiated values, taking some account of the irradiation temperature.

For the hollow rod fuel pin and the graphite block for which the temperature are lying in the ranges 750-800°C and 675-725°C respectively only one value has been used in the analysis in each case since in these temperatures ranges Young's modulus changes little after reaching the saturated value.

The value used in the analysis of hollow rod fuel pin was:

$$E = E_{unirrad.} + 38\% = 1.189 \times 10^6 N/cm^2$$

and for graphite block:

$$E = E_{unirrad.} + 44\% = 1.241 \times 10^6 N/cm^2$$

Most of the teledial temperatures are above 900°C and in this region the Young's modulus changes substantially with equivalent dose not only initially, but also later in life time (see Fig.18). The changes of Young's modulus used in analysis with respect to dose and temperature have therefore been considered in a exact step-wise way.

Thus, the values of Young's modulus follow closely the 900°C and 1200°C curves interpolating later linearly between the curves for the high equivalent dose.

Value of Poissons ration 0.18 was used in all calculations.

Table II gives the approximate strength of unirradiated pressed Gilsocarbon graphite over the temperature range of interest (600-1200°C).

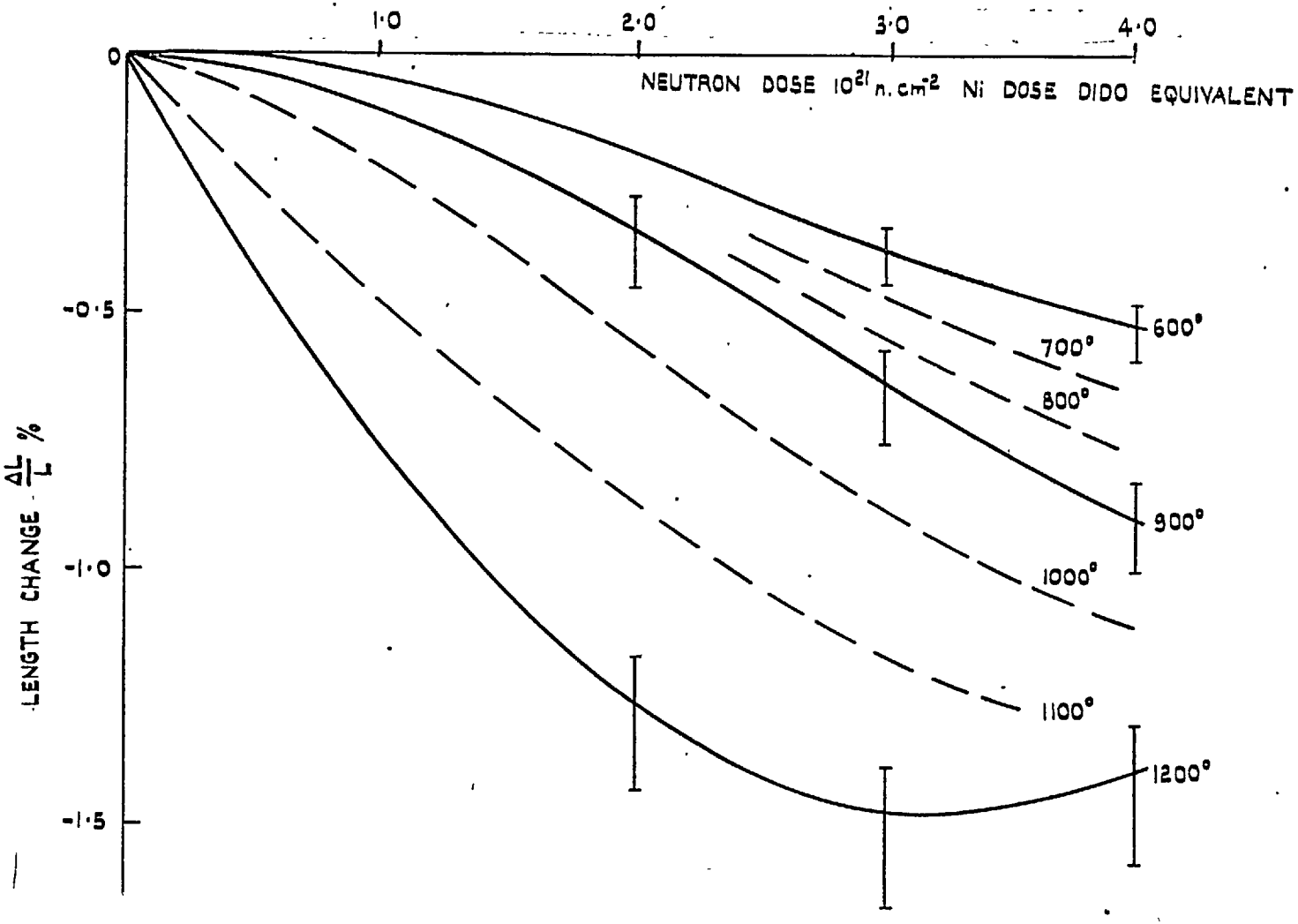

Fig.15

PRESSED GILSOCARBON GRAPHITE.
IRRADIATION INDUCED DIMENSIONAL
CHANGES, TRANSVERSE DIRECTION.

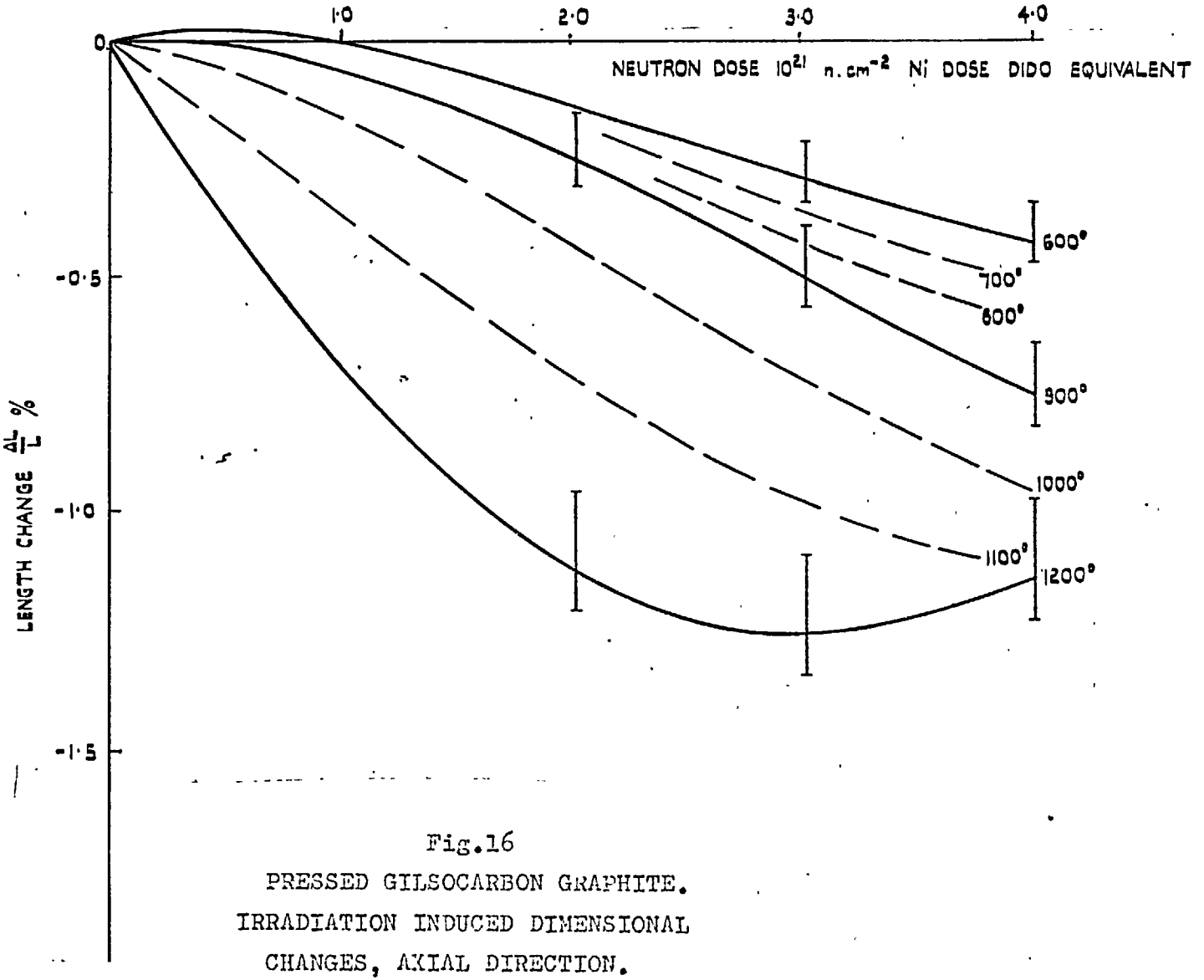

Fig.16

PRESSED GILSOCARBON GRAPHITE.
IRRADIATION INDUCED DIMENSIONAL
CHANGES, AXIAL DIRECTION.

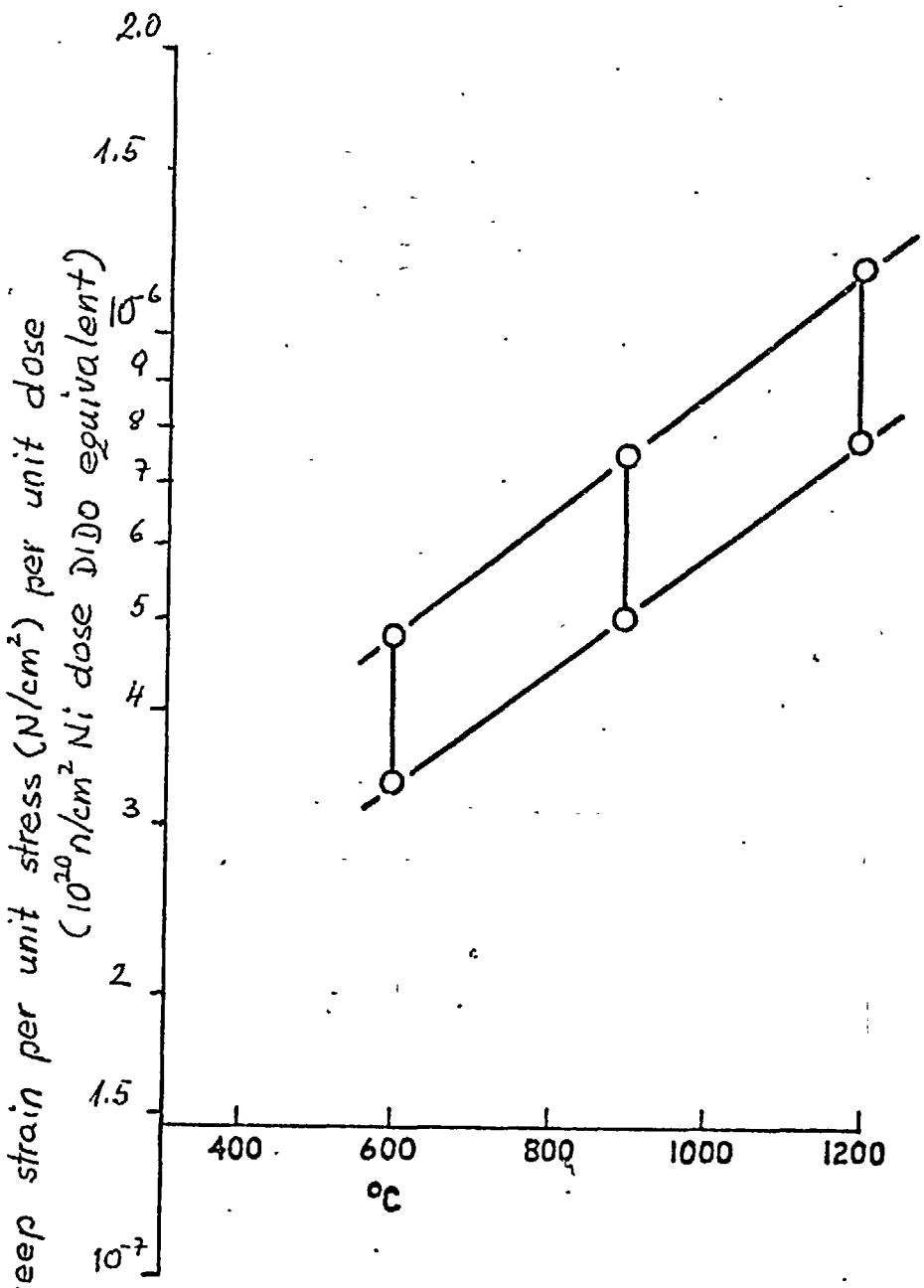

Fig.17

VARIATION OF CREEP COEFFICIENT WITH TEMPERATURE (RESULTS OF MEASUREMENTS ON SEVERAL TYPES OF GRAPHITE)

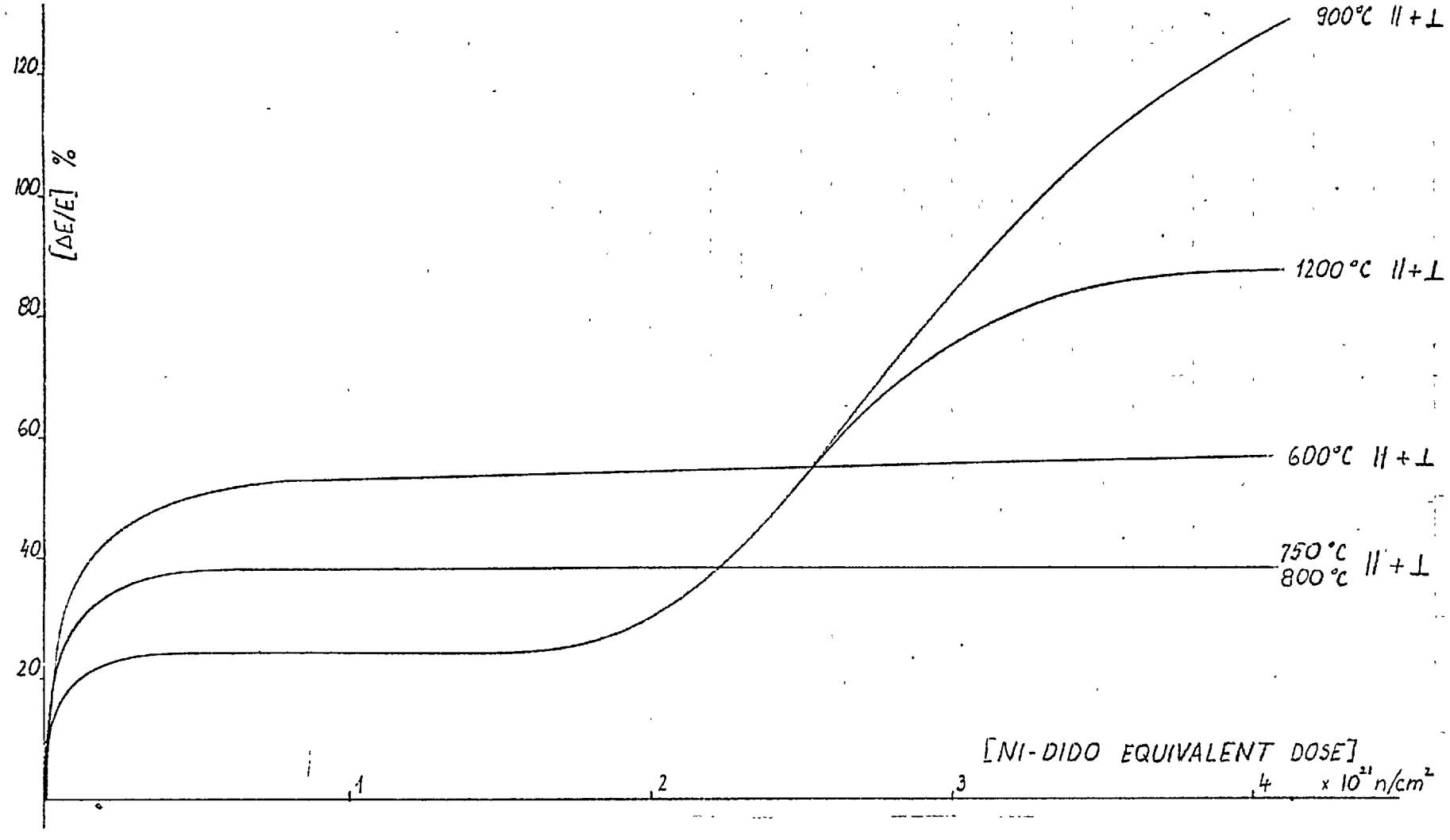

Fig.18

PRESSED GILSOCARBON GRAPHITE.

IRRADIATION INDUCED CHANGES OF YOUNG'S MODULUS.

TABLE II

Strength of unirradiated pressed isotropic Gilsocarbon graphite in temperature range 600-1200°C

Direction	Tensile Strength N/cm^2	Compressive Strength N/cm^2
Longitudinal	1,200	6,100
Transverse	1,400	6,100

5.5 The input of data and interpolation techniques

Thermal conductivity, dimensional change, thermal expansion, creep rate and Young's modulus data are all functions of current temperature and irradiation dose (Fig.14,15,16,17,18). In most cases the equations which describe this dependence can be simplified by use of linear interpolation without decreasing the accuracy but this is not so for changes of thermal conductivity and Wigner strains.

It can be seen from Fig.14 and Fig's 15, 16 that the thermal conductivity and Wigner strains change non-linearly over a wide range of temperature and irradiation doses. A standard procedure to obtain the values for an arbitray temperature and dose by interpolating linearly between different temperatures and doses (this procedure is refered sometimes as double linear interpolation) will clearly oversimplify the changes of the corresponding variable. If for example the equivalent dose at a point in the graphite component increases from a value just below 5×10^{20} to a value just above 5×10^{20} n/cm^2 Ni-Dido and the temperature remains the same 500°C, reference to Fig. 14 shows that linear interpolation implies a discontinuity in change of thermal conductivity. This is certainly an unrealistic

representation of the physical behaviour of the graphite and has an effect on the accuracy of results. The same conclusions apply for dimensional changes.

In this analysis polynomials were fitted to the data by the method of least squares. It was found that second order polynomials adequately fitted the experimental curves for thermal conductivity (Fig.14) and third order polynomials the experimental curves for dimensional changes (Fig.15,16). Between the polynomials the values have been interpolated nonlinearly using Newton forwards and Newtons backward's difference formulas (equations are given by Conte [41]) of the second order for thermal conductivity changes and of the third order for dimensional changes, both with constant step.

It is thought that the use of polynomials and nonlinear interpolation represents better the temperature and dose dependence of thermal conductivity and dimensional changes than linear interpolation. The analyses have indicated for example that the use of linear interpolation for dimensional changes can cause the stresses to be as much as 10% - 30% different from nonlinear interpolation for certain graphites. Further, if more data are available, nonlinear interpolation can be improved also by the use of higher order difference formulas.

In using nonlinear finite difference interpolation, it is necessary that the temperature and dose steps between the polynomials are constant. If the temperature or dose step are not constant other approaches have to be used such as Newtons divided difference interpolation (see for example Noble [42]).

6. RESULTS

6.1 Review of analysis

The first step in checking the finite element program (STAG) for graphite core components was to compare the results of the finite element stress analysis with earlier results calculated by Nessan III program for Dragon fuel tubes with symmetrical temperature and equivalent dose distribution. After results obtained from STAG showed a resonable agreement with the Nessan III results the comparison between results of the iterative and direct versions of STAG was made. The iterative version of STAG has been chosen for use in further analysis, since it was faster for the same accuracy and considered more suitable. Further comparative analyses of a Dragon tube with symmetrical loading have been performed examining the influence of mesh size, mesh pattern, element shape and different time steps on the results. After initial comparative studies the stress analysis of three particular more complex graphite components has been attempted: a hollow rod fuel pin under temperature tilt, a teledial fuel pin, and a multichannel graphite block.

In all analyses the equivalent neutron flux was assumed to be uniform over the cross-section of graphite components (Ch.5.3). If not stated otherwise on the graphs, equal dose increments of 1×10^{20} Ni-Dido were used. All analyses except that of graphite block (calculated to a dose 10×20^{20} n/cm^2 Ni-Dido) were continued to a Dido equivalent Ni-dose of 40×10^{20} n/cm^2.

6.2 Analyses of hollow rod fuel pin

6.2.1 Comparative analysis of hollow rod with symmetrical temperature and equivalent dose distribution

The hollow rod fuel pin with a symmetric temperature distribution and a constant equivalent dose across the tube

has been analysed in some detail using a step-by-step method of solution with computer program Nessan III and the results show a reasonable agreement with experimental values obtained by the Dragon Project (see Jezernik & Head [4,5]). The Nessan III results have therefore been considered as the starting point for the present work.

The stress analysis has been performed for half of the graphite tube using two different mesh sizes (Fig.9, Fig.10). A half of the hollow rod fuel pin was analysed instead of a narrow segment to study the influence of mesh pattern on the results as discused later. It is assumed that at the cross-sections at both ends of half ring, the nodal points on y axis are free to move in the y direction but restrained from moving in the x-direction. The mesh data have been calculated by the subroutine MESHR (Ch.5.1). The temperature at nodal points for both mesh sizes have been calculated using the subroutine TEMPR as explained in Ch.5.2 but considering a maximum of only 7 points across the tube wall in comparison with 10-point calculation in Nessan III. The difference between these temperature distributions can be regarded as negligible. The element temperatures have been calculated by averaging the node temperatures. It has been assumed that the temperature distribution changes with time due to fuel burnup and thermal conductivity change as discussed in Ch.5.2 and Ch.5.4. The initial and maximum temperature distribution through the fuel tube is given in Fig.19. The final temperature distribution is almost identical with initial temperature distribution.

In Fig.20 the minimum in-plane principal stress for element 10 and a coarse mesh* is compared using the direct and iterative codes (and some earlier values of elastic constants for Gilsographite). The results are in good agreement but the iterative version uses about 2.5 times less computer time. In both calculations the stiffness matrix for the whole structure has been

---

*In further analyses of the hollow rod fuel pin (Fig.20 to Fig.31) a fine mesh (Fig.10) is always used if not stated otherwise on the graph.

formed at each time step simulating the general case that the temperature and equivalent dose distribution of a graphite component changes continuously with time and therefore the elastic constants change with time also. It is in this case that the iterative method shows a relative advantage over direct approach but in addition less work is necessary to prepare the input data for the iterative program.

The accuracy of results is influenced by the magnitude of the element but the overall trend of stress changes/time remains similar (see Fig.21). In the calculations with a large number of elements the increased influence of rounding off errors was noticable and it appears that the accuracy could be improved by use of double precision for stiffness matrices. The shape of triangles with length/depth ratio close to 1:1 was found to give more accurate results than of those with ratios 3:1 or more. A mesh pattern of the type shown in Fig.9 and 10 where a number of symmetry lines can be drawn gave better results than a less symmetric mesh as indicated in Fig.9 by doted lines.

A large dose step causes slight oscillations in the plot of stresses against time since the creep strain increments are in turn over-estimated and under-estimated as shown in Fig.22. The oscillations are particularly marked if the stresses change rapidly with time.

A chosen set of STAG results for fine mesh and short dose step has been compared with Nessan III results in Fig.23,24 and 25. The results are in good agreement particularly the hoop and axial stresses. It will be noted that the hoop stress as calculated by STAG passes through zero slightly earlier and finally reaches slightly lower levels than the stresses calculated by Nessan III. The small difference initially is probably due to omission of the creep iteration process in the finite element analysis. In the step by step calculation the stresses from the previous time interval are always used in the calculation of the current creep strain increment and this in turn causes a slight overestimation of the creep strain increments when the

stress is rapidly reducing initially, hence the mentioned faster decrease of stress. Slightly lower values of stresses later in the lifetime (when the stress/time remains approximately constant) of the fuel pin are probably due to other reasons. The STAG residual stresses are slightly higher than Nessan III hoop stresses. The radial stresses calculated by STAG are higher than those estimated by Nessan III probably due to finite element idealization. The changes of axial stress/time compare with Nessan III. results slightly better than the changes of hoop stress/time.

6.2.2 Analysis of hollow rod under temperature tilt

The next analysis is related to a hollow rod fuel pin under temperature tilt as shown in Fig.26 and prevented from bowing. The principal stresses across the fuel tube for cross-sections C_1-C_1 and C_2-C_2 are plotted in Fig.27 for time zero. The overall shape of the variation of stress/radius is similar to that for the symmetric case but in addition axial stresses are all compressive on the hot side and tensile on the cooler side. With irradiation the stress distribution across the fuel tube is reversed as given in Fig.28 which relates to time int.35 (3.4×10^{21} N/cm^2 Ni-Dido). Cooling down of the reactor causes the stresses to rise since the thermal expansion effect, which opposes the dimensional change effect, vanishes. As a result, the residual stresses are always of the form of distribution shown in Fig.29, Figs.30 and 31 illustrate the variation with time of two of the principal stresses for two typical elements one at inner boundary of the tube and one at outer boundary (el.25 and 408).

6.2.3 Discussion of results

As shown in Figs.19 to Fig.31, good results can be obtained using constant stress triangular elements providing that sufficient are used. The results obtained by STAG compare favourably with the Nessan III. results (Ch.6.2.1).

In a hollow graphite tube under temperature tilt and restricted from bowing, the operating axial stresses are very high at the beginning of tube-life but decrease rapidly due to irradiation creep and differential dimensional changes. A shut down of the reactor will however cause the stresses to rise to high values with the possibility of failure. In reality the graphite tubes will be only partially restricted from bowing and therefore the axial stresses (operating and residual) will have lower values than those calculated. The amount of bowing depends on the clearance between the tube and channel and the amount of bowing of the multichannel graphite block. It is expected that the equivalent dose tilt will have similar effects on the stress pattern in the hollow tube as the temperature tilt.

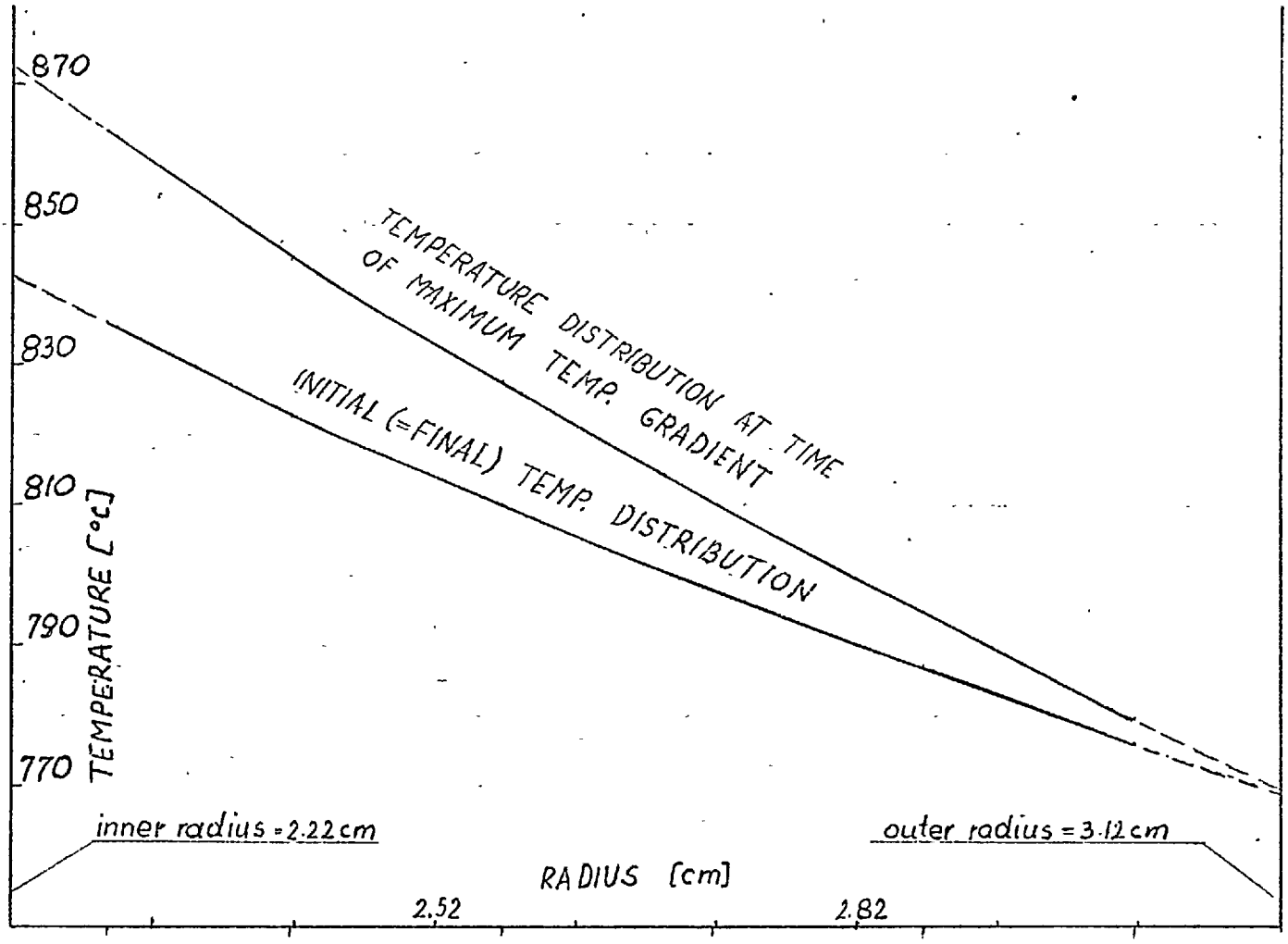

Fig.19

HOLLOW ROD FUEL PIN.

TUBE-WALL TEMPERATURE DISTRIBUTION AT A POINT CORRESPONDING TO 80 CM ABOVE CORE BASE PLANE IN THE DRAGON REACTOR.

(Constant temperature at outer radius = 769.4°C)

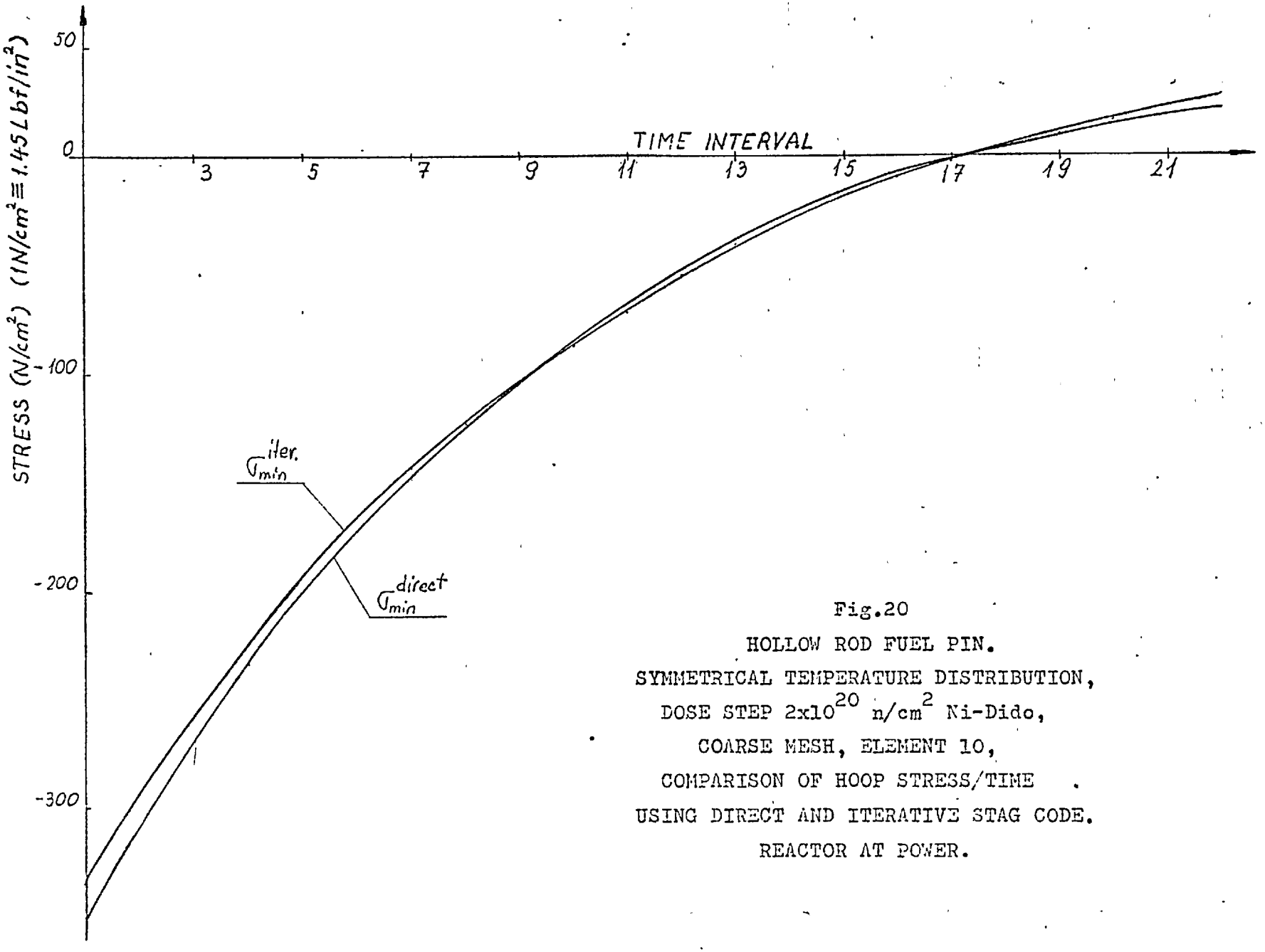

Fig.20

HOLLOW ROD FUEL PIN.
SYMMETRICAL TEMPERATURE DISTRIBUTION,
DOSE STEP 2×10^{20} n/cm^2 Ni-Dido,
COARSE MESH, ELEMENT 10,
COMPARISON OF HOOP STRESS/TIME .
USING DIRECT AND ITERATIVE STAG CODE.
REACTOR AT POWER.

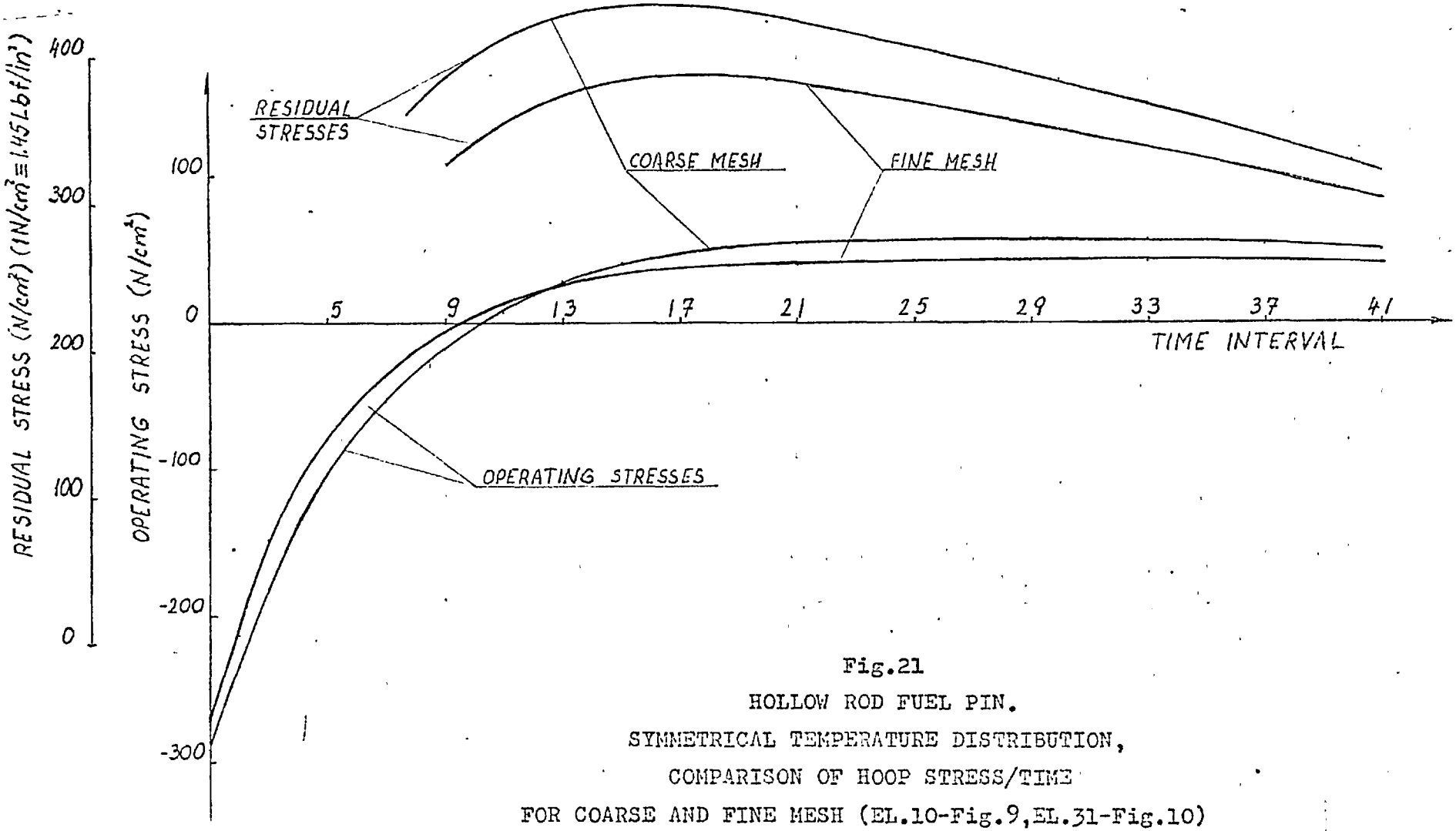

Fig.21

HOLLOW ROD FUEL PIN.

SYMMETRICAL TEMPERATURE DISTRIBUTION,

COMPARISON OF HOOP STRESS/TIME

FOR COARSE AND FINE MESH (EL.10-Fig.9, EL.31-Fig.10)

REACTOR AT POWER AND SHUT DOWN.

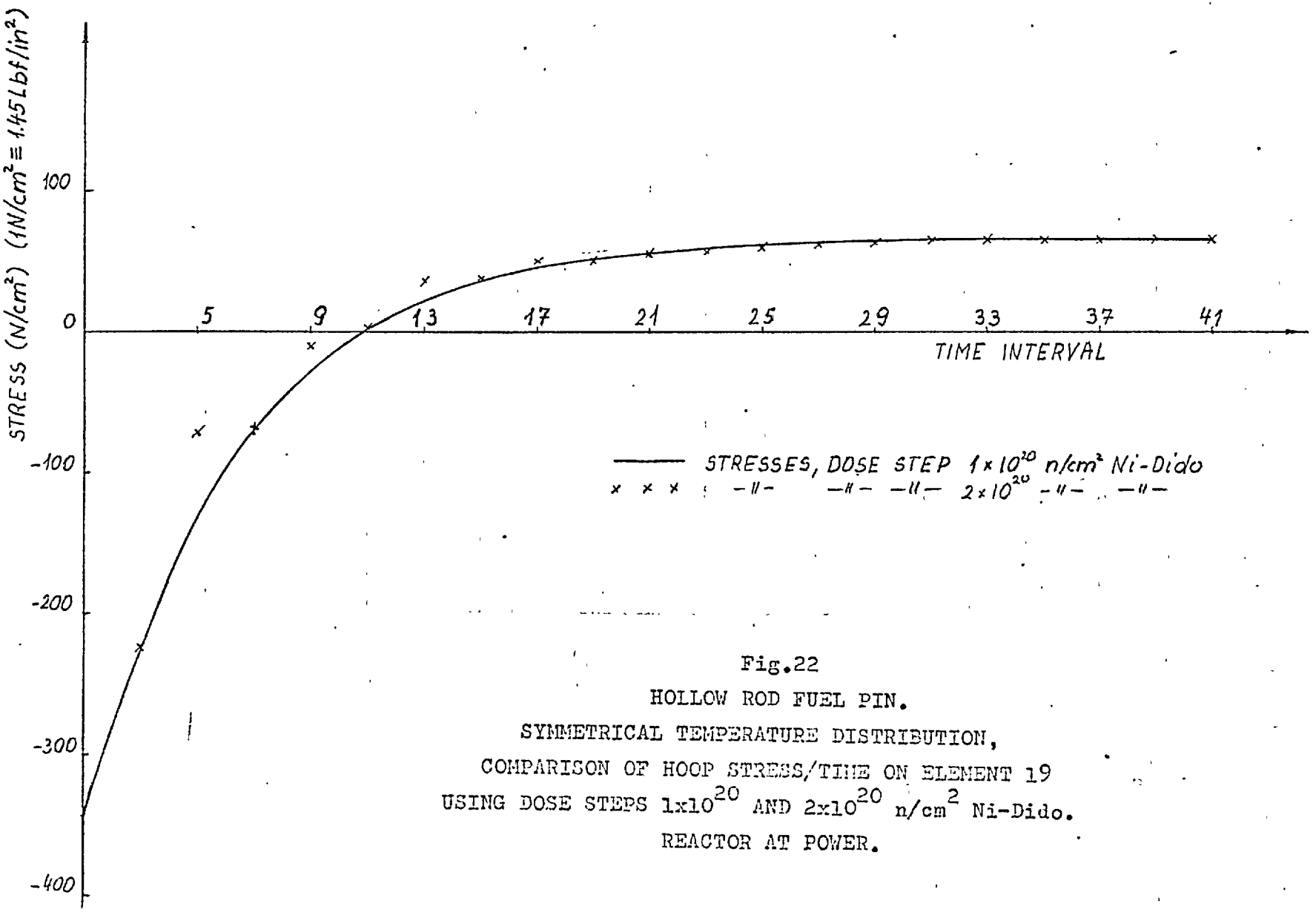

Fig.22

HOLLOW ROD FUEL PIN.

SYMMETRICAL TEMPERATURE DISTRIBUTION,

COMPARISON OF HOOP STRESS/TIME ON ELEMENT 19

USING DOSE STEPS 1×10^{20} AND 2×10^{20} n/cm^2 Ni-Dido.

REACTOR AT POWER.

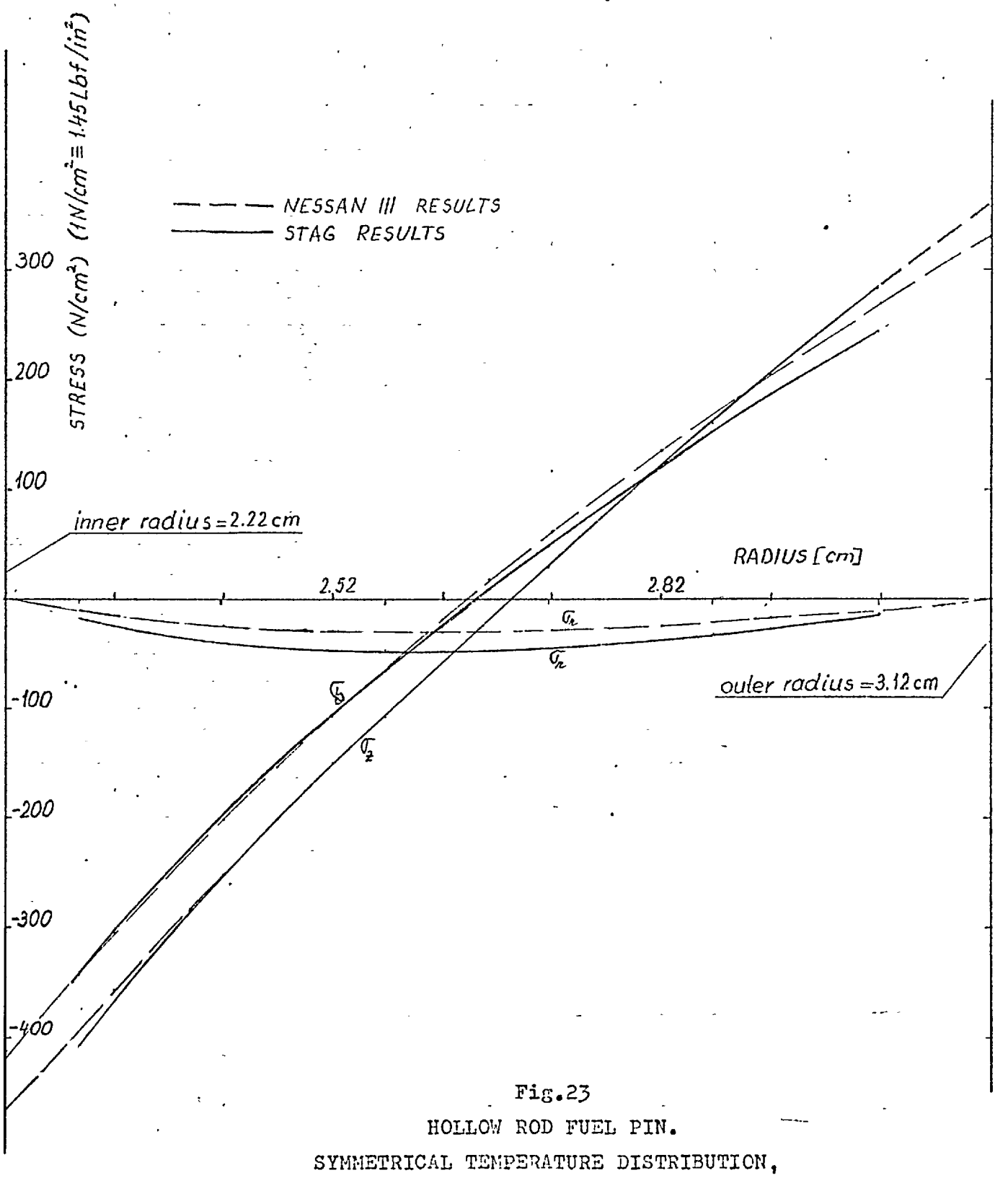

Fig.23

HOLLOW ROD FUEL PIN.

SYMMETRICAL TEMPERATURE DISTRIBUTION,

COMPARISON OF PRINCIPAL STRESSES ACROSS THE FUEL PIN

BETWEEN STAG (CROSS-SECTION C_1-C_1, see Fig.10)

AND NESSAN III CODE.

TIME ZERO.

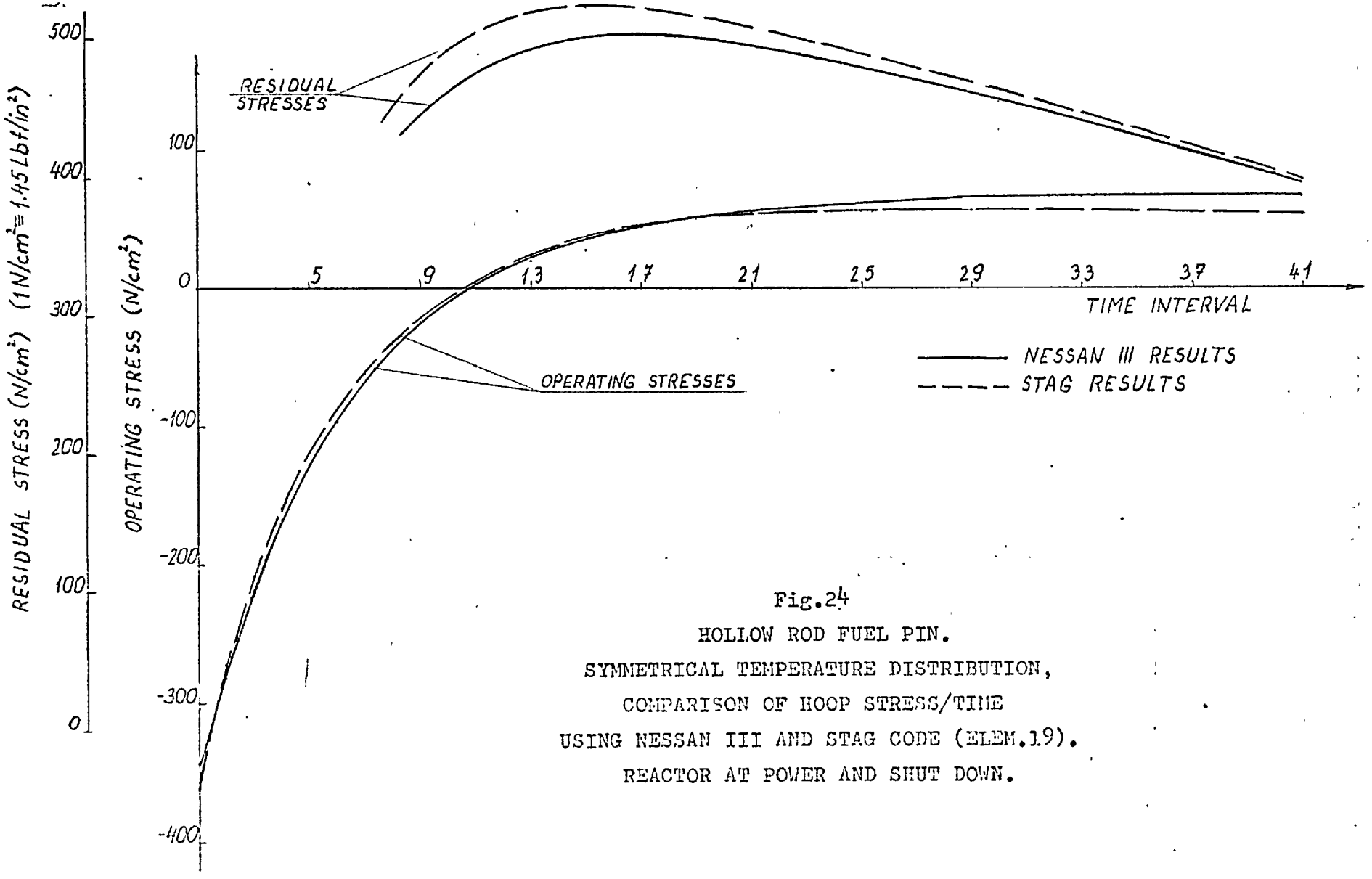

Fig.24

HOLLOW ROD FUEL PIN.

SYMMETRICAL TEMPERATURE DISTRIBUTION,

COMPARISON OF HOOP STRESS/TIME

USING NESSAN III AND STAG CODE (ELEM.19).

REACTOR AT POWER AND SHUT DOWN.

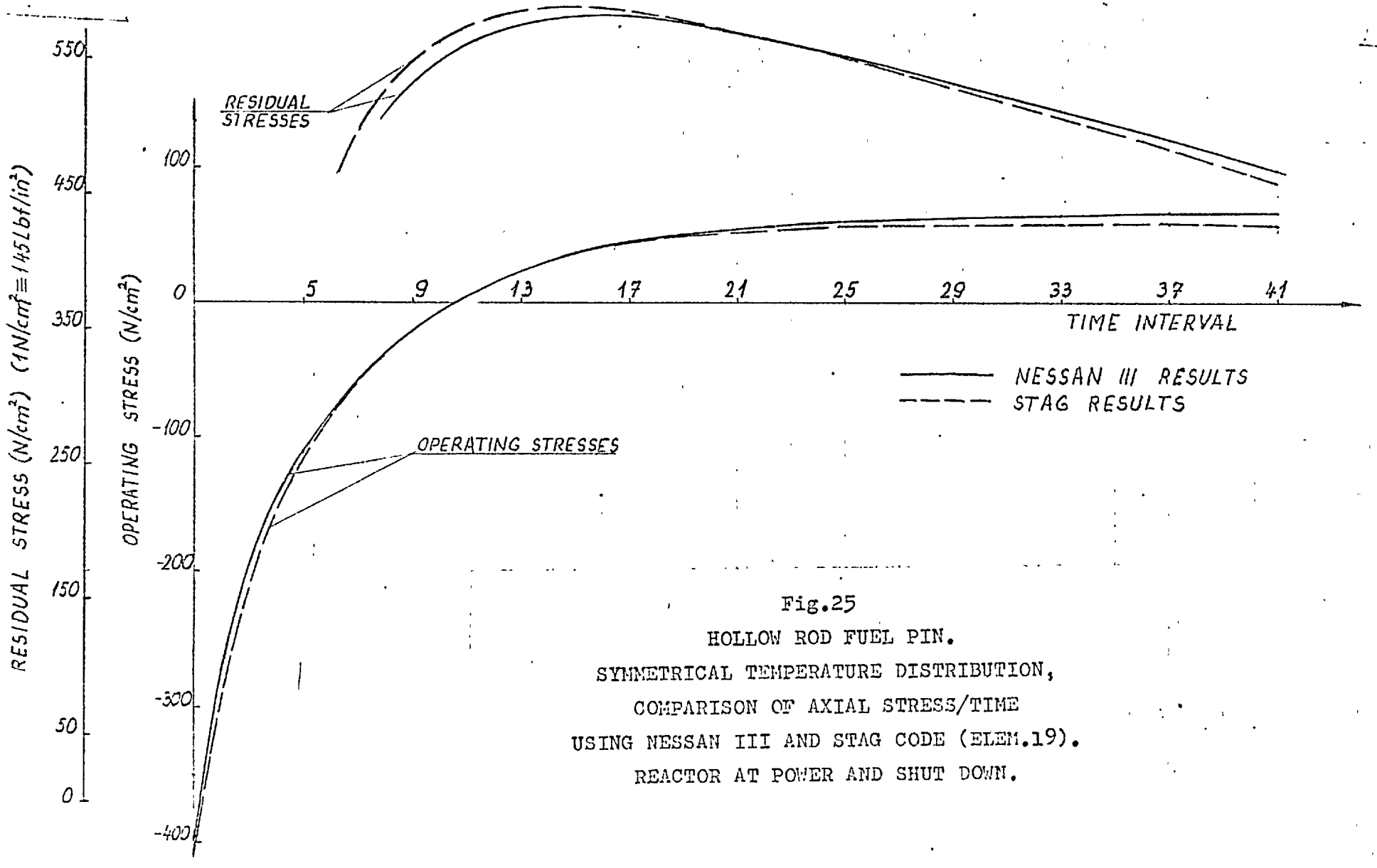

Fig.25

HOLLOW ROD FUEL PIN.

SYMMETRICAL TEMPERATURE DISTRIBUTION,

COMPARISON OF AXIAL STRESS/TIME

USING NESSAN III AND STAG CODE (ELEM.19).

REACTOR AT POWER AND SHUT DOWN.

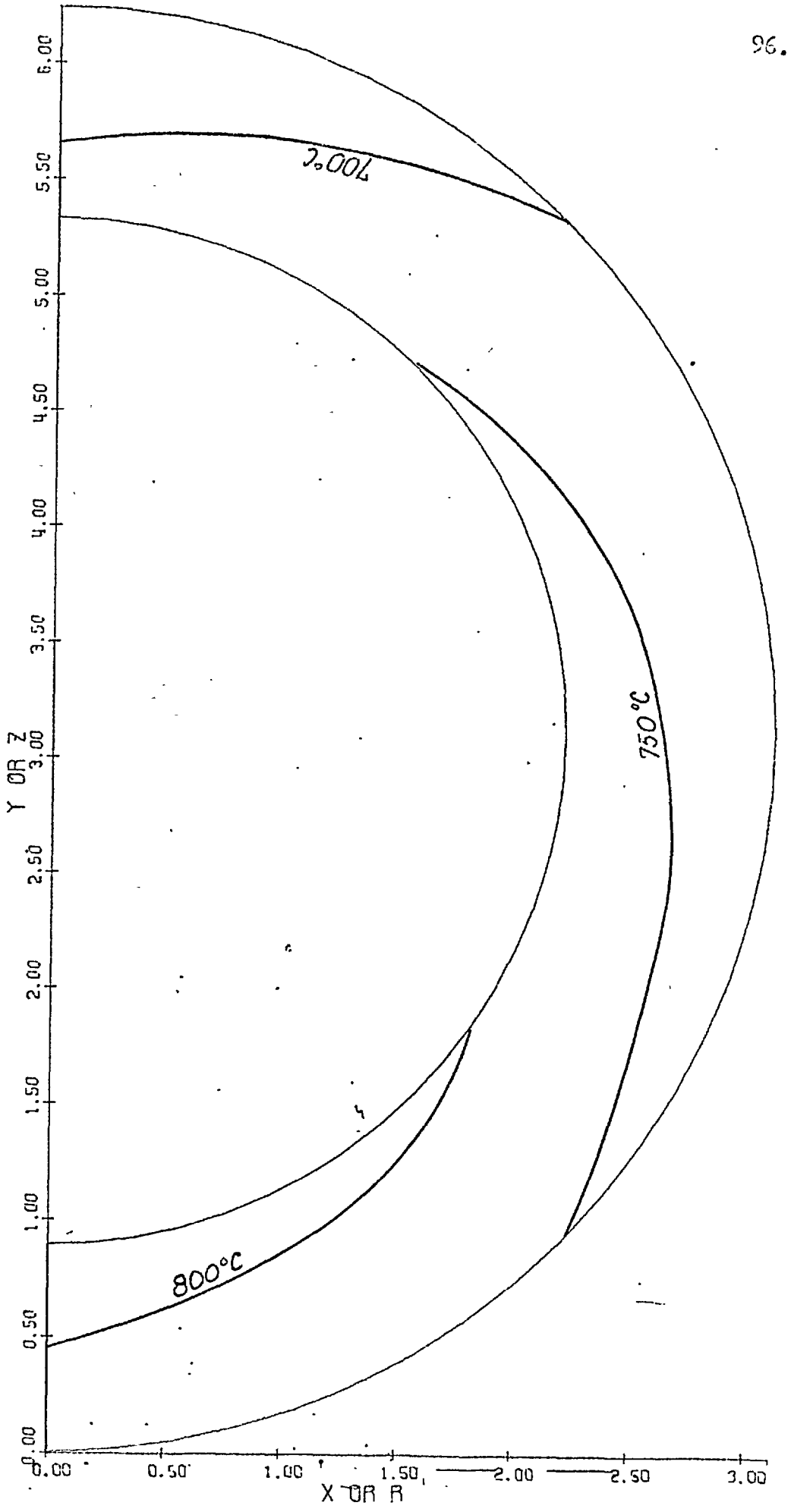

Fig.26

HOLLOW ROD FUEL PIN.

CONTOURS OF THE INITIAL NON-SYMMETRICAL TEMPERATURE DISTRIBUTION.

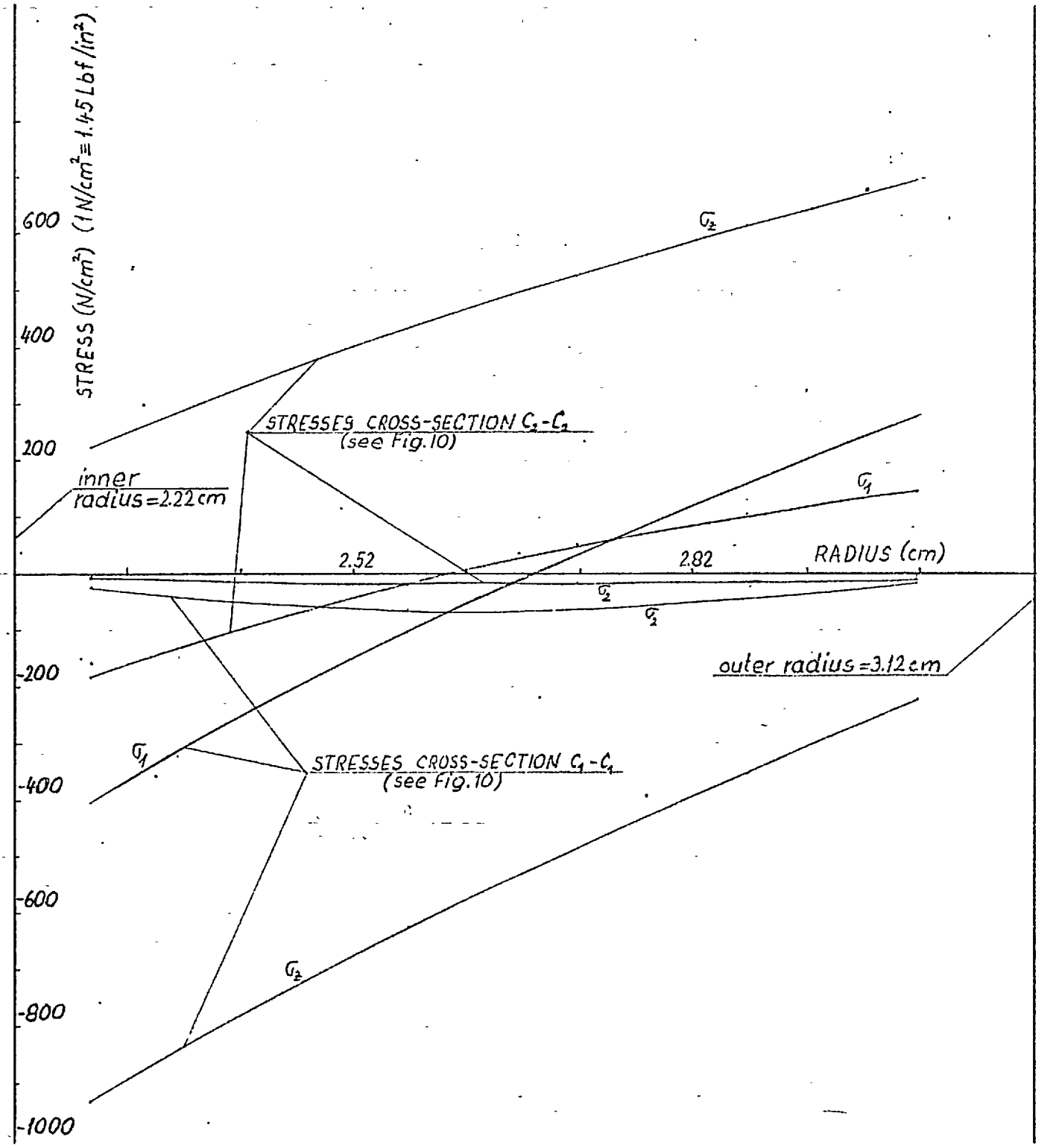

Fig.27

HOLLOW ROD FUEL PIN.

NON-SYMMETRICAL TEMPERATURE DISTRIBUTION,

PRINCIPAL OPERATING STRESSES

FOR CROSS-SECTIONS C_1-C_1 AND C_2-C_2 (see Fig.10).

TIME ZERO.

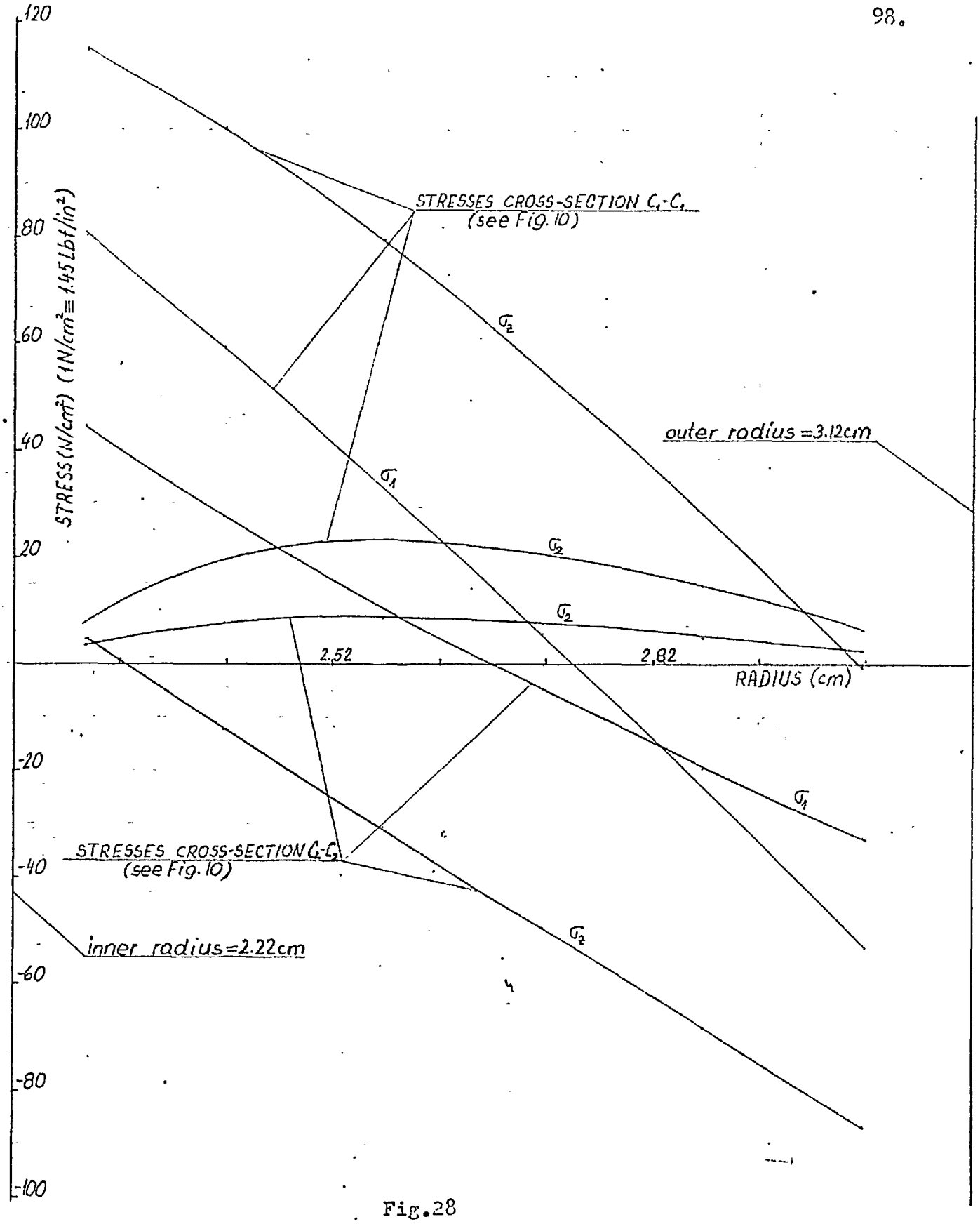

Fig.28

HOLLOW ROD FUEL PIN.

NON-SYMMETRICAL TEMPERATURE DISTRIBUTION,

PRINCIPAL STRESSES

FOR CROSS-SECTIONS C_1-C_1 AND C_2-C_2 (see Fig.10).

TIME INTERVAL 35 ($=34\times10^{20}$ n/cm^2 Ni-Dido).

REACTOR AT POWER.

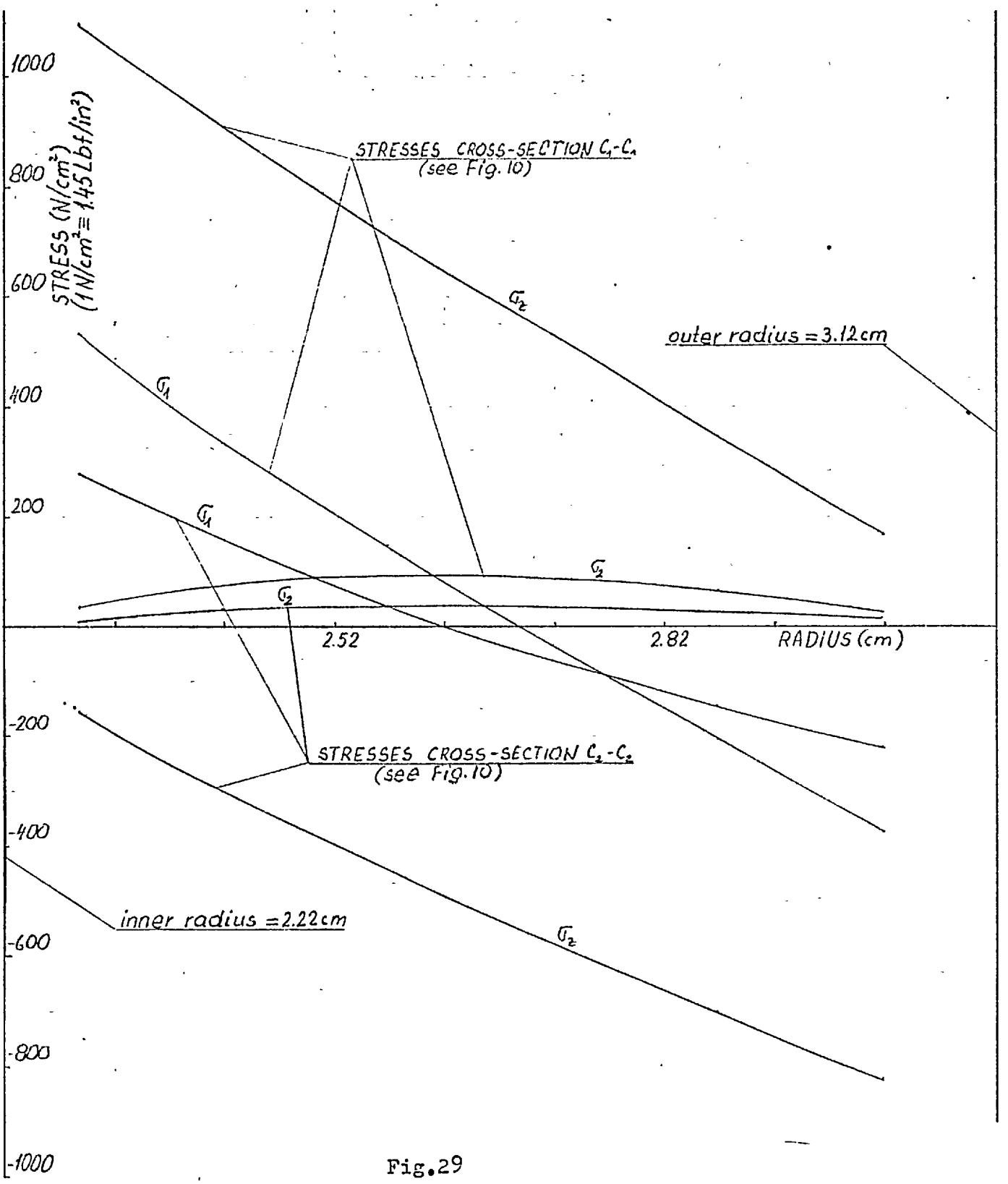

Fig.29

HOLLOW ROD FUEL PIN.

NON-SYMMETRICAL TEMPERATURE DISTRIBUTION,

PRINCIPAL STRESSES

FOR CROSS-SECTIONS C_1-C_1 AND C_2-C_2 (see Fig.10).

TIME INTERVAL 30 (=29×10^{20} n/cm^2 Ni-Dido).

REACTOR SHUT DOWN.

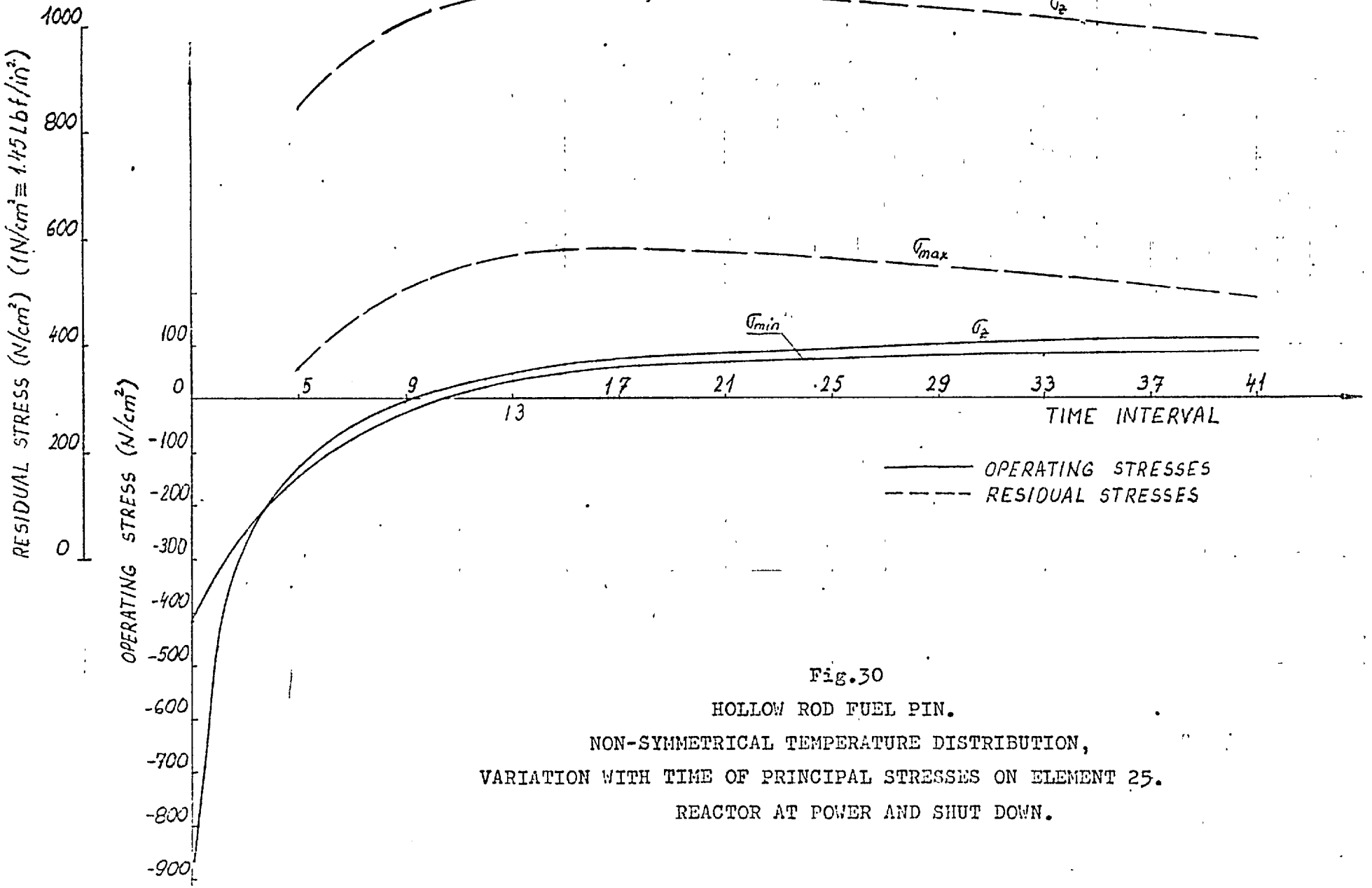

Fig.30

HOLLOW ROD FUEL PIN.

NON-SYMMETRICAL TEMPERATURE DISTRIBUTION,

VARIATION WITH TIME OF PRINCIPAL STRESSES ON ELEMENT 25.

REACTOR AT POWER AND SHUT DOWN.

Fig.31

HOLLOW ROD FUEL PIN.

NON-SYMMETRICAL TEMPERATURE DISTRIBUTION,

VARIATION WITH TIME OF PRINCIPAL STRESSES ON ELEMENT 408.

REACTOR AT POWER AND SHUT DOWN.

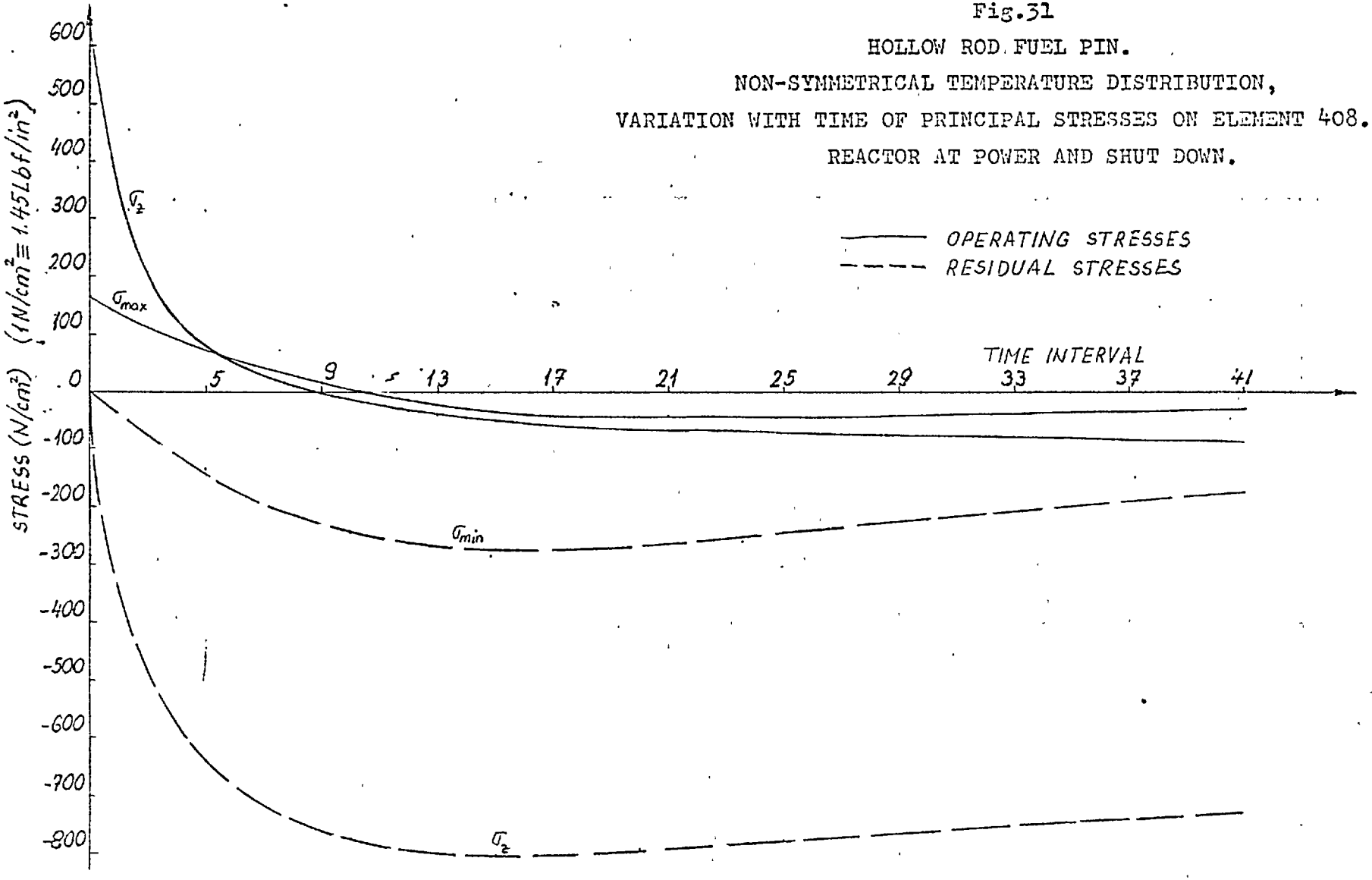

6.3 Analysis of teledial fuel pin

6.3.1 Basic data and results

Fig.9 shows a sector of the teledial fuel pin, bounded by planes of symmetry and the mesh used in the analysis. The assumed temperature distribution, shown in Fig.32 was provided by Kinkead [36] and corresponds to the time in the life of the fuel pin when the maximum fuel temperature occurs (see Ch.5.2).

The initial (thermal) stresses are shown in Figs.33, 34 and 35, Figs. 36, 37, 38 and 39 show the distribution of operational and residual principal stress in four most highly stressed regions of the fuel pin (as indicated in Fig.11) at several times in the life of the fuel pin. The region with highest stresses in axial direction is in the rib but the other two principal stresses there have low values. Figs. 40,41,42 and 43 show the variation with time of the stresses in highly stressed elements of the fuel pin crossection. These graphs again show the stresses on these elements with fuel pin at the operating temperature and also residual stresses assuming that the fuel pin is allowed to cool to a uniform temperature.

6.3.2 Discussion of results

As Fig.32 shows, the highest graphite temperature occurs in the ligaments between the fuel holes. With the particular boundary conditions used in the thermal analysis, the region inside the fuel hole pitch circle is generally hotter than the outer region. The lowest graphite temperature occurs in the rib, which locates the fuel pin in the channel. The high temperature in the ligaments causes a moderately high compressive radial stress initially in these regions (see Fig.34). The high temperature generally, inside the fuel hole pitch circle and lower temepratures in outer regions of fuel pin, cause in the x-y plane, compressive stresses in inner regions and tensile stresses in outer regions.

The compressive stresses in the inner region are concentrated around the inner edge of fuel hole (see Fig.34). It is in this region (el.488) that the highest stress in x-y plane occurs. Outside the fuel hole pitch circle, the tensile stresses in xy plane have moderate values (Fig.33) with a concentration in the corner of the rib. (The mesh used is too coarse to give a true indication of the peak stress). As shown in Fig.35, the highest axial stresses occur in the rib.

Figs.36, 38 and 40, 42 show the way the principal stresses vary with time in inner and outer regions. In the plane x-y the high compressive stresses developed around the inner edge of fuel hole and the more moderate tensile stresses in outer regions reduce rapidly in magnitude due to the combined effects of creep and a differential irradiation shrinkage of the graphite (the shrinkage rate generally increases with increasing temperature). It is apparent that towards the end of the life of the fuel pin, the stresses in these regions change sign and a form of reversed stress distribution is established.
If the reactor is shut-down, the stresses increase and high residual stresses of the reversed pattern are established*,

---

* A routine has been written to calculate elastic stress (the pin is assumed to be at a uniform temperature) due to internal pressure in the fuel hole of the teledial sector. By considering the elastic stresses in plane (xy) due to pressure and residual stresses after irradiation of the pin in the reactor and comparing the combined stresses with ultimate tensile strength (UTS) of the material, the pressure in the fuel hole can be calculated required to break an irradiated pin. Alternatively the pressure required to break a teledial fuel pin after irradiation in the reactor can be determined also experimentally. If the experimental and calculated values obtained for the required breaking pressure are compared some conclusions can be reached about the magnitude of maximum stress levels in a teledial pin after irradiation in the reactor. Stresses in a teledial sector at a uniform temperature of 20°C with internal pressure 1 bar (=10 N/cm^2) were calculated for the Dragon Project (where they intend to perform the experiment) but results are not given here.

an effect observed in the results of the analysis of the hollow rod fuel pin.

Figs, 37,39 and 41 show the pattern of changes of principal stresses in the ligament regions. It is possible to notice a similar rapid decrease with time in the magnitude of the stresses and the formation of a reverse stress pattern later in life of fuel pin. Again high residual stresses of a reversed pattern are developed if the reactor is shut down.

Fig.43 shows the variation of axial stress for el.4 in the rib. Very high residual axial compressive stresses develop if reactor is shut down.

Fig.32
TELEDIAL FUEL PIN.
TEMPERATURE DISTRIBUTION (°C)

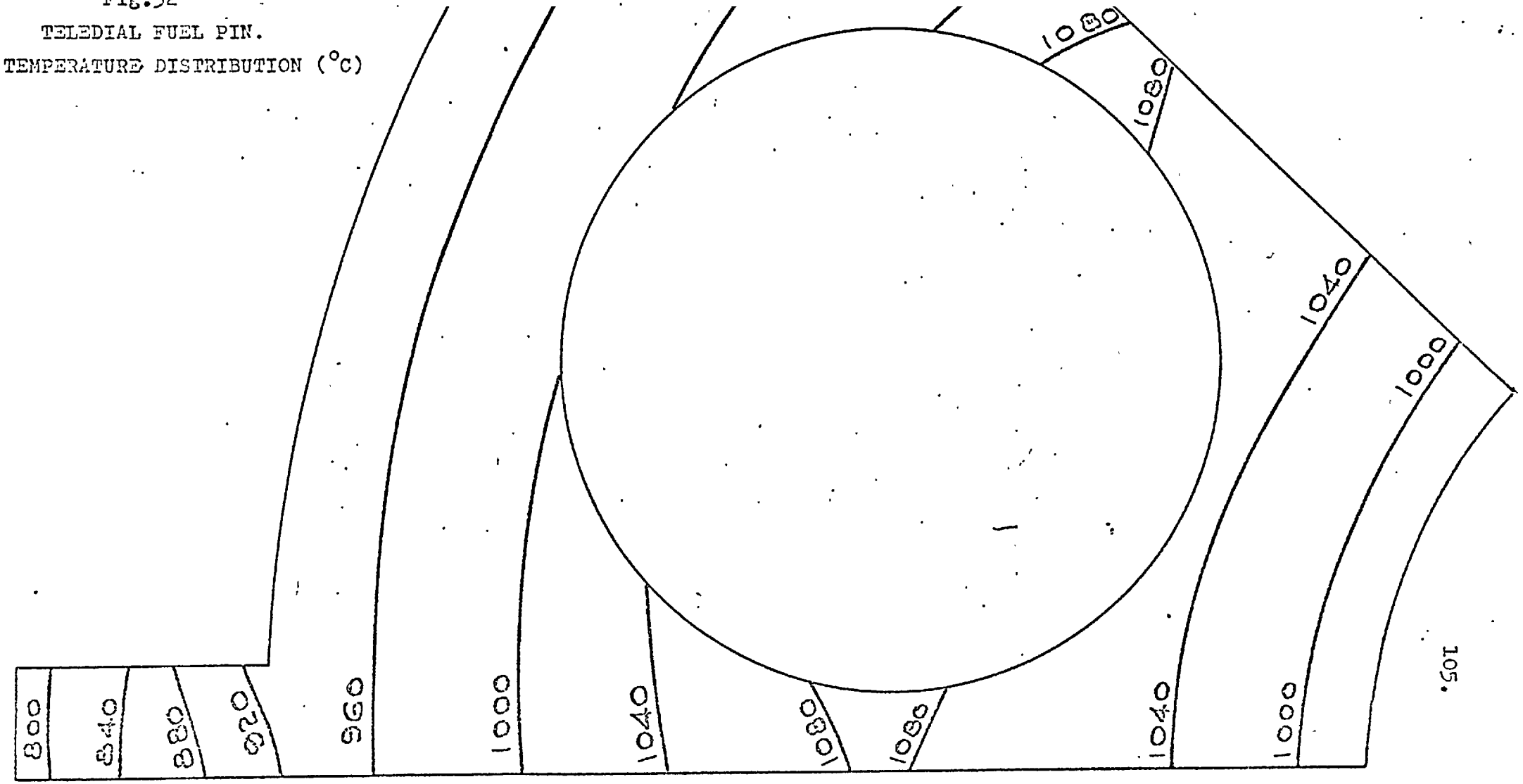

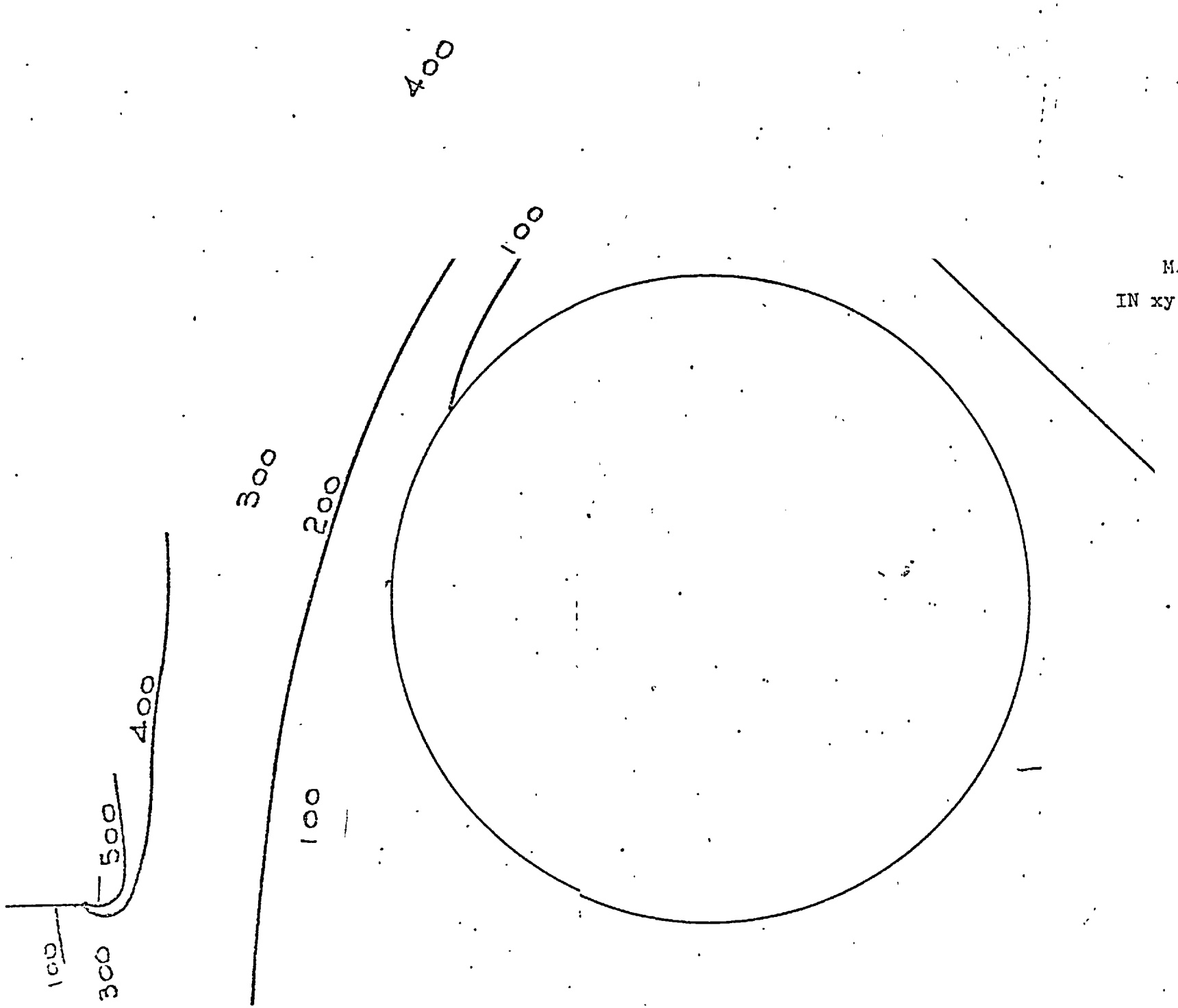

Fig.33
TELEDIAL FUEL PIN.
MAXIMUM PRINCIPAL STRESS
IN xy PLANE AT TIME ZERO (N/cm^2).

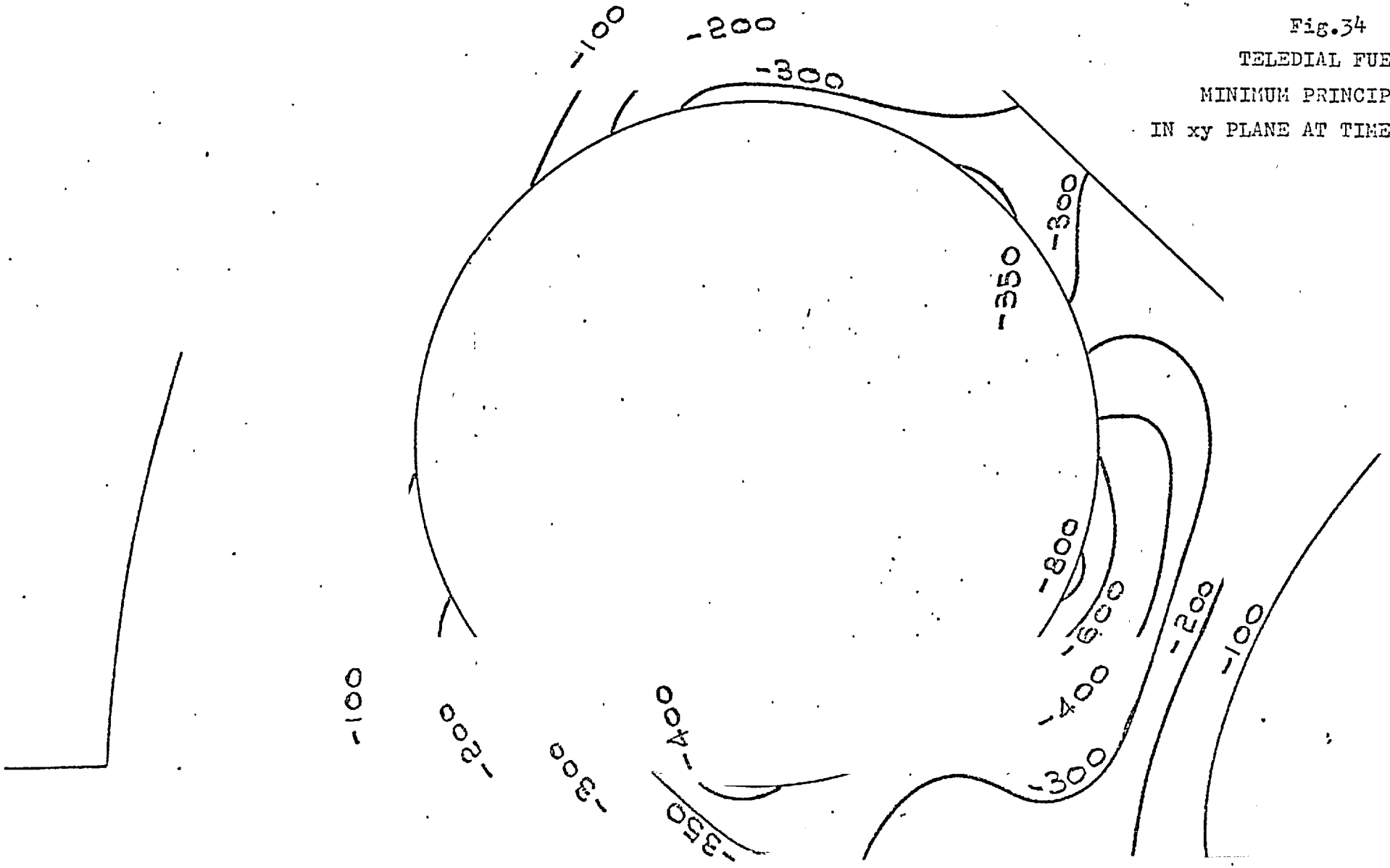

Fig.34
TELEDIAL FUEL PIN.
MINIMUM PRINCIPAL STRESS
IN xy PLANE AT TIME ZERO (N/cm^2).

Fig.35
TELEDIAL FUEL PIN.
STRESS IN AXIAL DIRECTION
AT TIME ZERO (N/cm^2).

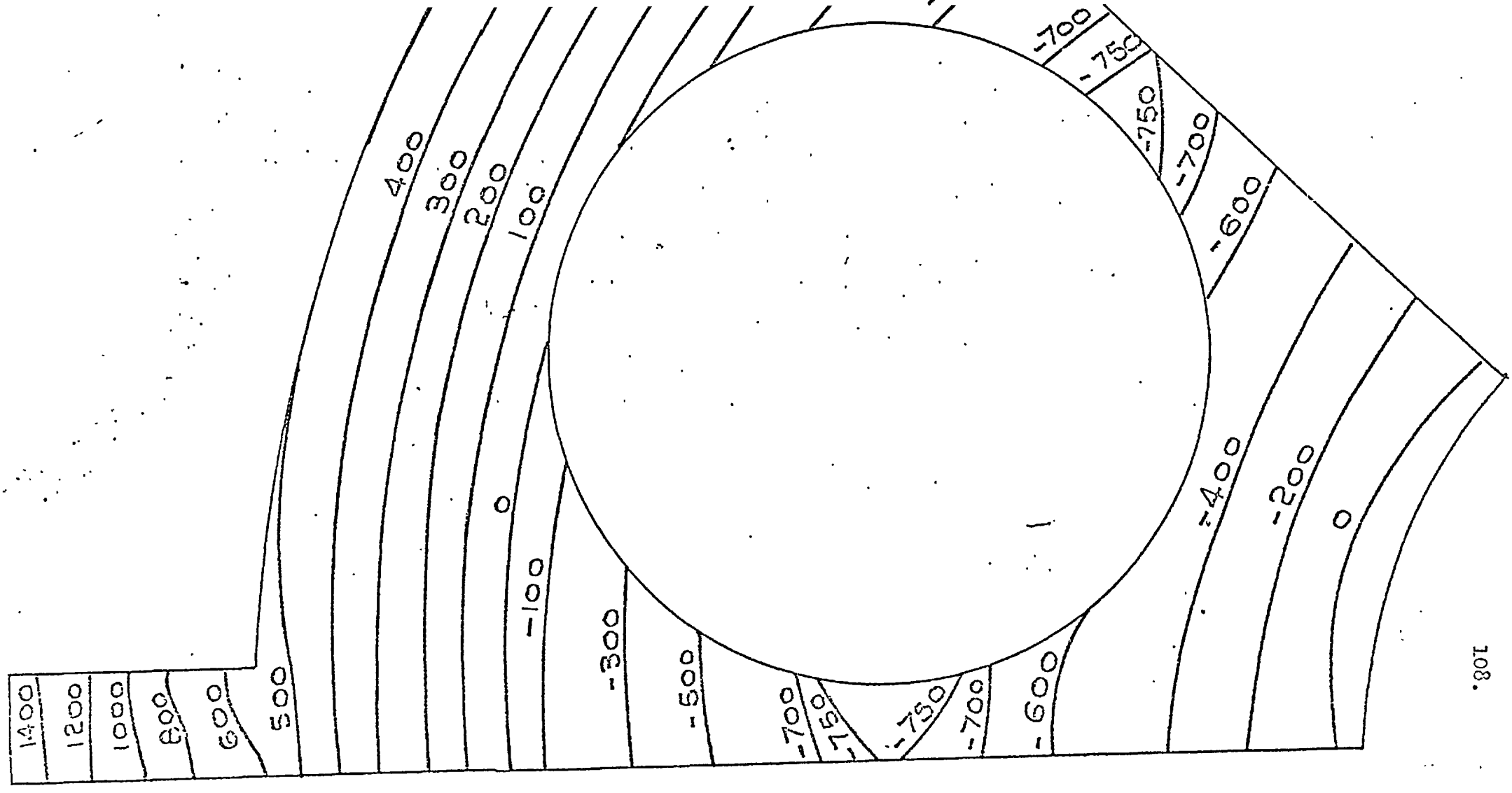

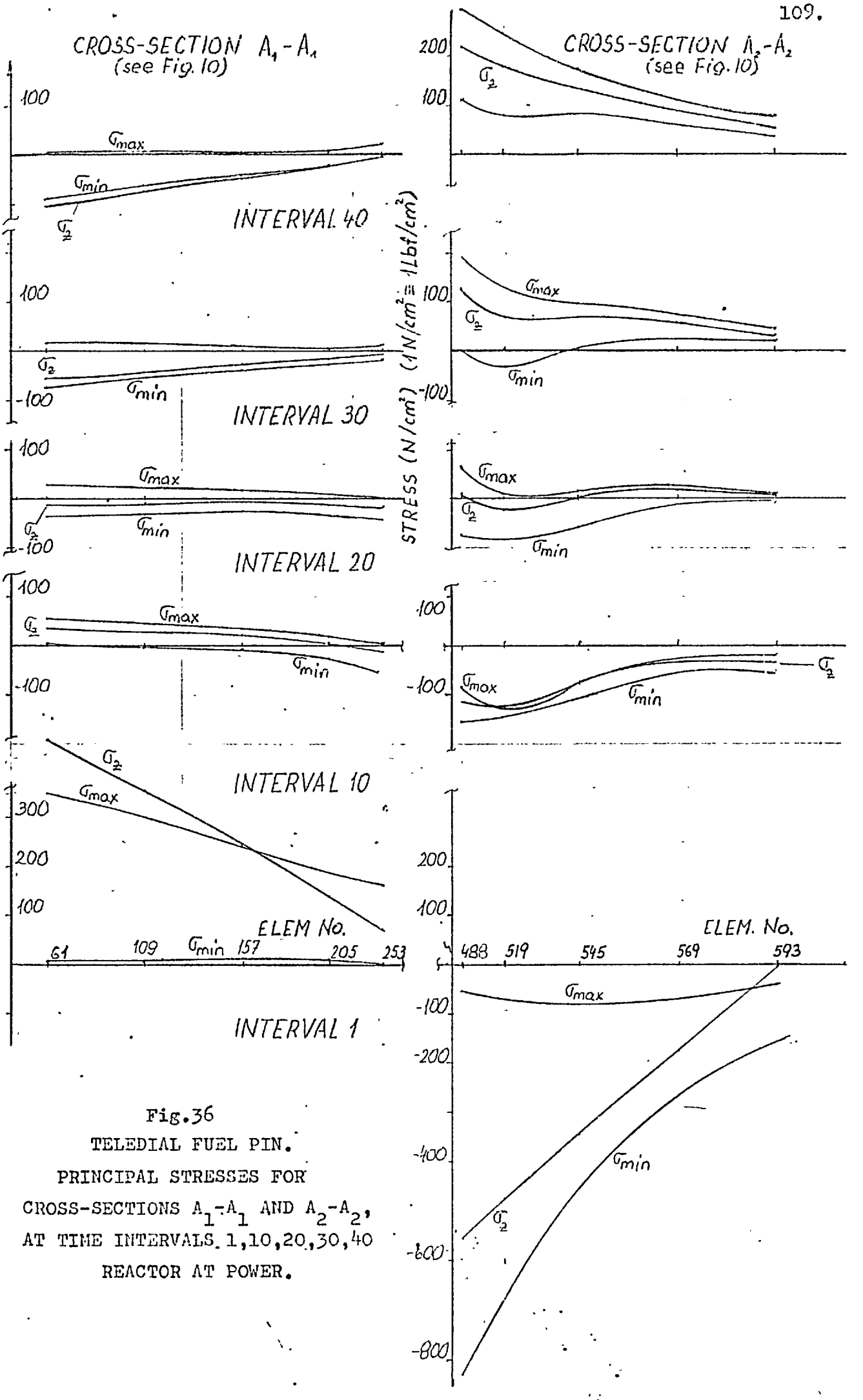

Fig.36
TELEDIAL FUEL PIN.
PRINCIPAL STRESSES FOR
CROSS-SECTIONS A_1-A_1 AND A_2-A_2,
AT TIME INTERVALS 1,10,20,30,40
REACTOR AT POWER.

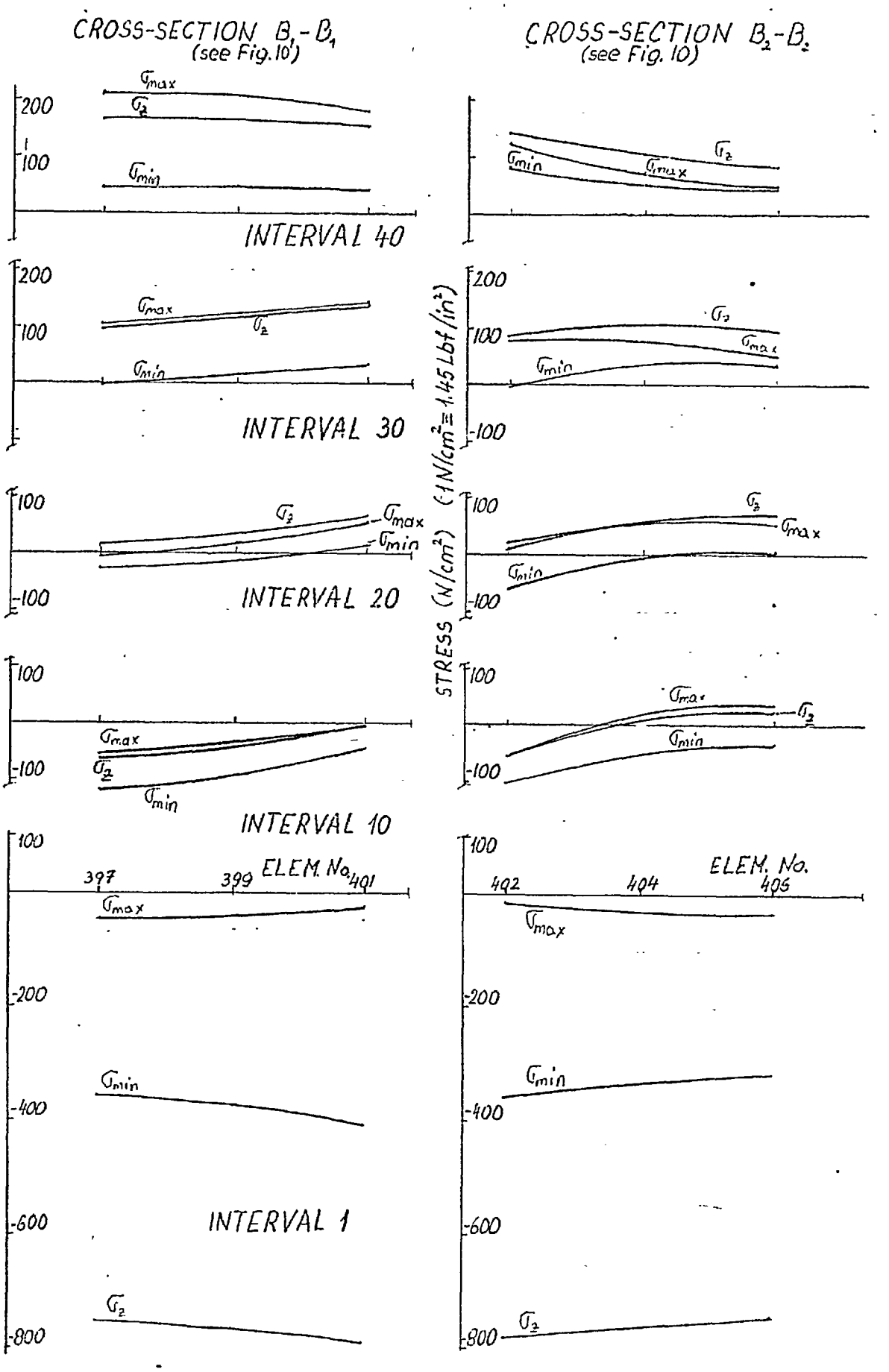

Fig.37

TELEDIAL FUEL PIN.

PRINCIPAL STRESSES FOR CROSS-SECTIONS B_1-B_1 AND B_2-B_2 ,

AT TIME INTERVALS 1,10,20,30,40

REACTOR AT POWER.

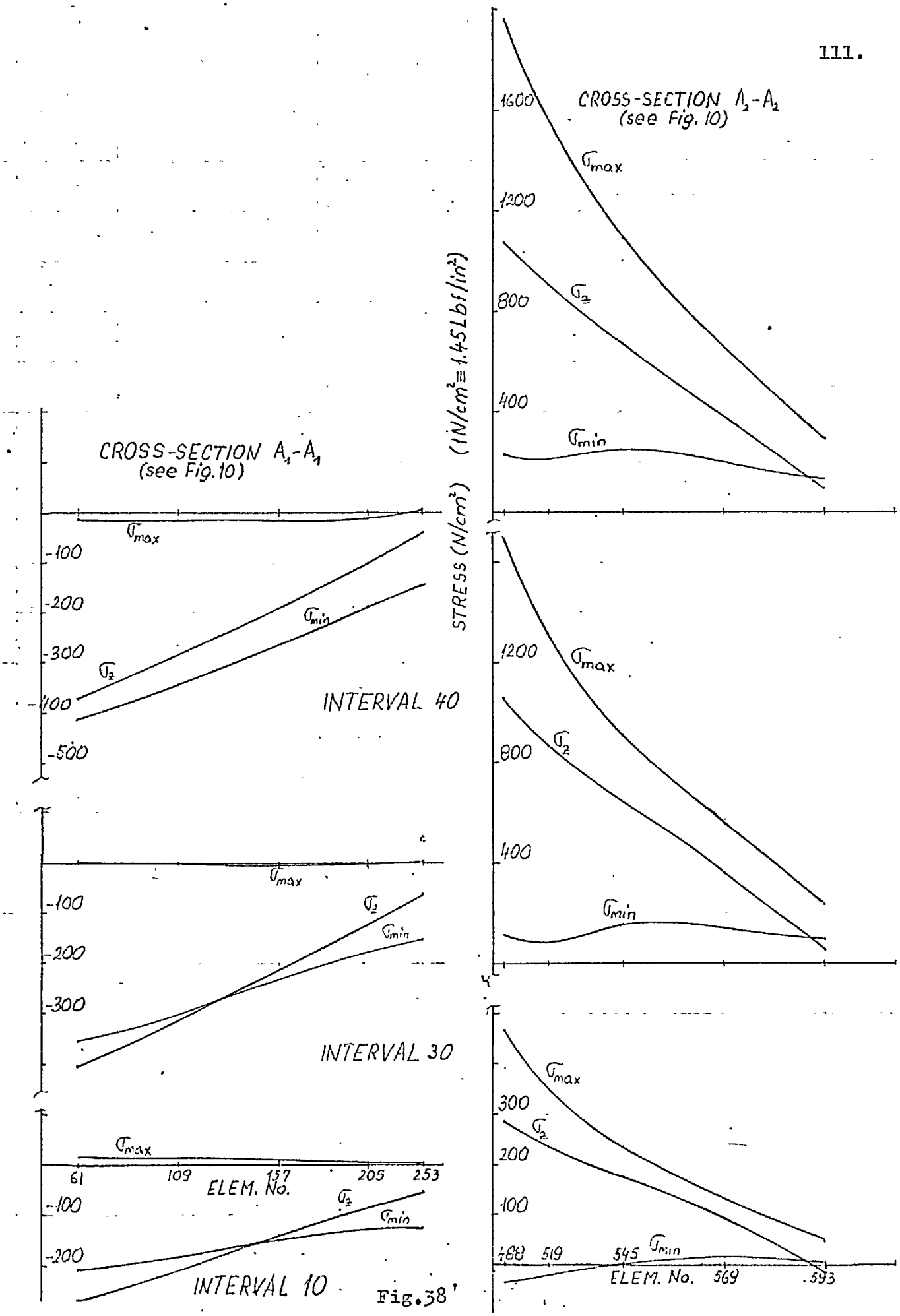

Fig.38

TELEDIAL FUEL PIN.

PRINCIPAL STRESSES FOR CROSS-SECTIONS A_1-A_1 AND A_2-A_2,

AT TIME INTERVALS 10,30,40

REACTOR SHUT DOWN.

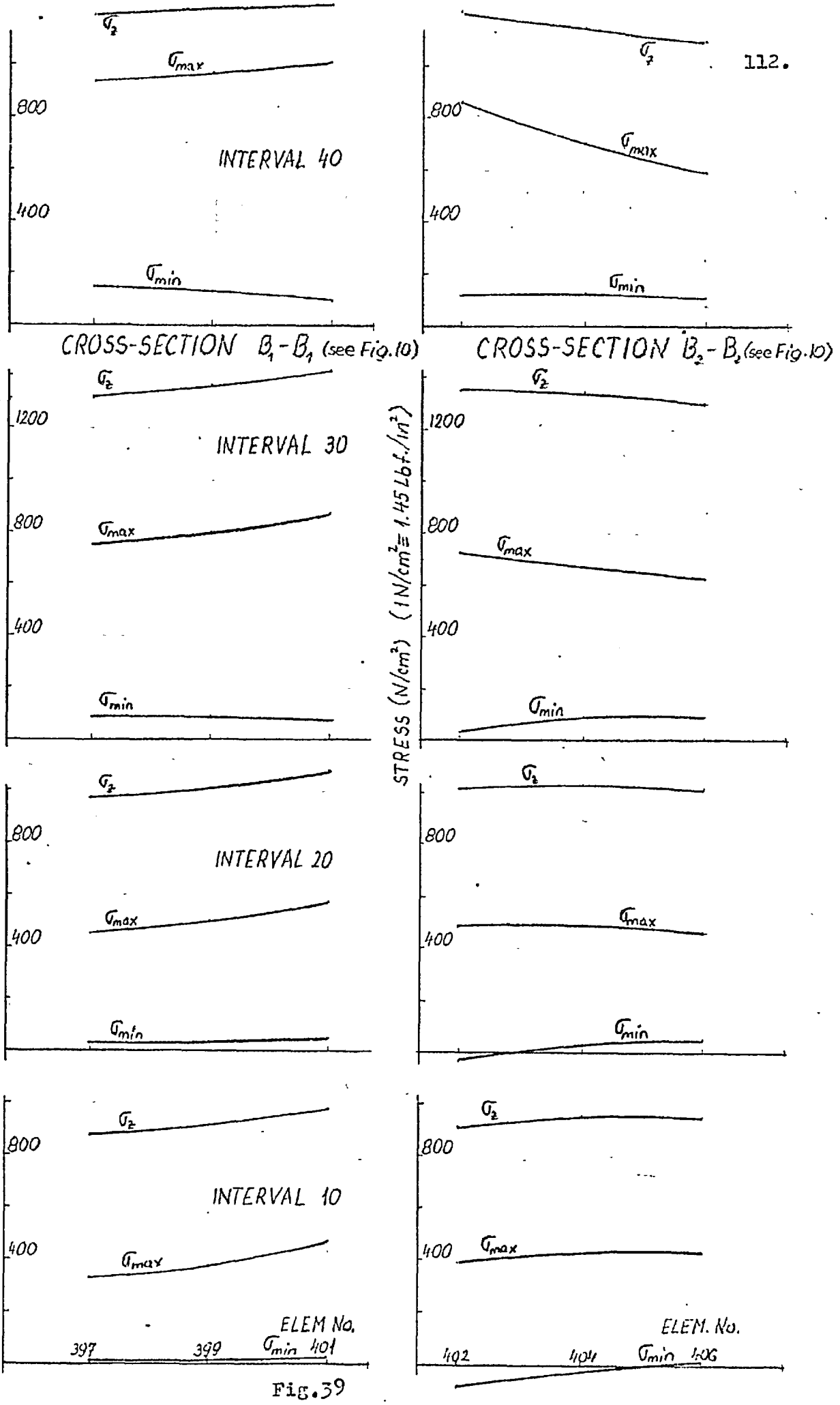

Fig.39

TELEDIAL FUEL PIN.

PRINCIPAL STRESSES FOR CROSS-SECTIONS B_1-B_1 AND B_2-B_2, AT TIME INTERVALS 10,20,30,40. REACTOR SHUT DOWN.

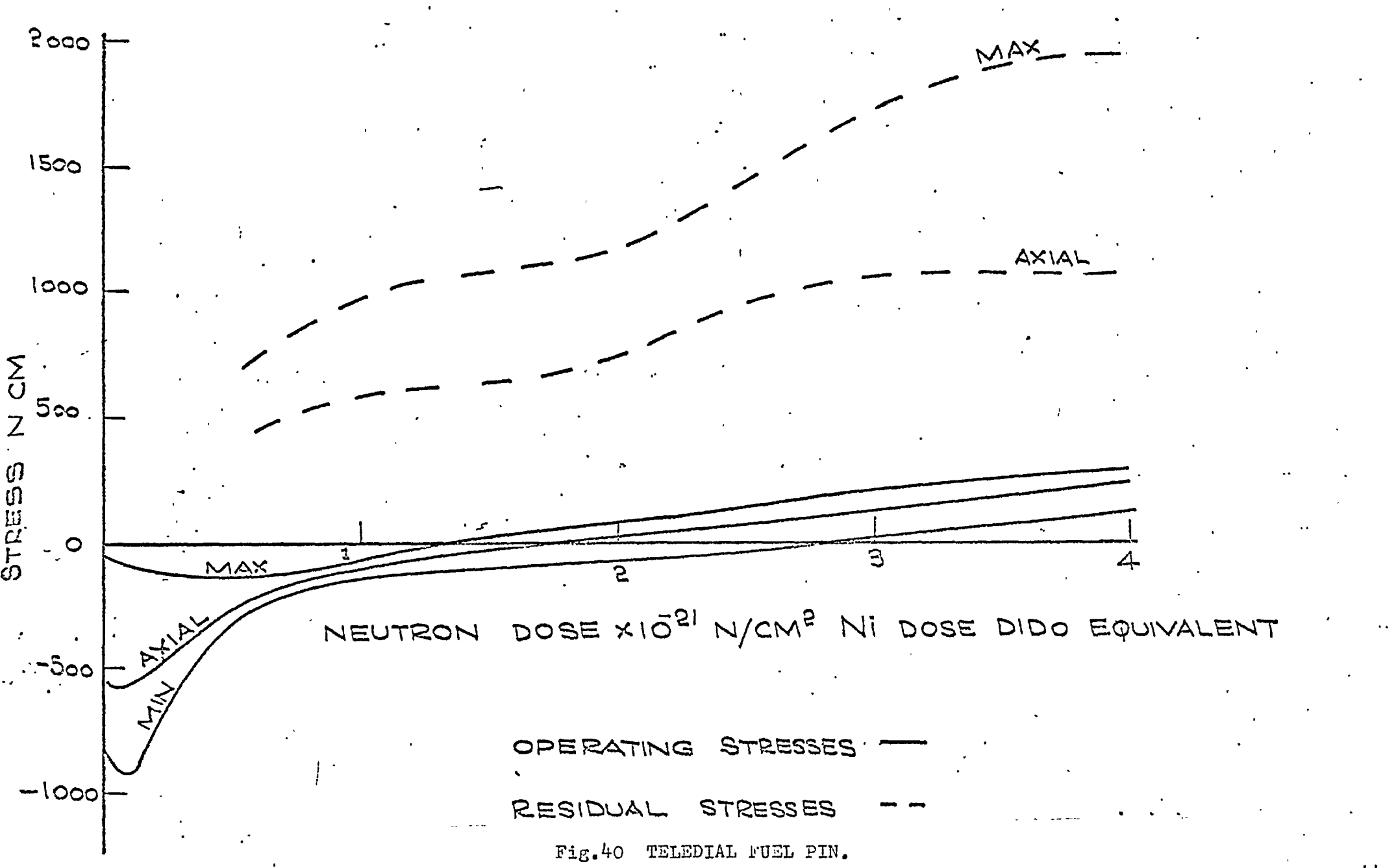

Fig.40 TELEDIAL FUEL PIN.
VARIATION WITH TIME OF PRINCIPAL STRESSES ON ELEMENT 488 -
REACTOR AT POWER AND SHUT DOWN.

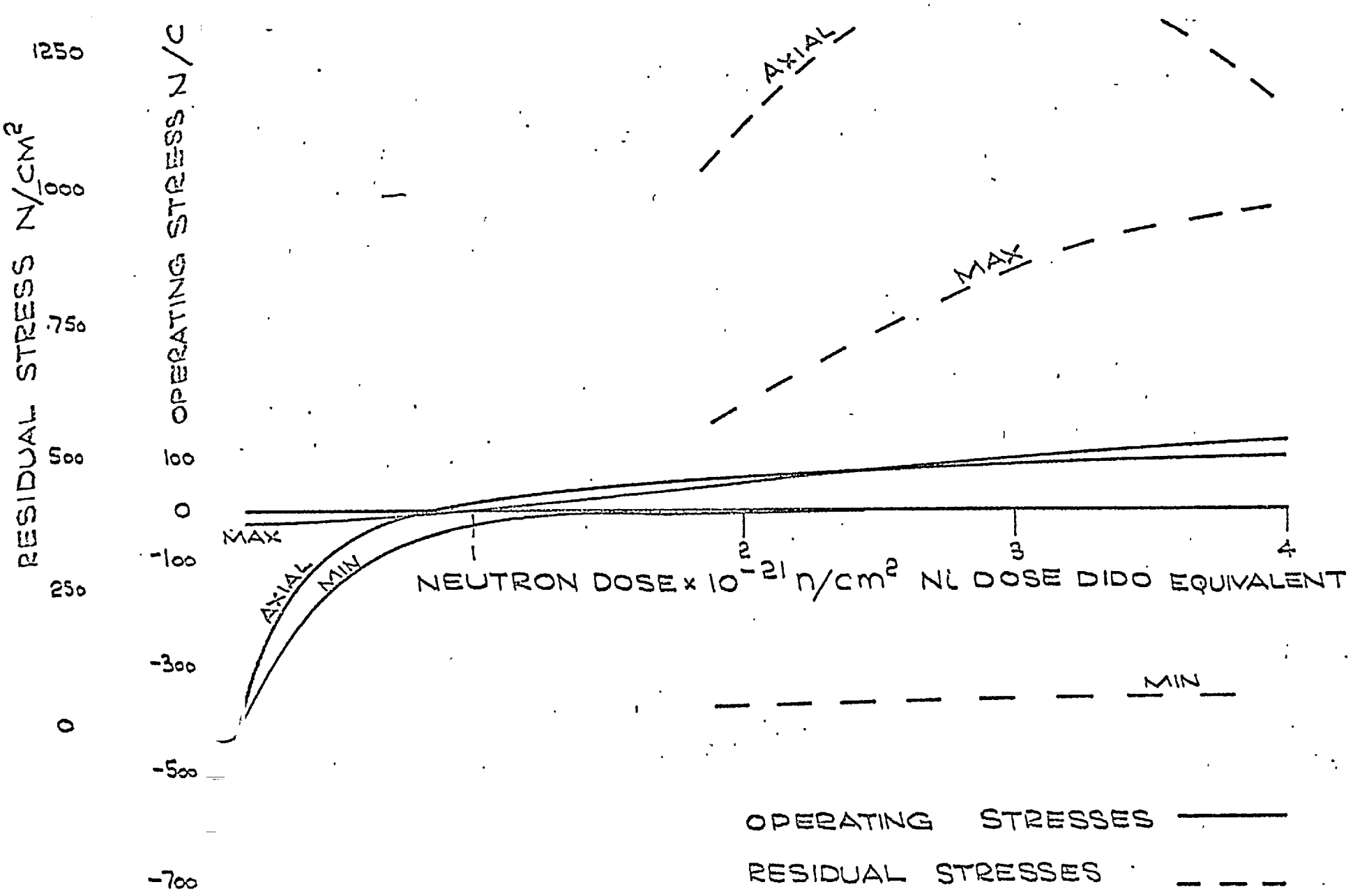

Fig.41 TELEDIAL FUEL PIN
VARIATION WITH TIME OF PRINCIPAL STRESSES ON ELEMENT 401 - REACTOR AT POWER AND SHUT DOWN.

Fig.42 TELEDIAL FUEL PIN
VARIATION WITH TIME OF PRINCIPAL STRESSES ON ELEMENT 49 -
REACTOR AT POWER AND SHUT DOWN.

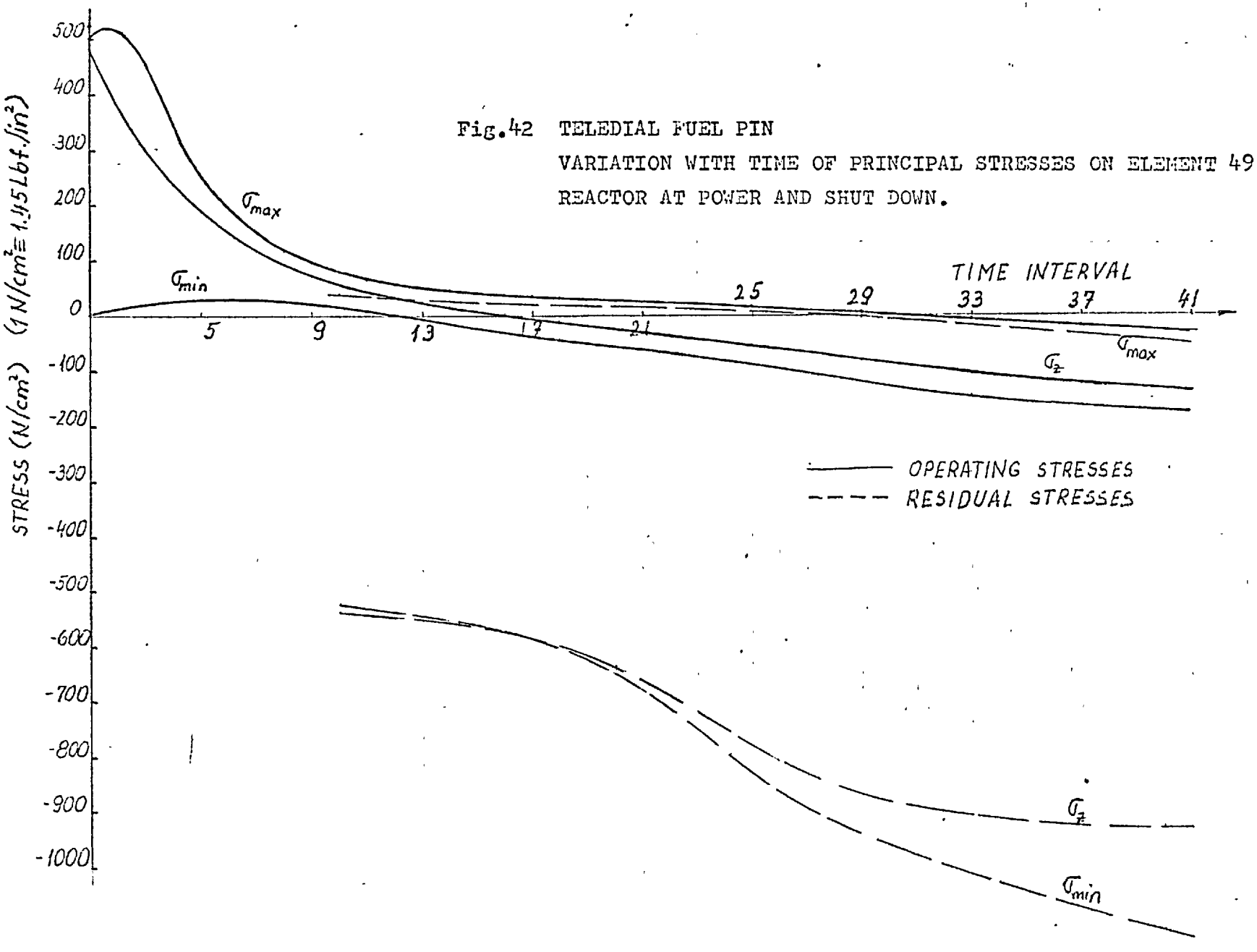

Fig.43 TELEDIAL FUEL PIN

VARIATION WITH TIME OF AXIAL STRESS ON ELEMENT 4 -

REACTOR AT POWER AND SHUT DOWN.

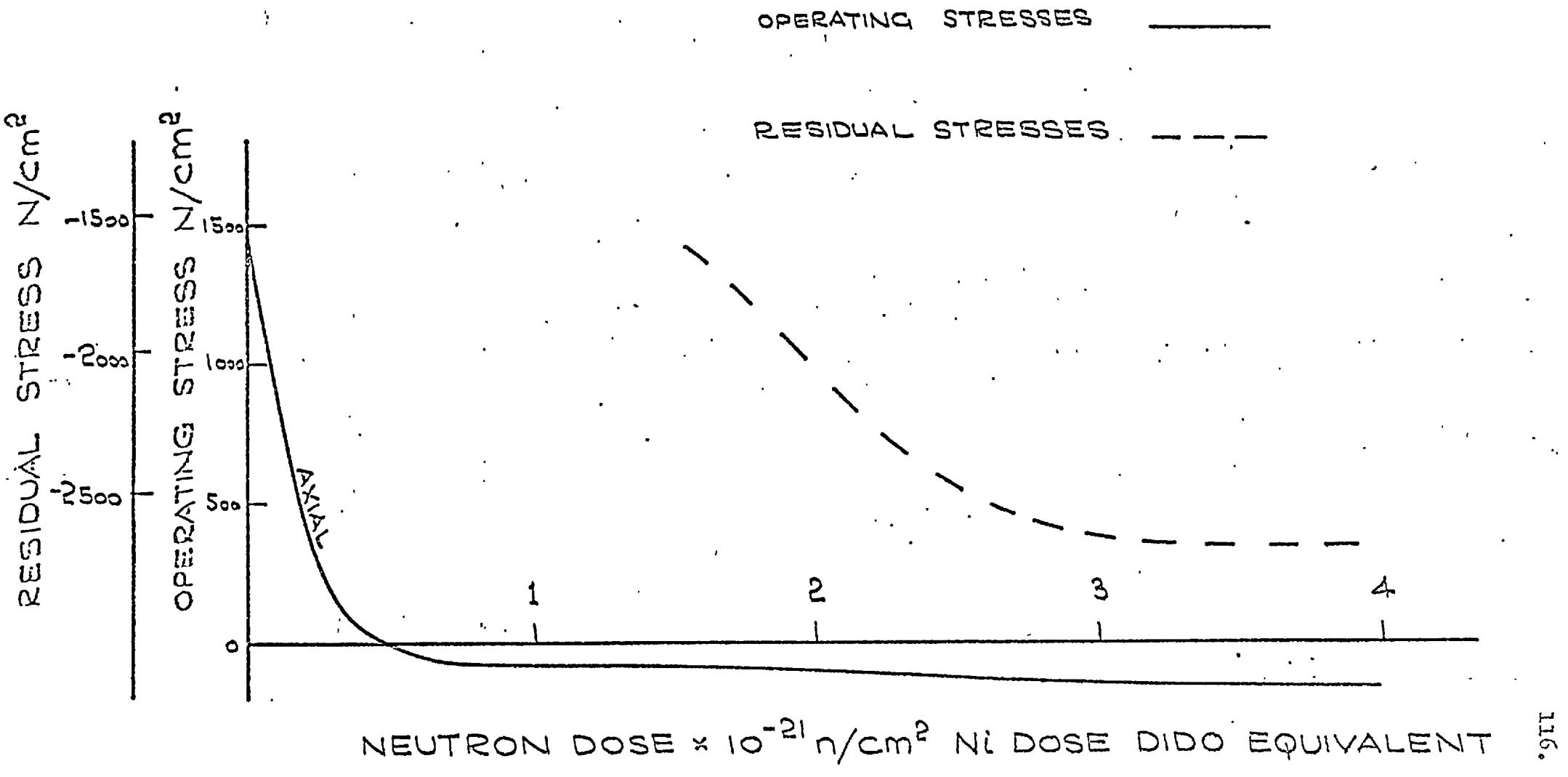

6.4. Analysis of a HTR multichannnel graphite block

6.4.1 Basic data and results

A half of a typical hexagonal multichannel graphite block as shown in Fig.44 has been analysed using a coarse mesh of a similar pattern as in Fig.12 with approximately 350 elements. The graphite block was assumed to be under an arbitrary temperature tilt and approximate temperatures are indicated in Fig.44 (see also Ch.5.2). The results presented in Table III. should provide some indications about stresses in graphite blocks under real conditions in a HTR, The assumption that the equivalent dose is constant accross the graphite block is unrealistic, but it is possible to apply, at least in part, the conclusions derived from the results for a temperature tilt to indicate the behaviour of the graphite block under a neutron dose tilt.

Some characteristic results are presented in Table III and areas with maximum stresses indicated in Fig.44. In general the left hand side of the graphite block is hotter than the right hand side. In addition all outside boundary regions are hotter than inner regions of the block. The temperature differences in ligaments between the holes are moderate (5°C to 10°C).

At time 0 the highest stresses are axial stresses, being compressive at the hotter left hand side and tensile at the cooler right hand side of the block. The highest principal stresses in plane develop at the inner part of the graphite block along the horizontal symmetry-line. It is interesting to note that only relatively moderate stresses (in plane and axially) develop in the ligaments between the holes. (see Table III)

The operating stresses are rapidly relaxed with time and it can be assumed that an axial stress distribution of a reversed pattern with tensile axial operating stresses at the left hand side and compressive stresses at the right hand side of the block will be established later in the life-time of graphite block. The principal stresses in plane x-y are relaxed to more moderate

values with compressive and tensile values close to zero. If the reactor is shut down the stresses rise and an axial stress distribution of reverse pattern is established.

6.4.2 Discusion of results

It is possible to conclude from characteristic results presented*, that the highest operating and residual stresses in a graphite block under temperature tilt (at for example core reflector boundary) are axial stresses and that the magnitude of these stresses depends on the temperature difference across block, the equivalent dose and graphite block dimensions. The axial stresses will be partially relaxed by the bowing of the block and it is the amount of bowing which will determine the magnitude of the maximum axial stress levels in the block. An equivalent dose tilt across the block will have similar effects as a temperature tilt. If the structure is already under temperature tilt and in addition there is a neutron dose tilt across the structure of the same shape the axial stress pattern in the structure will be amplified.

---

* By the time this thesis was completed, the input data and STAG program have been prepared for very complex stress analyses of graphite blocks under arbitrary temperature and equivalent dose distribution and using a large number of elements (fine mesh). Thus for example mesh data for a half of a large hexagonal graphite block have been calculated with appr. 1500 elements and 1000 nodes. The block has more than 30 holes and a part of the mesh is shown in Fig.12. The results of this work are commercial and are therefore not included.

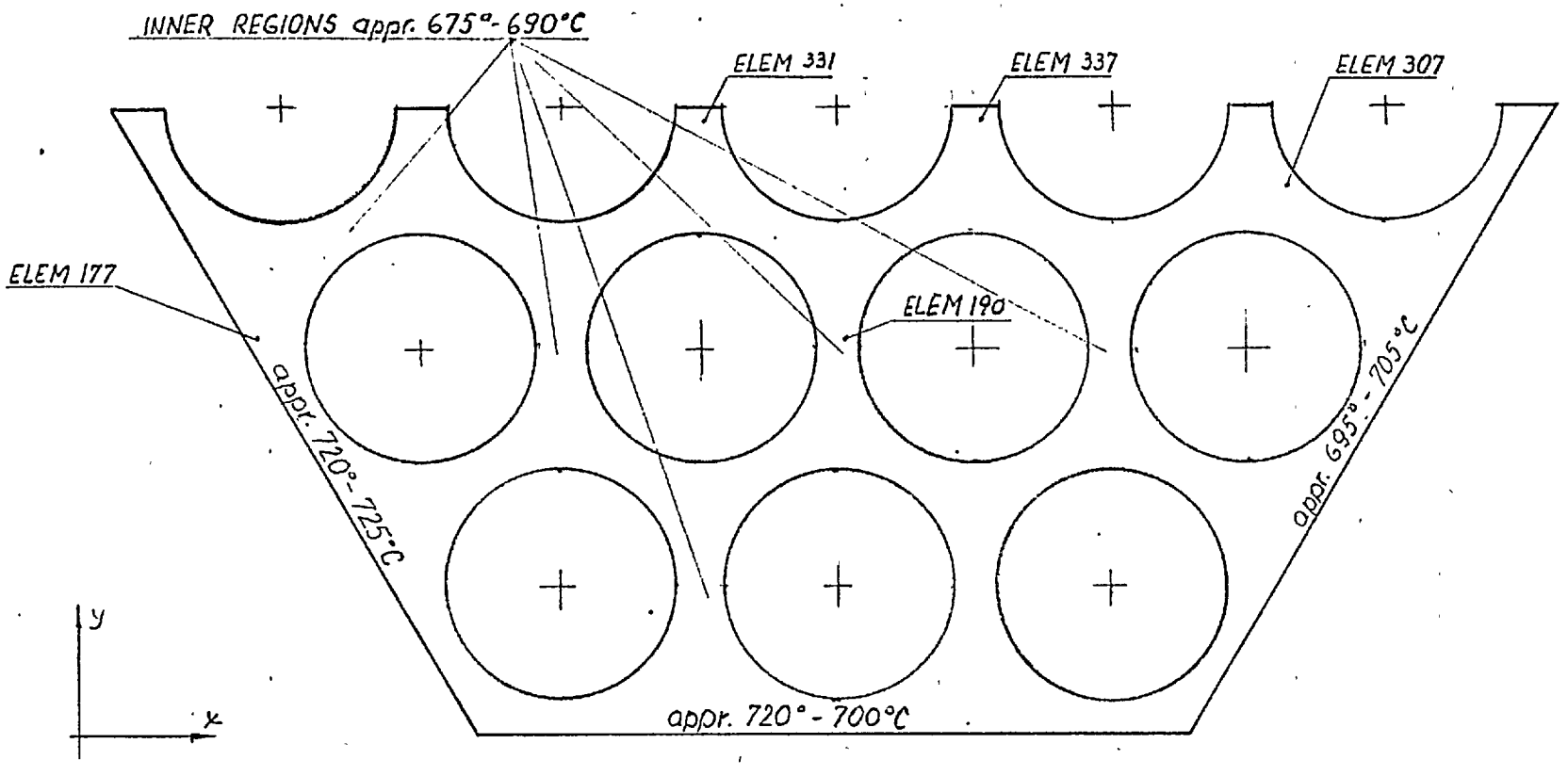

Fig.44

GRAPHITE BLOCK.

TEMPERATURE DISTRIBUTION,

HIGHLY STRESSED REGIONS (ELEMENTS 331,337,307,177),

AND A TYPICAL LIGAMENT REGION (ELEMENT 190)

(see TABLE III).

TABLE III.

	OPERATING STRESSES (N/cm^2)			RESIDUAL STRESSES (N/cm^2)		
DOSE 0 (Int.1)	σ_{max}	σ_{min}	σ_z	σ_{max}	σ_{min}	σ_z
ELEM.337	195.3	-11.3	173.5			
331	42.0	-236.7	- 27.5			
307	88.3	11.6	269.7			
177	-18.5	-110.9	-326.7			
190	73.5	- 16.1	136.8			
Dose 4 x 10^{20} n/cm^2 Ni-Dido (Int.5)						
ELEM.337	54.8	11.2	40.0	29.9	-147.9	-133.5
331	-59.5	-82.0	-68.5	167.7	-114.7	- 41.0
307	39.0	23.5	34.6	13.6	- 51.6	-235.1
177	-16.8	-38.8	-31.1	79.8	- 5.9	±295.5
190	19.0	-20.4	4.8	- 4.4	- 54.6	-132.0
Dose 9 x 10^{20} n/cm^2 Ni-Dido (Int.10)						
ELEM.337	30.9	11.3	18.7			
331	-60 .1	-74.6	-68.1			
307	27.1	24.1	17.2			
177	-10.0	-18.8	- 4.3			
190	1.9	-18.0	-11.0			

The maximum stresses develop in el.s 337, 331, 307 and 177 and in each element the underlined value represents the maximum stress. Stresses which develop in el.190 represent typical value for ligament regions.

7. SUMMARY, CONCLUSIONS AND SUGGESTIONS FOR FURTHER WORK

In previous Chapters a finite element stress analysis model for irradiation induced stresses of graphite core components has been developed and demonstrated. It appears that by using the step-by-step method and triangular elements with linear displacement field, sufficient accuracy can be achieved, provided sufficient numbers of elements are used. The accuracy of results depends on the mesh size, element shape and mesh pattern in a similar way as in elastic analysis. Creep iteration has not been used in the computations since the computing time involved makes its application uneconomic at present. However, with the choice of a suitable time (dose) step, depending on the rate of change of stress with time, the results were found to be sufficiently accurate.

For the given type of problem, a graphite core component with continously changing temperature and equivalent dose distribution and therefore with elastic constants changing with time (and position) the iterative method of solving for nodal point displacements has been found to be faster and more suitable than direct band method. If the elastic constants can be assumed constant during the life of a graphite component in the reactor, the direct tri-band and iterative methods may well use a comparable amount of computer time since the lengthy inversion of stiffness matrices for the structure partitions (in the direct program) has to be performed only once and not at each time interval. If the iterative mathix displacement method is used structures with up to 1500-2000 constant stress, triangular elements can be analysed with the current large computers having approximately 100,000 words of central memory available. This seems to be sufficient for most (graphite reactor) engineering problems. Using the direct-band method possibility exists to analyse structures with appr. 3000-4000 elements for the same size of computer. Special program rewriting will be required for larger structures. It seems that other direct methods such as the

front method will be more suitable for very large structures using a smaller number of higher order (isoparametric) elements. In the analysis of graphite core components it is however unlikely that analysis of structures with many thousand elements will be needed. If so, the computer time required will run into hours.

At present the temperature distribution and equivalent dose changes with time can be read into the program from cards or tapes at the beginning of each time interval and these input data are calculated by separate programs. It is thought that this arrangment makes the program more flexible since intermediate results can be always checked and also turn-round time is shorter for a short program. The mesh data are calculated by a separate program and read in at the beginning of the calculation. For long runs a restart facility could be included to enable the termination and restart of the calculation at any time.

Several possible directions of further development are indicated by the present work. One desirable development is the inclusion in the STAG code of axi-symmetric and plane stress options for which the basic relationships have already been developed (Ch.3 and App.I). The partial creep iteration could be included as well.

Another attractive line of development is probably the comparison of different matrix displacement methods for viscoelastic and other time - dependent problems. It seems that not only the running time and central memory required but also the accuracy and stability of results vary for different matrix displacement methods. One particular matrix displacement method may well have advantages over others for a particular class of problem.

The time-dependent analysis of graphite components in three dimensions will probably remain for some time to come an uneconomic proposition because of the large amount of computing time required. It is possible that some conclusions

from comparative analyses of matrix displacement methods in two dimensions could contribute to the development of the three dimensional work.

The accuracy of peripheral programs which provide mesh data, material properties data etc, could significantly influence the results. The automatic mesh generation programs and nonlinear interpolation of material properties data are prefered to manual preparation of mesh data and linear interpolation. In general, the level of accuracy of peripheral programs should be comparable or better than the accuracy of suplied experimental values.

Finally some conclusions can be drawn regarding the relative suitability of different graphite core components.

Stresses in a hollow rod fuel pin under symmetric loading are relatively moderate. A substantial temperature tilt causes very high axial stresses if the pin is restricted from bowing. An equivalent dose tilt accross the rod of the same shape as temperature tilt is expected to amplify the exsisting stress pattern in the rod. Since it is unlikely that the graphite block and fuel pin will undergo the same amount of bowing, the fuel pins will be partially restrained and the amount of possible bowing of fuel pin will determine the magnitude of maximum axial stresses. The stresses in plane (x-y) are only slightly influenced by temperature (or dose) tilt and their values and pattern are similar to those for symmetric loading. The hollow rod pins are most likely to fail in regions of high tensile axial (residual) stresses due to restricted bowing. The magnitude of overall stress distribution for symmetric loading can be reduced by reducing the thickness of the hollow rod tube wall and for non-symmetric loading by reducing the tube diameter. However in both cases, this is clearly possible only to a limited extent due to other (for example reactor physics) design requirements.

The stresses in a teledial fuel pin are substantially higher than in the hollow rod fuel pin. The most serious conditions in a teledial seem to be at inner edge of the fuel hole (el.488,Fig.11)

for the temperature distribution without a temperature tilt. In the ribs of the teledial fuel pin very high stresses develop since they are normally overcooled. These very high stresses will however probably not cause a serious concern since they may cause only local cracking and can be to a large extent eleminated by cutting horizontal grooves into the rib at several positions along the fuel pin. The same conclusions can be applied for axial stresses in the ribs of a hollow rod fuel pin. A comment that may be made is that the calculated stresses in the teledial, particularly the residual stresses which occur at the end of the fuel pin life are almost certainly an overstimate of the true stresses, as the reduction of pin power, due to burn-up has been neglected.

For both fuel pins the residual or shut-down stresses are much higher than the operating stresses.

In a graphite block under temperature tilt the axial stresses reach the highest values. For the time (dose) range presented the highest are initial axial (thermal) stresses but it can be assumed that the residual axial stresses are most severe after a prolonged irradiation in the reactor. Similarly as for hollow rod fuel pin it is the amount of bowing which will determine the magnitude of the maximum axial stress levels. Equivalent dose tilt of the same shape as temperature tilt will amplify the existing stress pattern. The stresses which develop in the ligaments are relatively moderate. The most serious stress condition will probably be represented by a large size block at high temperature (for example 800°C - 1000°C) and under substantial temperature and flux gradients. In general a smaller graphite block may well be more desirable from the point of maximum stresses but again a very small block may be in contradiction with the other design requirements.

One general comment which can be made is that the stresses which develop in the graphite block for the temperature distribution assumed in the analysis are relatively moderate in comparison with the stresses which develop in fuel pins.

8. REFERENCES

1. Head, J.L., Sockalingam, K.C., 'Radiation-Damage Stresses in the Graphite of Power-Producing Nuclear Reactors', J.Mech.Engg.Sci., Vol 10, No.5,1968.

2. Head, J.L., 'The Effect of Radiation Creep on the Stresses in the Moderator Graphite of a Nuclear Reactor', PhD Disertation, University of London, 1970.

3. Jezernik A., 'Stresses in Graphite Tubes of a High Temperature Gas Cooled Reactor', M.Sc.Dissertation, University of London, 1968.

4. Jezernik A., Head, J.L., 'Stresses in the Graphite Fuel Tubes of a High Temperature Gas-cooled Reactor', Dragon Project Report 662, 1970.

5. Jezernik, A., Head, J.L., 'Calculation of Stresses in Graphite-Fuel-Tubes of a High Temperature Reactor', to be published in Atomkernenergie, 1971.

6. Head, J.L., Jezernik, A., 'A Comparison of the Stresses in HTR Fuel Tube made of Dragon Pechiney G5 and Pressed Isotropic Gilsocarbon Graphites', Dragon Project Report 705,1970.

7. Sockalingam, K.C., 'Stresses in Graphite Moderator Blocks' M.Sc.Dissertation, University of London, 1966.

8. Barnes, S.A., 'Stresses in Graphite Moderator Blocks of an Advanced Gas-Cooled Reactor', M.Sc. Dissertation, University of London, 1968.

9. Alujevič, A., Head, J.L., 'Heat Transfer and Stress/Strain Analysis of Tubular Fuel Elements', Dragon Project Report, to be published in 1971.

10. Shepherd, L.R., 'High Temperature Reactor and the Dragon Reactor Experiment', The Journal of British Nuclear Energy Society, Vo.5, No.3, 1966.

11. Lockett, G.E., Hosegood, S.E., (assembled and edited), 'Preliminary Study for a 630MW(e) low enriched Homogeneous High Temperature Gas Cooled Reactor', Dragon Project Report 558, 1968.

12. Smith, E., Fuel Elements for the first core loading of the Dragon Reactor, Dragon Project Report 342, 1965.

13. Mendelson, A., Hirschberg, M.M., Manson, S.S., 'A General Approach to the Practical Solution of Creep Problems', J.Basic Engg., Trans A.S.M.E, 81D, 1959.

14. Smith, E.M., 'Primary Creep Behaviour of Thick Tubes', Thermal Loading and Creep in Structures and Components, Proc.Instn.Mech.Engrs. 1963-4, Vol.178 (Part 3L).

15. Turner, H.J., Clough, R.W., Martin, H.C., Topp, L.J., 'Stiffness and Deflection Analysis of Complex Structures', J.Aero Sci. 23, 1956.

16. Clough, R.W., 'The Finite Element in Plane Stress Analysis', Proc., 2nd ASCE Conf. on Electronic Computattion, Pittsburgh, Pa., 1960.

17. Argyris, J.H., 'Energy Theorems and Structural Analysis', Butterworth, London (1960). (Reprinted from Aircraft Eng.1954-55).

18. Zienkiewicz, O.C., Cheung, Y.K., 'The Finite Element Method in Structural and Continuum Mechanics', McGraw-Hill,1967.

19. Wilson, E.L., 'Finite Element Analysis of Two-Dimensional Structures', Ph.D.Dissertation, University of California, 1963.

20. Fraeys de Veubeke, B., Displacement and Equilibrium Models in the finite Element Method, (Ch.9 Stress Analysis), O.C.,Zienkiewicz and G.,Holister, edited by, J.,Wiley Son (1965).

21. Argyris, J.H., 'Matrix Analysis of Three-Dimensional Elastic Media. Small and large,Displacements', J.AIAA, 3,1965.

22. Ergatoudis, J., Irons, B.M., and Zienkiewicz, O.C., 'Curved Isoparametric Quadrilateral Elements in Finite Element Analysis', Int.J.Solids Struct.4, 1968.

23. Przemieniecki J.S, 'Theory of Matrix Structural Analysis', McGraw Hill, 1968.

24. Nettley, P.T., Martin, W.H., 'The Irradition Behaviour of Graphite High Temperature Nuclear Fuels', Holden, A.N. (Editor), Gordon Breach, London, 1968.

25. Everett, M.R., Graham, L.W., 'Physical Property and Irradiation Data on Isotropic Gilsocarbon Graphite', Dragon Project Internal Document DPRDD/1666, 1968.

26. Blackstone, R., Graham, L.W., Everett, M.R., and Delle,W., 'Irradiation Data on Gilsocarbon Graphites for High Temperature Nuclear Reactors', IAEA Symposium on Radiation Damage in Reactor Materials, Vienna, 1969.

27. Cornwall, W.S., Jobson, D.A., 'Wigner Stresses in Graphite, Allowing for the effects of Irradiation Creep', U.K.A.E.A Report TRG 672 (R), 1964.

28. Witt, F.J., Greenstreet, B.L., 'Influence of Cross-Sectional Shape on Irradiation - Induced Stresses in Graphite Columns', Nucl.Sci Engg., Vol.25, No.2, 1966.

29. Chang, T.Y., Rashid, Y.R., 'Viscoelastic Response of Graphitic Materials in Irradiation Enviromments', Nuclear Engineering Design, 1970.

30. Marcal, V.P., 'On General Purpose Programs for Finite Element Analysis, with Special Reference to Geometric and Material Nonlinearities', Symposium on Numerical Solution of Partial Differential Equations, University of Maryland,1970.

31. Greenbaum, G.A., Rubinstein, M.F., 'Creep Analysis of Axi-symmetric Bodies using Finite Elements', Nuclear Engineering and Design 7, 1968.

32. Perks, A.J., Simmons, J.H.W., 'Radiation Induced Creep of Graphite', U.K.A.E.A. Report AERE-R 4372, 1963.

33. Irons, B.M., 'A Frontal Solution Program for Finite Element Analysis', International Journal for Numerical Methods in Engineering, Vol.2, No.1, 1970.

34. Frederick, C.O., Wong, Y.C., and Edge, F.W., 'Two-Dimensional Automatic Mesh Generation for Structural Analysis', International Journal for Numerical Methods in Engineering, Vol.2., No.1, 1970.

35. Lewis, D.J., Fullard, K., 'Experience in the Use of Finite Elements in Stress Analysis.' CEGB Report.

36. Kinkead, N., Private Communication, 1970.

37. Bell, J.C., Bridge, H., Cottrell, A.H., Greenough, G.B., Reynolds, W.N., Simmons, J.H.W., 'Stored Energy in the Graphite of Power Producing Reactors', Phil.Trans.Roy.Soc. (A), Vol.254, 1962.

38. Reed, D.L., Everett, M.R., and Blackstone, R., 'The Correlation of Graphite Irradiations in the High Flux Reactor Petten and in High Temperature Reactors', I.A.E.A., Symposium on Radiation Damage in Reactor Materials, Vienna, June 1969, Paper SM - 120/E-7.

39. Everett, M.R., Manzel, R., 'Summary of Physical Properties and Irradiation Data on Gilsocarbon Graphite', Dragon Project Internal Document DPRDD/1794, 1969.

40. Dragon Project Private Communication.

41. Conte, S.D., 'Elementary Numerical Analysis an Algorithmic Approach', McGraw Hill, 1965.

42. Noble, B., 'Numerical Methods 2' - Oliver and Boyd Ltd., Edinburgh, 1964.

43. Wood, W.G., Blomfield, J.A., 'Postgraduate Lectures on Finite Element Method', Imperial College of Sc. and Technology 1968/69.

44. Sokolnikov, I.S., 'Mathematical Theory of Elasticity', McGraw Hill, 1956.

45. Hearmon, R.F.S., 'An Introduction to Applied Anisotropic Elasticity', Oxford University Press, 1961.

46. Kaae, J.L., 'On Irradiation - Induced Creep of Pyrolitic Carbon in a General State of Stress', J.Nucl.Mats.,Vol.34, 1970.

47. P.J., Allen, 'Central Electricity Generating Board (London) Private Communication'.

9. NOTATION

A	area of element
$[B]$	displacement/strain transformation matrix
$C_{1,2,3,4}$	constants
C_I, C_{II}, C_N	stiffness matrices for subregions (partitions)
$[D]$	elasticity matrix
De	equivalent neutron dose
E	Young's modulus
$[K]$	stiffness matrix for complete assembly
$[K_I], [K_{II}], [K_N]$	stiffness matrices for subregions (partitions)
$[k]$	stiffness matrix for element
P	axial restraining force
$[Q]$	creep compliance matrix
$\{R\}$	nodal force matrix
$\{R'\}$	nodal forces to suppress displacement
$\{S\}$	element corner force matrix
$[s]$	6 x 6 elastic compliance matrix
T	temperature
U,V	elements of 4 x 4 creep compliance matrix
u,v	element displacements in plane
x,y	cartesian coordinates
r,z,θ	axi-symmetrical coordinates
α	thermal expansion coefficient
β	the convergence factor
$\{\delta\}$	element corner or structure displacement matrix
$\{\varepsilon\}$	total strain matrix
$\{\varepsilon^e\}$	elastic strain matrix
$\{\varepsilon^n\}$	nonelastic strain matrix
$\{\varepsilon^c\}$	creep strain matrix
$\{\varepsilon^t\}$	thermal strain matrix
$\{\varepsilon^W\}$	Wigner strain matrix

ν	Poissons's ratio
$\{\sigma\}$	stress matrix
τ	shear stress
γ	shear strain

Subscripts

x,y,z	cartesian coordinates
z,O,r	axi-symmetrical coordinates
i,j,k	node numbers
$\parallel, \perp$	parallel, perpendicular directions

Superscripts

e	elastic
n	nonelastic
c	creep
W	wigner
t	thermal

Other symbols are defined where they occur in the text

Units

Stress: 1 N/cm^2 = 1.45 psia

Temperature ^oC

Length (dimensions): cm

Neutron dose: Calder equivalent dose 1000MWD/Ate = 10^{20} n/cm^2 Ni-dido dose

APPENDIX I , THEORETICAL ANALYSIS

The matrix equations for plane stress/strain and axisymmetric problems are derived here in detail considering the derivations by Wilson [19], Head [2] and notes of selective postgraduate lectures about the finite element method at Imperial College given by Wood and Blomfield in 1968/69 [43] .

A.1.1 Strain/displacement relationship

Displacements with an element with an assumed linear displacement field are defined for plane stress/strain (eq's 3.2a, 3.2b in Ch.3) by:

$$u = u_i + C_1(x - x_i) + C_2(y - y_i) \qquad (A.1.1)$$

$$v = v_i + C_3(x - x_i) + C_4(y - y_i) \qquad (A.1.2)$$

The equations are of the same form for axisymmetric analysis (eq.3.24) except that coordinates x and y have to be replaced by r and z. We can define six simultaneous equations of the above form and the constants C_1, C_2, C_3 and C_4 can be determined in terms of nodal displacements (eq.3.3):

$$\begin{bmatrix} C_1 \\ C_2 \\ C_3 \\ C_4 \end{bmatrix} = \frac{1}{2\Delta} \begin{bmatrix} y_j-y_k & 0 & -(y_i-y_k) & 0 & (y_i-y_j) & 0 \\ -(x_j-x_k) & 0 & (x_i-x_k) & 0 & -(x_i-x_j) & 0 \\ 0 & y_j-y_k & 0 & -(y_i-y_k) & 0 & (y_i-y_j) \\ 0 & -(x_j-x_k) & 0 & (x_i-x_k) & 0 & -(x_i-x_j) \end{bmatrix} \begin{Bmatrix} u_i \\ v_i \\ u_j \\ v_j \\ u_k \\ v_k \end{Bmatrix}$$

and

$$\frac{1}{2\Delta} = \frac{1}{x_i(y_j-y_k) - x_j(y_i-y_k) + x_k(y_i-y_j)} \qquad (A.1.3)$$

The strains within the element can be obtained from the assumed displacement field (see eq's 3.5 and 3.26),

$$\{\varepsilon\} = [B] \quad \{\delta\} \qquad (A.1,4)$$

The matrix $[B]$ for plane strain/stress and for axi-symmetric geometry is given in detailed form at the end of this Appendix.

A 1.2 Stress/Strain Relationship

A 1.2.1 The Strain Matrix

It is assumed that the total strain matrix can be separated into elastic thermal, Wigner and creep strain matrices (see eq's 3.9):

$$\{\varepsilon\} = \{\varepsilon^e\} + \{\varepsilon^t\} + \{\varepsilon^W\} + \{\varepsilon^c\} \qquad (A.1.5)$$

These matrices have been given in expanded form in Ch.3. In this Chapter the derivation of the elasticity matrix $[D]$ and creep compliance matrix $[Q]$ are discused or given in more detail, for different 2-dimensional cases.

A 1.2.2 Stress/Elastic Strain Relationship

In the general three-dimensional case and for anisotropic material the stress/strain relationship is of the form:

$$\{\sigma\} = [D] \quad \{\varepsilon\} \qquad (A\ 1.6)$$

The elasticity matrix $[D]$ can be derived as follows: Hooke's law, for small strains, may be written:

$$\varepsilon^e_{ij} = s_{ijkl} \ \sigma_{kl} \qquad (A\ 1.7)$$

where s_{ijkl} = elastic compliance tensor.

The compliance tensor is of the fourth order and has 81 elements. It can be shown (see for example Sokolnikov [44]) that since:

$$\sigma_{ij} = \sigma_{ji} \qquad \text{(A 1.8)}$$

and

$$\varepsilon_{ij} = \varepsilon_{ji} \qquad \text{(A 1.9)}$$

only 36 of elements are independent and we may restate Hooke's law in the form of the matrix equation:

$$\{\varepsilon^e\} = [s] \cdot \{\sigma\} \qquad \text{(A 1.10)}$$

where

$\{\varepsilon^e\}$ = 6 x 1 elastic strain matrix, the elements of which are the strains

$\{\sigma\}$ = 6 x 1 stress matrix, the elements of which are the stresses

$[s]$ = 6 x 6 compliance matrix

Hearmon [45] uses the principle of conservation of energy to show that 6 x 6 compliance matrix $[s]$ is symmetrical and has therefore only 21 independent elements in the case of a completely anisotropic material.

The properties of graphite usually do not vary significantly between directions in a plane transverse to extrusion or pressing: in other words material is transversely isotropic. Thus, if we assume that the direction of the z axis coincides with the extrusion or pressing direction of the graphite block or fuel pin, the compliance matrix should be invariant with respect to any rotation about z - axis. It can be shown that the number of independent compliances is reduced to 5 for a transversely isotropic material. Equation (A 1.10), written in expanded form, therefore becomes:

$$\begin{Bmatrix} \varepsilon_x^e \\ \varepsilon_y^e \\ \varepsilon_z^e \\ \gamma_{yz} \\ \gamma_{zx} \\ \gamma_{xy} \end{Bmatrix} = \begin{bmatrix} s_{11} & s_{12} & s_{13} & 0 & 0 & 0 \\ s_{12} & s_{11} & s_{11} & 0 & 0 & 0 \\ s_{13} & s_{13} & s_{33} & 0 & 0 & 0 \\ 0 & 0 & 0 & s_{44} & 0 & 0 \\ 0 & 0 & 0 & 0 & s_{44} & 0 \\ 0 & 0 & 0 & 0 & 0 & 2(s_{11}-s_{12}) \end{bmatrix} \begin{Bmatrix} \sigma_x \\ \sigma_y \\ \sigma_z \\ \tau_{yz} \\ \tau_{zx} \\ \tau_{xy} \end{Bmatrix} \qquad (A\ 1.11)$$

We must now relate the elements of the compliance matrix to experimentally measured elastic constants. For graphite, the constants which are normally measured are as follows:

$E_{\parallel}$, $E_{\perp}$ = Young's modulus measured on specimens cut with their axes respectively parallel and perpendicular to the extrusion (or pressing) direction.

$\nu_{\perp\perp}$ = Poisson's ratio measured in a plane transverse to the extrusion (or pressing) direction.

$\nu_{\perp\parallel}$ = Poisson's ratio measured in a plane parallel to the extrusion (or pressing) direction: ratio of strain in the direction perpendicular to extrusion (or pressing) to strain in the direction parallel to extrusion (or pressing).

Expressing the compliances in terms of these elastic constants, we have for example:

s_{11} = strain in coordinate direction x due to unit stress in direction x

$$= \frac{1}{E_{\perp}}$$

and similarly

$$s_{12} = -\frac{\nu_{\perp\perp}}{E_{\perp}}, \quad s_{13} = -\frac{\nu_{\perp\parallel}}{E_{\perp}}, \quad s_{33} = \frac{1}{E_{\parallel}}, \quad s_{44} = \frac{1}{G} \qquad (A\ 1.12)$$

In terms of the experimentally measured elastic constants equation (A 1.11) may be written:

$$\begin{Bmatrix} \varepsilon_x^e \\ \varepsilon_y^e \\ \varepsilon_z^e \\ \gamma_{yz}^e \\ \gamma_{zx}^e \\ \gamma_{xy}^e \end{Bmatrix} = \begin{bmatrix} \frac{1}{E_\perp} & -\frac{\nu_{\perp\perp}}{E_\perp} & -\frac{\nu_{\perp\parallel}}{E_\parallel} & 0 & 0 & 0 \\ -\frac{\nu_{\perp\perp}}{E_\perp} & \frac{1}{E_\perp} & -\frac{\nu_{\perp\parallel}}{E_\parallel} & 0 & 0 & 0 \\ -\frac{\nu_{\perp\parallel}}{E_\parallel} & -\frac{\nu_{\perp\parallel}}{E_\parallel} & \frac{1}{E_\parallel} & 0 & 0 & 0 \\ 0 & 0 & 0 & 1/G & 0 & 0 \\ 0 & 0 & 0 & 0 & 1/G & 0 \\ 0 & 0 & 0 & 0 & 0 & \frac{2(1+\nu_{\perp\perp})}{E_\perp} \end{bmatrix} \begin{Bmatrix} \sigma_x \\ \sigma_y \\ \sigma_z \\ \tau_{yz} \\ \tau_{zx} \\ \tau_{xy} \end{Bmatrix} \qquad \text{(A 1.13)}$$

Equation (1.13) can be regarded as origin for deriving all $[D]$ matrices for plane stress/strain and axi-symmetrical geometry for fully isotropic and transversely isotropic materials.
Eq. (A 1.11) or (A 1.13) can be written in symbolic form also:

$$\{\sigma\} = [s]^{-1} \quad \{\varepsilon\} = [D] \quad \{\varepsilon\} \qquad \text{(A 1.14)}$$

or

$$[s]^{-1} = [D] \qquad \text{(A 1.15)}$$

By omitting the corresponding rows and columns of matrix $[s]$ for plane stress/strain and axi-symmetric geometry and by inverting it, the corresponding matrix $[D]$ can be obtained.

Thus, for example, for plane strain and transversely isotropic material the forth and fifth columns and rows of matrix $[s]$ have to be omitted and after inversion matrix $[D]$ is as follows:

$$D = \frac{\begin{bmatrix} 1-m^2\nu_{\perp\parallel}^2 & \nu_{\perp\perp}+m^2\nu_{\perp\parallel}^2 & \nu_{\perp\perp}(1+\nu_{\perp\perp}) & 0 \\ \nu_{\perp\perp}+m^2\nu_{\perp\parallel}^2 & 1-m^2\nu_{\perp\parallel}^2 & \nu_{\perp\parallel}(1+\nu_{\perp\perp}) & 0 \\ (1+\nu_{\perp\perp}) & \nu_{\perp\parallel}(1+\nu_{\perp\perp}) & -\frac{1}{2}(1-\nu_{\perp\perp}^2) & 0 \\ 0 & 0 & 0 & \frac{1}{2}-(1-\nu_{\perp\perp}-2m^2\nu_{\perp\parallel}^2) \end{bmatrix}}{(1+\nu_{\perp\perp})(1-\nu_{\perp\perp}-2m^2\nu_{\perp\parallel}^2)} \qquad \text{(A 1.16)}$$

where $m^2 = E_\perp / E_\parallel$

If material is fully isotropic $E_{\perp} = E_{\parallel} = E$ and $\nu_{\perp\parallel} = \nu_{\perp\perp} = \nu$ and the above matrix $[D]$ for plane strain simplifies to:

$$D = \frac{E(1-\nu)}{(1+\nu)(1-2\nu)} \begin{bmatrix} 1 & \nu/(1-\nu) & \nu/(1+\nu) & 0 \\ \nu/(1-\nu) & 1 & \nu/(1+\nu) & 0 \\ \nu/(1+\nu) & \nu/(1+\nu) & 1 & 0 \\ 0 & 0 & 0 & (1-2\nu)/2(1-\nu) \end{bmatrix} \quad \text{(A1.17)}$$

In a similar way the matrices $[D]$ can be derived for plane stress and axi-symmetric geometry, for transversely isotropic or fully isotropic materials.

A 1.2.3 Creep Strain matrix

As derived by Head [2] for a transversely isotropic Maxwell material the creep compliance matrix in 2 dimensions is of the form:

$$\begin{Bmatrix} \dot{\varepsilon}_x^c \\ \dot{\varepsilon}_y^c \\ \dot{\varepsilon}_z^c \\ \dot{\gamma}_{xy}^c \end{Bmatrix} = \begin{bmatrix} q_{11} & q_{12} & q_{13} & 0 \\ q_{12} & q_{11} & q_{13} & 0 \\ q_{13} & q_{13} & q_{33} & 0 \\ 0 & 0 & 0 & 2(q_{11}-q_{12}) \end{bmatrix} \begin{Bmatrix} \sigma_x \\ \sigma_y \\ \sigma_z \\ \tau_{xy} \end{Bmatrix} \quad \text{(A 1.18)}$$

where the dot indicates the rate of change with respect to neutron dose. Compliances q_{11} and q_{33} have been measured experimentally, but compliances q_{12} and q_{13} have not been measured.

In this analysis, q_{12} and q_{13} were obtained by assuming that creep occurs at constant volume. There is some evidence that this is the case for pyrocarbon (see Kaae [46]). Kelly has suggested recently that nuclear graphite exhibits a volume change, and that compliances q_{12} and q_{13} are related to q_{11} and q_{33} by the elastic Poissons ratios (see footnote, Ch.3.3.2.3.5).

The assumption that there is no permanent volume change implies additional relationships between the elements of the creep compliance matrix. The rate of change of volume of an element of material will be:

$$\dot{\varepsilon}_x^c + \dot{\varepsilon}_y^c + \dot{\varepsilon}_z^c = (q_{11}+q_{12}+q_{13})(\sigma_x+\sigma_y) + (2q_{13}+q_{33})\sigma_z \qquad \text{(A 1.19)}$$

If the right hand side of equation (A 1.19) is to be zero for all stress conditions, the following equations between the creep compliances must be satisfied:

$$\begin{aligned} q_{11} + q_{12} + q_{13} &= 0 \\ 2q_{13} + q_{33} &= 0 \end{aligned} \qquad \text{(A 1.20)}$$

Using equations (A 1.20) to eliminate q_{12} and q_{13} and multiplying the right hand side by the neutron dose increment, equation (A 1.18) can be written as follows:

$$\begin{Bmatrix} \delta\varepsilon_x^c \\ \delta\varepsilon_y^c \\ \delta\varepsilon_z^c \\ \delta\gamma_{xy}^c \end{Bmatrix} = \delta(De) \begin{bmatrix} q_{11} & -(q_{11}-q_{33}/2) & -q_{33}/2 & \\ -(q_{11}-q_{33}/2) & q_{11} & -q_{33}/2 & \\ -q_{33}/2 & -q_{33}/2 & q_{33} & \\ 0 & 0 & 0 & 4q_{11}-q_{33} \end{bmatrix} \begin{Bmatrix} \sigma_x \\ \sigma_y \\ \sigma_z \\ \tau_{xy} \end{Bmatrix} \qquad \text{(A.1.21)}$$

Introducing a simplified notation:

$$\begin{aligned} U &= q_{11} - q_{33}/2 \\ V &= q_{33}/2 \end{aligned} \qquad \text{(A 1.22)}$$

the equation (3.13) are obtained:

$$\begin{Bmatrix} \delta\varepsilon_x^c \\ \delta\varepsilon_y^c \\ \delta\varepsilon_z^c \\ \delta\gamma_{xy}^c \end{Bmatrix} = \delta(De) \begin{bmatrix} (U+V), & -U, & -V, & 0 \\ -U, & (U+V), & -V, & 0 \\ -V, & -V, & 2V, & 0 \\ 0, & 0, & 0, & (4U+2V) \end{bmatrix} \begin{Bmatrix} \sigma_x \\ \sigma_y \\ \sigma_z \\ \tau_{xy} \end{Bmatrix} \qquad \text{(A 1.23)}$$

If the material is fully isotropic U = V and the eq. 3.13 is simplified.

Equation (A 1.21) is the required flow rule from which the incremental creep strains can be derived.

A 1.3 Stress resultants and element stiffness

The corner forces expressed in terms of three components of stress are given in Ch.3 (eqs. 3.14 and 3.27), or in terms of the corner displacements, for plane stress/strain we have (eqs 3.16

$$\{S\} = [B]^T [D][B]\{\delta\} \qquad \text{(A 1.24)}$$

and for axisymmetrical geometry (eq.3.31) we have:

$$\{S\} = -2\pi \Delta [B]^T \bar{r} [D] [\bar{B}] \{\delta\} \qquad \text{(A 1.25)}$$

or in both cases (eq. 3.17 and 3.32)

$$\{S\} = [k] \{\delta\} \qquad \text{(A 1.26)}$$

where $[k]$ is the stiffness matrix for one element.

For plane strain and isotropic material the detailed form of eq's is as follows:

$$[k] = 1/2 \underbrace{\begin{bmatrix} (y_j-y_k), & 0 & -(x_j-x_k) \\ 0 & -(x_j-x_k), & (y_j-y_k) \\ -(y_i-y_k), & 0 & (x_i-x_k) \\ 0 & (x_i-x_k), & -(y_i-y_k) \\ (y_i-y_j), & 0 & -(x_i-x_j) \\ -0 & -(x_i-x_j), & (y_i-y_j) \end{bmatrix}}_{\Delta \cdot [B]^T} \cdot \underbrace{\frac{E}{(1+\nu)(1-2\nu)} \begin{bmatrix} 1-\nu & \nu & 0 \\ \nu & 1-\nu & 0 \\ 0 & 0 & \frac{1-2\nu}{2} \end{bmatrix}}_{[D]} \cdot$$

$$\cdot \underbrace{\frac{1}{x_j y_k - x_x y_j} \begin{bmatrix} y_j-y_k & 0 & -(y_i-y_k) & 0 & -(y_j-y_k) & 0 \\ 0 & -(x_j-x_k) & 0 & (x_i-x_k) & 0 & -(x_i-x_j) \\ -(x_i-x_k) & (y_j-y_k) & (x_i-x_k) & -(y_i-y_k) & -(x_i-x_j) & -(y_j-y_k) \end{bmatrix}}_{[B]} \qquad \text{(A 1.27)}$$

and

$$\{\delta\} = \begin{Bmatrix} u_i \\ v_i \\ u_j \\ v_j \\ u_k \\ v_k \end{Bmatrix} \qquad \text{(A 1.28)}$$

For different plane cases (plane stress, transversely isotropic material etc) only matrix $[D]$ have to be replaced.

$[D]$ is here a 3 x 3 matrix, see footnote Ch.3.3.2.4

For axisymmetrical geometry:

$$\left[\bar{B}\right] = -\frac{1}{2\Delta} \cdot$$

$$\cdot\begin{bmatrix} 0 & ,-(r_j-r_k), & 0 & ,(r_i-r_k), & 0 & ,-(r_i-r_j) \\ (z_j-z_k) & , 0 & ,-(z_i-z_k) & , 0 & , (z_i-z_j), & 0 \\ (r_jz_k-r_kz_j)/r_j+ & , 0 & ,(z_k-r_k\cdot\frac{z}{r}), & 0 & ,r_j\cdot\frac{z}{r}-z_j), & 0 \\ +(z_j-z_k)-(r_j-r_k)/r, & & & & & \\ -(r_j-r_k) & , (z_j-z_k),(r_i-r_k) & ,-(z_i-z_k),-(r_i-r_j),(z_i-z_j) & & & \end{bmatrix}$$

(A 1.29)

where

$$\frac{1}{2\Delta} = \frac{1}{r_i(z_j-z_k)-r_j(z_i-z_k)+r_k(z_i-z_j)} \qquad \text{(A 1.30)}$$

and

$$\Delta \cdot \left[\bar{B}\right]^T =$$

$$= \frac{1}{2}\cdot\begin{bmatrix} 0 & ,(z_j-z_k), & \frac{r_jz_k-r_kz_j}{r}+(z_j-z_k)-(r_i-r_k)\cdot\frac{z}{r}, & -(r_i-r_k) \\ -(r_j-r_k), & 0 & , 0 & , (z_j-z_k) \\ 0 & ,-(z_i-z_k), & (z_k-r_k\cdot\frac{z}{r}) & , (r_i-r_k) \\ -(r_i-r_k), & 0 & , 0 & ,-(z_i-z_k) \\ 0 & , (z_i-z_j), & (r_j\cdot\frac{z}{r}-z_j) & ,-(r_i-r_j) \\ -(r_i-r_j), & 0 & , 0 & , (z_i-z_j) \end{bmatrix} \qquad \text{(A 1.31)}$$

The detailed expression for corner forces $\{S\}$ can be derived from eq. (3.32). The matrix $[D]$ can be derived from eq.A 1.13.

APPENDIX II

LISTING OF PROGRAMS STAG

(ITERATIVE AND DIRECT VERSION)

```
JOB(UMEM040,J12,CM40000,T500)                    JEZERNIK , STAG , ITERATIVE
FUN(S,,,,,,11554)
LGO.
'
      PROGRAM STAG (INPUT,OUTPUT,TAPE5=INPUT,TAPE6=OUTPUT)
      DIMENSION TAE(10),RCEN(10),HEADX(6)
     1,HEADY(6),TITLE(6),XLIM(2),YLIM(2)
      DIMENSION NPNUM(300),DSX(300),DSY(300),XLOAD(300),YLOAD(300)
      DIMENSION NUME(500),SIGXX(500),SIGYY(500),SIGXY(500),SLOPE(300)
     1,SIGZZ(500),NPB(300),NFIX(300),      LM(3),A(6,6),S(6,6),B(6,6)
     2,ECX(500),ECY(500),ECXY(500),ECZ(500),COC(500)
     3,STXR(500),STYR(500),STZR(500),STXYR(500)
     4,NOW(50)
      COMMON NPI(500),NPJ(500),NPK(500),XORD(300),YORD(500),TIEL(500)
     1,TAEL(500),EWX(500),EWZ(500),JO,QC,QG,NUMEL,NUMNP,TOS,DOSE,NUSIZE
     2,NURAE,NUSEC,NUELE
      COMMON C11,C12,C13,C14,C15,C16,C17,C18,C19,C20,C21,C22,C23,C24,C25
     1,C26,C27,C28,C29,C30,C31,C32,C33,C34,C35,C36,C37,C38,C39,C40,C41
     2,C42,C43,C44,C45,C46,C47,C48,C49,C50,C51,C52,C53,C54,C55,C56,C57
C
C     READ AND PRINT OF DATA
      READ(5,31) ARA,AZA,ARB,ARC
      QG=2.
      NUSIZE=1
      NWRITE=2
      NUMEL=108
      NUMNP=76
      NUMBC=8
      NOPIN=1000
      NCPIN=1000
      NCYCM=2000
      PRESS=10.
      NBNP=58
      TOLER=0.00002
      XFAC=1.85
      DATA(E900(J),J=1,2)/0.862,1.0344/
      DO 36 J=3,17
   36 E900(J)=1.0689
      DATA(E900(J),J=18,41) /1.077,1.086,1.103,1.125,1.155,1.198,
     11.241,1.293,1.345,1.414,1.474,1.526,1.577,1.625,1.672,1.715,
     21.758,1.802,1.821,1.824,1.827,1.83,1.832,1.833/
      DO 37 J=1,26
   37 E1200(J)=E900(J)
      DATA(E1200(J),J=27,41) /1.396,1.439,1.483,1.513,1.534,1.552,
     11.569,1.577,1.586,1.59,1.595,1.595,1.595,1.595,1.59/
      DO 38 J=1,41
      E900(J)=E900(J)*1000000.
   38 E1200(J)=E1200(J)*1000000.
      WRITE(6,31) (E900(I),I=1,41)
      WRITE(6,31) (E1200(I),I=1,41)
      WRITE(6,11)NUMEL
      WRITE(6,12)NUMNP
      WRITE(6,13)NUMBC
      WRITE(6,14)NCPIN
      WRITE(6,15)NOPIN
      WRITE(6,16)NCYCM
      WRITE(6,17)TOLER
      WRITE(6,18)XFAC
      DATA (NPB(L),L=1,8)/1,2,3,4,73,74,75,76/
```

```
      DO 45 L=1,8
      NFIX(L)=1
   45 CONTINUE
      READ(5,36) E,PR
      READ(5,36) CU
   36 FORMAT(2F15.4)
      READ(5,31)C11,C12,C13,C14,C15,C16,C17,C18,C19,C20,C21,C22,C23,C24,
     1C25
      READ(5,31)C26,C27,C28,C29,C30,C31,C32,C33,C34,C35,C36,C37,C38,
     1C39,C40,C41,C42,C43,C44,C45,C46,C47,C48,C49,C50,C51,C52,C53,
     2C54,C55,C56,C57
      DO 46 JO=1,50
   46 NOW(JO)=0.0
      DO 47 JO=5,30,5
   47 NOW(JO)=JO
      CALL MESHR
      DO 700 MOVE=1,8
      READ(5,32) INC,POS,QC,TOS
      DO 700 JO=1,40
      ETX=1
      STEP=FLOAT(INC)
      MA=INC*(JO-1)
      DOSE=FLOAT(MA)
      CALL TEMPRI
      IF(JO.LE.1) GO TO 52
      CALL WIGN
      GO TO 56
   52 CONTINUE
      DO 55 I=1,NUMEL
      EWX(I)=0.0
      EWZ(I)=0.0
      ECX(I)=0.0
      ECY(I)=0.0
      ECXY(I)=0.0
      ECZ(I)=0.0
   55 CONTINUE
   56 CONTINUE
      IF(JO-1) 62,62,59
   59 DO 60 I=1,NUMEL
   60 CONTINUE
   62 CONTINUE
      DO 57 M=1,NUMNP
      XLOAD(M)=0.0
      YLOAD(M)=0.0
      DSX(M)=0.0
      DSY(M)=0.0
   57 CONTINUE
      SURF=0.0
      DO 180 N=1,NUMEL
      IF(TAEL(N).LE.900.) GO TO 109
      E=E900(JO)-((E900(JO)-E1200(JO))*(TAEL(N)-900.))/300.
      GO TO 110
  109 E=E900(JO)
  110 CONTINUE
      IF(ETX.EQ.0.0) GO TO 65
      TADA=TAEL(N)-500.
      ARTO=ARA+ARB*TADA
      AZTO=AZA+ARC*TADA
      TADB=TAEL(N)-20.
```

```
      ETX=ARTO*TADB
      ETZ=AZTO*TADB
   65 CONTINUE
      I=NPI(N)
      J=NPJ(N)
      K=NPK(N)
      AJ=XORD(J)-XORD(I)
      AK=XORD(K)-XORD(I)
      BJ=YORD(J)-YORD(I)
      BK=YORD(K)-YORD(I)
      SUR=(AJ*BK-BJ*AK)/2.
      CU=CV=FUNCT0(TAEL(I),DOSE)
      CW=4.*CU+2.*CV
      ECX(I)=FUNCT1(CU,CV,STXR(I),STYR(I),STZR(I),STEP,1)
      ECY(I)=FUNCT1(CU,CV,STXR(I),STYR(I),STZR(I),STEP,2)
      ECZ(I)=FUNCT1(CV,CV,STXR(I),STYR(I),STZR(I),STEP,3)
      ECXY(I)=FUNCT1(CW,0.,STXYR(I),0.,0.,STEP,4)
      XLOAD(I)=FUNCT2(ETX,ETY,EWX(N),EWY(N),ECX(N),ECY(N),ECXY(N),
     1 XORD(I),YORD(I),XORD(J),YORD(J),XORD(K),YORD(K),E,PR,1)
      YLOAD(I)=FUNCT3(ETX,ETY,EWX(N),EWY(N),ECX(N),ECY(N),ECXY(N),
     1 XORD(I),YORD(I),XORD(J),YORD(J),XORD(K),YORD(K),E,PR,1)
      XLOAD(J)=FUNCT2(ETX,ETY,EWX(N),EWY(N),ECX(N),ECY(N),ECXY(N),
     1 XORD(I),YORD(I),0.,0.,XORD(K),YORD(K),E,PR,2)
      YLOAD(J)=FUNCT3(ETX,ETY,EWX(N),EWY(N),ECX(N),ECY(N),ECXY(N),
     1 XORD(I),YORD(I),0.,0.,XORD(K),YORD(K),E,PR,2)
      XLOAD(K)=FUNCT2(ETX,ETY,EWX(N),EWY(N),ECX(N),ECY(N),ECXY(N),
     1 XORD(I),YORD(I),XORD(J),YORD(J),0.,0.,E,PR,3)
      YLOAD(K)=FUNCT3(ETX,ETY,EWX(N),EWY(N),ECX(N),ECY(N),ECXY(N),
     1 XORD(I),YORD(I),XORD(J),YORD(J),0.,0.,E,PR,3)
      SURF=SURF+SUR
  180 CONTINUE
C     TUBE UNDER INTERNAL PRESSURE
      FORCE=10.*PRESS
      DATA(NOVI(N),N=1,6)/251,259,267,275,283,284/
      DO 120 N=7,21
  120 NOVI(N)=N+286
      DATA(NOVI(N),N=22,37)/285,286,276,268,260,252,244,236,228,220,211,
     1210,199,198,185,184/
      DO 121 N=38,48
  121 NOVI(N)=206-N
      DATA(NOVI(N),N=49,60)/182,183,196,197,208,209,219,227,235,243,
     1251,259/
      XCEN=3.3465-1.935*COS(0.39270)
      YCEN=1.935*SIN(0.39270)
      RA=0.6025
      DO 130 N=1,NBNP
      I=NOVI(N)
      J=NOVI(N+1)
      K=NOVI(N+2)
      XA=XORD(I)-XORD(J)
      YA=YORD(I)-YORD(J)
      XYA=SQRT(XA**2+YA**2)
      XB=XORD(J)-XORD(K)
      YB=YORD(J)-YORD(K)
      XYB=SQRT(XB**2+YB**2)
  130 FANOD(N+1)=(XYA+XYB)/2.
      FANOD(1)=FANOD(NBNP+1)
      DO 140 N=1,NBNP
      ASIGN=1.
```

```
      BSIGN=1.
      CSIGN=1.
      I=NOVI(N)
      IF(XORD(I).LT.XCEN)ASIGN=-1
      DSA=(XORD(I)-XCEN)*ASIGN
      ALFA(N)=ASIN(DSA/RA)
      IF(XORD(I).LT.XCEN) BSIGN=-1.
      IF(YORD(I).LT.YCEN) CSIGN=-1.
      AXLOAD=FORCE*SIN(ALFA(N))*BSIGN*FANOD(N)
      AYLOAD=FORCE*COS(ALFA(N))*CSIGN*FANOD(N)
      XLOAD(I)=XLOAD(I)+AXLOAD
      YLOAD(I)=YLOAD(I)+AYLOAD
  140 CONTINUE
      WRITE(6,25) (XLOAD(I),I=1,NUMNP)
      WRITE(6,25) (YLOAD(I),I=1,NUMNP)
  141 CONTINUE
C     INITIALIZATION
      NCYCLE=0
      NUMPT=NCPIN
      NUMOPT=NOPIN
      DO 175 L=1,NUMNP
      DO 170 M=1,9
      SXX(L,M)=0.0
      SYX(L,M)=0.0
      SXY(L,M)=0.0
      SYY(L,M)=0.0
  170 NP(L,M)=0
      NP(L,10)=0
  175 NP(L,1)=L
C     FORMATION OF STIFFNESS ARRAY
      DO 200 N=1,NUMEL
      IF(TAEL(N).LE.900.) GO TO 177
      E=E900(JO)-((E900(JO)-E1200(JO))*(TAEL(N)-900.))/300.
      GO TO 178
  177 E=E900(JO)
  178 CZ=E
      I=NPI(N)
      J=NPJ(N)
      K=NPK(N)
      AJ=XORD(J)-XORD(I)
      AK=XORD(K)-XORD(I)
      BJ=YORD(J)-YORD(I)
      BK=YORD(K)-YORD(I)
      SUR=(AJ*BK-BJ*AK)/2.
      COC(N)=(SUR*NUMEL)/SURF
      COMM=0.25*E*(1.-PR)/((1.+PR)*(1.-2.*PR)*SUR)
      A(1,1)=BJ-BK
      A(1,2)=0.0
      A(1,3)=BK
      A(1,4)=0.0
      A(1,5)=-BJ
      A(1,6)=0.0
      A(2,1)=0.0
      A(2,2)=AK-AJ
      A(2,3)=0.0
      A(2,4)=-AK
      A(2,5)=0.0
      A(2,6)=AJ
      A(3,1)=AK-AJ
```

```
      A(3,2)=BJ-BK
      A(3,3)=-AK
      A(3,4)=BK
      A(3,5)=AJ
      A(3,6)=-BJ
      B(1,1)=COMM
      B(1,2)=COMM*PR/(1.-PR)
      B(1,3)=0.0
      B(2,1)=B(1,2)
      B(2,2)=COMM
      B(2,3)=0.0
      B(3,1)=0.0
      B(3,2)=0.0
      B(3,3)=COMM*(1.-2.*PR)/(2.*(1.-PR))
      DO 182 J=1,6
      DO 182 I=1,3
      S(I,J)=0.0
      DO 182 K=1,3
  182 S(I,J)=S(I,J)+B(I,K)*A(K,J)
      DO 183 J=1,6
      DO 183 I=1,3
  183 B(J,I)=S(I,J)
      DO 184 J=1,6
      DO 184 I=I,6
      S(I,J)=0.0
      DO 184 K=1,3
  184 S(I,J)=S(I,J)+B(I,K)*A(K,J)
C
      LM(1)=NPI(N)
      LM(2)=NPJ(N)
      LM(3)=NPK(N)
      DO 200 L=1,3
      DO 200 M=1,3
      LX=LM(L)
      MX=0
  185 MX=MX+1
      IF(NP(LX,MX)-LM(M)) 190,195,190
  190 IF(NP(LX,MX)) 185,195,185
  195 NP(LX,MX)=LM(M)
      IF (MX-10) 196,702,702
  196 SXX(LX,MX)=SXX(LX,MX)+S(2*L-1,2*M-1)
      SXY(LX,MX)=SXY(LX,MX)+S(2*L-1,2*M)
      SYX(LX,MX)=SYX(LX,MX)+S(2*L,2*M-1)
  200 SYY(LX,MX)=SYY(LX,MX)+S(2*L,2*M)
C     COUNT OF ADJACENT NODAL POINTS
      DO 206 M=1,NUMNP
      MX =1
  205 MX=MX+1
      IF (NP(M,MX)) 206,206,205
  206 NAP(M)=MX-1
C
C     INVERSION OF NODAL POINT STIFFNESS
      DO 210 M=1,NUMNP
      COMM=SXX(M,1)*SYY(M,1)-SXY(M,1)*SYX(M,1)
      TEMP=SYY(M,1)/COMM
      SYY(M,1)=SXX(M,1)/COMM
      SXX(M,1)=TEMP
      SXY(M,1)=-SXY(M,1)/COMM
  210 SYX(M,1)=-SYX(M,1)/COMM
```

```
C       MODIFICATION OF BOUNDARY FLEXIBILITIES
        DO 240 L=1,NUMBC
        M=NPB(L)
        NP(M,1)=0
        IF(NFIX(L)-1)225,220,215
  215 C=(SXX(M,1)*SLOPE(L)-SXY(M,1))/(SYX(M,1)*SLOPE(L)-SYY(M,1))
        R=1.0-C*SLOPE(L)
        SXX(M,1)=(SXX(M,1)-C*SYX(M,1))/R
        SXY(M,1)=(SXY(M,1)-C*SYY(M,1))/R
        SYX(M,1)=SXX(M,1)*SLOPE(L)
        SYY(M,1)=SXY(M,1)*SLOPE(L)
        GO TO 240
  220 SYY(M,1)=SYY(M,1)-SYX(M,1)*SXY(M,1)/SXX(M,1)
        GO TO 230
  225 SYY(M,1)=0.0
  230 SXX(M,1)=0.0
  235 SXY(M,1)=0.0
        SYX(M,1)=0.0
  240 CONTINUE
C
C       ITERATION ON NODAL POINT DISPLACEMENTS
C
  243 WRITE(6,21)
  244 SUM=0.0
        SUMD=0.
        DO 290 M=1,NUMNP
        NUM=NAP(M)
        IF (SXX(M,1)+SYY(M,1)) 275,290,275
  275 FRX=XLOAD(M)
        FRY=YLOAD(M)
        DO 280 L=2,NUM
        N=NP(M,L)
        FRX=FRX-SXX(M,L)*DSX(N)-SXY(M,L)*DSY(N)
  280 FRY=FRY-SYX(M,L)*DSX(N)-SYY(M,L)*DSY(N)
  281 DX=SXX(M,1)*FRX+SXY(M,1)*FRY-DSX(M)
        DY=SYX(M,1)*FRX+SYY(M,1)*FRY-DSY(M)
  297 DSX(M)=DSX(M)+XFAC*DX
        DSY(M)=DSY(M)+XFAC*DY
        SUMD=SUMD+ABS(DSX(M))+ABS(DSY(M))
        IF(NP(M,1))285,290,285
  285 SUM=SUM+ABS(DX)+ABS(DY)
  290 CONTINUE
        SUM=SUM/SUMD
C
C       CYCLE COUNT AND PRINT CHECK
C
        NCYCLE=NCYCLE +1
        IF (NCYCLE-NUMPT) 305,300,300
  300 NUMPT=NUMPT+NCPIN
        WRITE(6,22) NCYCLE,SUM,SUMD
  305 IF(SUM-TOLER) 400,400,310
  310 IF(NCYCM-NCYCLE)400,400,315
  315 IF (NCYCLE-NUMOPT) 244,320,320
  320 NUMOPT=NUMOPT+NOPIN
C
C       PRINT OF DISPLACEMENTS AND STRESSES
C
  400 CONTINUE
```

```
      CZ=1330000.
      P=0.0
      DO 390 I=1,NUMEL
      IF(ETX.EQ.0.0) GO TO 388
      TADA=TAEL(I)-500.
      AZTO=AZA+ARC*TADA
      TADB=TAEL(I)-20.
      ETZ=AZTO*TADB
  388 CONTINUE
      P=P+(ETZ+EWZ(I)+ECZ(I))*CZ*COC(I)
  390 CONTINUE
  672 IF(JO.GT.1) GO TO 676
      WRITE(6,673)POS
  673 FORMAT(1H0,18H CHANNEL POSITION ,F5.1,3H CM)
  676 WRITE(6,679) JO,DOSE
  679 FORMAT(17H0 INTERVAL NUMBER,I3,18H   EQUIVALENT DOSE,F8.1)
      NCASE=NWRITE/2
      GO TO (680,682,684) NCASE
  680 WRITE(6,681)
  681 FORMAT(2(67H ELEM NODE NO TEMP  X-, Y-, MAX-, MIN-, Z-, AND XY-, S
     1TRESSES ANGLE))
      GO TO 685
  682 WRITE(6,683)
  683 FORMAT(4(33H ELEM  PRINCIPAL STRESSES 1,2,3,  ))
      GO TO 685
  684 CONTINUE
  685 CONTINUE
      K1=1
      K2=2
      K3=3
      K4=4
      DO 420 N=1,NUMEL
      IF(TAEL(N).LE.900.) GO TO 402
      E=E900(JO)-((E900(JO)-E1200(JO))*(TAEL(N)-900.))/300.
      GO TO 403
  402 E=E900(JO)
  403 CZ=E
      NUME(N)=N
      IF(ETX.EQ.0.0) GO TO 690
      TADA=TAEL(N)-500.
      ARTO=ARA+ARB*TADA
      AZTO=AZA+ARC*TADA
      TADB=TAEL(N)-20.
      ETX=ARTO*TADB
      ETZ=AZTO*TADB
  690 CONTINUE
      I=NPI(N)
      J=NPJ(N)
      K=NPK(N)
      AJ=XORD(J)-XORD(I)
      AK=XORD(K)-XORD(I)
      BJ=YORD(J)-YORD(I)
      BK=YORD(K)-YORD(I)
      EPX=FUNCT4(YORD(I),YORD(J),YORD(K),DSX(I),DSX(J),DSX(K),1)
      EPY=FUNCT4(XORD(I),XORD(J),XORD(K),DSY(I),DSY(J),DSY(K),2)
      GAM=FUNCT5(XORD(I),XORD(J),XORD(K),YORD(I),YORD(J),YORD(K),DSX(I),
     1 DSX(I),DSY(I),DSX(J),DSY(J),DSX(K),DSY(K))
      X=FUNCT6(EPX,EPY,ETX,ETY,EWX(N),EWY(N),ECX(N),ECY(N),ECXY(N),E,PR,
     1 XORD(I),XORD(J),XORD(K),YORD(I),YORD(J),YORD(K),1)
```

```
      Y=FUNCT6(EPX,EPY,ETX,ETY,EWX(N),EWY(N),ECX(N),ECY(N),ECXY(N),E,PR,
     1 XORD(I),XORD(J),XORD(K),YORD(I),YORD(J),YORD(K),2)
      XY=FUNCT7(GAM,ECXY(N),E,PR,XORD(I),XORD(J),XORD(K),YORD(I),YORD(J)
     1,YORD(K))
      SIGXX(N)=X
      SIGYY(N)=Y
      SIGXY(N)=XY
      C=(X+Y)/2.0
      R=SQRT(((Y-X)/2.0)**2+XY**2)
      XMAX=C+R
      XMIN=C-R
      PA=0.5*57.29578*ATAN(2.*XY/(Y-X))
      IF(2.*X-XMAX-XMIN) 405,414,414
  405 IF (PA) 410,414,412
  410 PA=PA+90.0
      GO TO 414
  412 PA=PA-90.0
  414 CONTINUE
      SIGZZ(N)=P*COC(N)/NUMEL-(ETZ+EWZ(N)+ECZ(N))*CZ*COC(N)
     1+PR*(SIGXX(N)+SIGYY(N))
      IF(N.NE.K1) GO TO 415
      XMAXA=XMAX
      XMINA=XMIN
      PAA=PA
      K1=K1+NWRITE
  415 IF(N.NE.K2) GO TO 416
      XMAXB=XMAX
      XMINB=XMIN
      PAB=PA
      K2=K2+NWRITE
      IF(NWRITE.EQ.4) GO TO 416
      WRITE(6,4) NUME(N-1),NPI(N-1),NPJ(N-1),NPK(N-1),TAEL(N-1),
     1SIGXX(N-1),SIGYY(N-1),XMAXA,XMINA,SIGZZ(N-1),SIGXY(N-1),PAA,
     2NUME(N),NPI(N),NPJ(N),NPK(N),TAEL(N),SIGXX(N),SIGYY(N),XMAXB,
     3XMINB,SIGZZ(N),SIGXY(N),PAB
      GO TO 420
  416 CONTINUE
      IF(N.NE.K3) GO TO 417
      XMAXC=XMAX
      XMINC=XMIN
      PAC=PA
      K3=K3+NWRITE
  417 IF(N.NE.K4) GO TO 420
      XMAXD=XMAX
      XMIND=XMIN
      PAD=PA
      WRITE(6,5) NUME(N-3),XMAXA,XMINA,SIGZZ(N-3),PAA,NUME(N-2),XMAXB,
     1XMINB,SIGZZ(N-2),PAB,NUME(N-1),XMAXC,XMINC,SIGZZ(N-1),PAC,
     2NUME(N),XMAXD,XMIND,SIGZZ(N),PAD
      K4=K4+NWRITE
  420 CONTINUE
    4 FORMAT(2(I4,3I3,6F7.1,2F6.0))
    5 FORMAT(4(I5,4F7.1))
C
      IF (SUM-TOLER) 440,440,430
  430 IF (NCYCM-NCYCLE) 440,440,243
C
  440 CONTINUE
C
```

```
C      PRINT OF ERRORS IN INPUT DATA
C
  701 WRITE(6,28)
  702 WRITE(6,29)
      IF(ETX.EQ.0.0) GO TO 695
      DO 470 I=1,NUMEL
      STXR(I)=SIGXX(I)
      STYR(I)=SIGYY(I)
      STXYR(I)=SIGXY(I)
      STZR(I)=SIGZZ(I)
  470 CONTINUE
      IF(JO.NE.NOW(JO)) GO TO 695
      ETX=0.0
      ETZ=0.0
      GO TO 62
  695 CONTINUE
      CALL START(2)
      READ(5,103) (HEADX(I),I=1,6)
  103 FORMAT(6A6)
      READ(5,103) (HEADY(I),I=1,6)
      READ(5,103) (TITLE(I),I=1,6)
      READ(5,100) (XLIM(I),I=1,2),(YLIM(I),I=1,2)
  100 FORMAT(4F10.2)
      CALL CPLOT (XLIM,YLIM,2,0,HEADX,HEADY,TITLE,2,2,5)
      NPTS=3
      DO 696 I=1,3
      II=NPI(I)
      JJ=NPJ(I)
      KK=NPK(I)
      XCEN=(XORD(II)+XORD(JJ)+XORD(KK))/3.
      YCEN=(YORD(II)+YORD(JJ)+YORD(KK))/3.
      RCEN(I)=SQRT(XCEN**2+(3.12-YCEN)**2)
  696 TAE(I)=TAEL(I)
      CALL CPLOT (RCEN,TAE,NPTS,1,HEADX,HEADY,TITLE,2,2,2)
      CALL ENPLOT
  700 CONTINUE
C
C      FORMAT STATEMENTS
C
    2 FORMAT(1215)
    3 FORMAT(I5,2F15.6,I5,2F15.8)
   11 FORMAT(29HONUMBER OF ELEMENTS          =,I4/)
   12 FORMAT(29H NUMBER OF NODAL POINTS      =,I4/)
   13 FORMAT(29H NUMBER OF BOUNDARY POINTS   =,I4/)
   14 FORMAT(29H CYCLE PRINT INTERVAL        =,I4/)
   15 FORMAT(29H OUTPUT INTERVAL OF RESULTS  =,I4/)
   16 FORMAT(29H CYCLE LIMIT                 =,I4/)
   17 FORMAT(29H TOLERANCE LIMIT             =,E12.4/)
   18 FORMAT(29H OVER RELAXATION FACTOR      =1F6.3)
   20 FORMAT (20H BOUNDARY CONDITIONS)
   21 FORMAT(34H0          CYCLE      FORCE UNBALANCE)
   22 FORMAT(I11,2E20.6)
   23 FORMAT (42HONODAL POINT X-DISPLACEMENT Y-DISPLACEMENT)
   24 FORMAT(3(I11,2E15.8))
   25 FORMAT(15F9.2)
   26 FORMAT(120H1  ELEMENT              X-STRESS              Y-STRESS
     1       XY-STRESS           MAX-STRESS    MIN-STRESS        DIRECTION)
   27 FORMAT(1110,6F20.8)
   28 FORMAT (32HOZERO OR NEGATIVE AREA, EL. NO.=114)
```

```
   29 FORMAT (33HOOVER 8 N.P. ADJACENT TO N.P. NO.114)
   31 FORMAT(4E16.9)
   32 FORMAT(I10,3F10.2)
   33 FORMAT(2F15.8)
      STOP
       END



      SUBROUTINE MESHR
      DOUBLE PRECISION ALSTEP
      DIMENSION RI(20),X(300,2),NOD(500,3)
      COMMON NPI(500),NPJ(500),NPK(500),XORD(300),YORD(500),TIEL(500)
     1,TAEL(500),EWX(500),EWZ(500),JO,QC,QG,NUMEL,NUMNP,TOS,DOSE,NUSIZE
     2,NURAE,NUSEC,NUELE
      IF(NUSIZE.GT.1) GO TO 50
C     INPUT DATA LARGE MESH SIZE (108 EL,S,76 NODES-HALF TUBE)
      DATA(RI(I),I=1,4)/2.22,2.52,2.82,3.12/
      NUSEC=10
      NURAS=1
      NURAE=4
      NUJUMP=36
      NUNEXT=6
      NELEM=108
      NPOIN=76
      GO TO 52
   50 CONTINUE
C     INPUT DATA SMALL MESH SIZE (432 EL=SS,259 NODES-HALF TUBE)
      DO 51 I=2,7
      RI(I)=RI(I-1)+0.15
   51 CONTINUE
      NUSEC=19
      NURAS=1
      NURAE=7
      NUJUMP=126
      NUNEXT=12
      NELEM=432
      NPOIN=259
   52 CONTINUE
C     CALCULATION
C     ADITIONAL INPUT DATA
      NUSEGM=2*(NUSEC-1)
      TOSEGM=FLOAT(NUSEGM)
      NUELE=NURAE-1
C     CALCULATION OF COORDINATES X AND Y FOR ONE QARTER
C     ANGLE STEP
      ALSTEP=31415926.53589793/(TOSEGM*10**7)
      ALPHE=0.0
      DO 54 IB=NURAS,NURAE
      K=IB
      DO 53 IA=1,NUSEC
      X(K,1)=RI(IB)*SIN(ALPHE)
      X(K,2)=3.12-RI(IB)*COS(ALPHE)
      K=K+NURAE
      ALPHE=ALPHE+ALSTEP
   53 CONTINUE
      ALPHE=0.0
   54 CONTINUE
```

```
C       X AND Y COORDINATES IN SECOND QARTER
        DO 56 ID=NURAS,NURAE
        K=ID+NUJUMP
        DO 55 IC=1,NUSEC
        X(K,1)=RI(ID)*COS(ALPHE)
        X(K,2)=3.12+RI(ID)*SIN(ALPHE)
        K=K+NURAE
        ALPHE=ALPHE+ALSTEP
   55   CONTINUE
        ALPHE=0.0
   56   CONTINUE
C       CALCULATION OF NODE NO'S FOR ONE HALF OF TUBE
        K=0
        DO 61 IE=1,NUSEGM
        NEW1=NUNEXT*(IE-1)
        NEW2=NEW1+NUELE
        DO 60 IG=1,NUELE
        NOD(IG+NEW1,1)=IG+K
        NOD(IG+NEW1,2)=IG+K+NURAS
        NOD(IG+NEW1,3)=IG+K+ NURAE
        NOD(IG+NEW2,1)=IG+K+NURAE
        NOD(IG+NEW2,2)=IG+K+NURAS
   60   NOD(IG+NEW2,3)=IG+K+NURAS+NURAE
   61   K=K+NURAE
C       WRITING AND PUNCHING OF RESULTS
    2   FORMAT(3(I8,3I5))
    3   FORMAT(I5,2F15.8,I5,2F15.8)
   70   CONTINUE
        DO 72 I=1,NUMNP
        XORD(I)=X(I,1)
   72   YORD(I)=X(I,2)
        DO 74 J=1,NUMEL
        NPI(J)=NOD(J,1)
        NPK(J)=NOD(J,2)
   74   NPJ(J)=NOD(J,3)
        RETURN
         END


        SUBROUTINE TEMPR
        DIMENSION CDD(50),QCC(50),QGG(50),XB(20),TCB(20),TCD(20),TCE(20),
       1TCF(20),DEB(20),DEC(20),DED(20),DSQA(20),DSQB(20),DCUA(20),
       2DA(50),DD(50),DC(50),TCA(20),TC(19),XA(19),R(20),TA(20),TI(20)
       3,TINOD(150),TANOD(150),TINODE(3),TANODE(3)
        COMMON NPI(500),NPJ(500),NPK(500),XORD(300),YORD(500),TIEL(500)
       1,TAEL(500),EWX(500),EWZ(500),JO,QC,QG,NUMEL,NUMNP,TOS,DOSE,NUSIZE
       2,NURAE,NUSEC,NUELE
        COMMON C11,C12,C13,C14,C15,C16,C17,C18,C19,C20,C21,C22,C23,C24,C25
       1,C26,C27,C28,C29,C30,C31,C32,C33,C34,C35,C36,C37,C38,C39,C40,C41
       2,C42,C43,C44,C45,C46,C47,C48,C49,C50,C51,C52,C53,C54,C55,C56,C57
        DATA (R(I),I=1,7)/2.22,2.37,2.52,2.67,2.82,2.97,3.12/
        J=JO
        TI(7)=TOS
        IF(J.GT.1) GO TO 161
       DO 160 K=1,6
        I=7-K
        XA(I)=(TI(I+1)+3.)/1000.
        TC(I)=(C13*XA(I)+C12)*XA(I)+C11
```

```
      TI(I)=TI(I+1)+0.159155*(QC+QG*(R(I)**2-R(1)**2)*3.14159)
     1*ALOG(R(I+1)/R(I))/TC(I)+0.25*QG*(R(I+1)**2-R(I)**2
     .2-2.*R(I)**2*ALOG(R(I+1)/R(I)))/TC(I)
  160 CONTINUE
  161 CONTINUE
      CDD(J)=1.-(DOSE-10000.)/20000.
      QCC(J)=QC-0.5*QC*DOSE/40000.
      QGG(J)=QG-0.5*QG*DOSE/40000.
      TA(7)=TOS
      DO 250 K=1,6
      I=7-K
      IF(TOS.LT.820.) GO TO 211
      XB(I)=(TA(I+1)+3.)/1000.
      GO TO 214
  211 XB(I)=(TA(I+1)+4.)/1000.
  214 TCB(I)=(C13*XB(I)+C12)*XB(I)+C11
      TCD(I)=(C19*XB(I)+C18)*XB(I)+C17
      TCE(I)=(C22*XB(I)+C21)*XB(I)+C20
      TCF(I)=(C25*XB(I)+C24)*XB(I)+C23
      DEB(I)=TCD(I)-TCB(I)
      DEC(I)=TCE(I)-TCD(I)
      DED(I)=TCF(I)-TCE(I)
      DSQA(I)=DEC(I)-DEB(I)
      DSQB(I)=DED(I)-DEC(I)
      DCUA(I)=DSQB(I)-DSQA(I)
      IF(DOSE.GT.5000.) GO TO 215
      DA(J)=DOSE/5000.
      DD(J)=DA(J)*(DA(J)-1.)/2.
      DC(J)=DA(J)*(DA(J)-1.)*(DA(J)-2.)/6.
      TCA(I)=TCB(I)+DA(J)*DEB(I)+DD(J)*DSQA(I)+DC(J)*DCUA(I)
      GO TO 217
  215 IF(DOSE.GT.10000.) GO TO 216
      DA(J)=(DOSE-5000.)/5000.
      DD(J)=DA(J)*(DA(J)-1.)/2.
      DC(J)=DA(J)*(DA(J)+1.)*(DA(J)-1.)/6.
      TCA(I)=TCD(I)+DA(J)*DEC(I)+DD(J)*DSQA(I)+DC(J)*DCUA(I)
      GO TO 217
  216 TCA(I)=TCF(I)+(TCE(I)-TCF(I))*CDD(J)
  217 TA(I)=TA(I+1)+0.159155*(QCC(J)+QGG(J)*(R(I)**2-R(1)**2)*3.14159)
     1*ALOG(R(I+1)/R(I))/TCA(I)+0.25*QGG(J)*(R(I+1)**2-R(I)**2
     2-2.*R(I)**2*ALOG(R(I+1)/R(I)))/TCA(I)
  250 CONTINUE
      L=0
      DO 260 I=1,NURAE
      TINOD(I)=TI(I+L)
      TANOD(I)=TA(I+L)
      IF(NUSIZE.GT.1) GO TO 260
      L=L+1
  260 CONTINUE
      NUSEGM=2*(NUSEC-1)
      K=NURAE
      DO 262 J=1,NUSEGM
      DO 261 I=1,NURAE
      TINOD(I+K)=TINOD(I)
  261 TANOD(I+K)=TANOD(I)
      K=K+NURAE
  262 CONTINUE
      DO 265 N=1,NUMEL
      JJ=NPI(N)
```

```
      KK=NPK(N)
      LL=NPJ(N)
      TIEL(N)=(TINOD(JJ)+TINOD(KK)+TINOD(LL))/3.
      TAEL(N)=(TANOD(JJ)+TANOD(KK)+TANOD(LL))/3.
  265 CONTINUE
      RETURN
       END



      SUBROUTINE WIGN
      COMMON NPI(500),NPJ(500),NPK(500),XORD(300),YORD(500),TIEL(500)
     1,TAEL(500),EWX(500),EWZ(500),JO,QC,QG,NUMEL,NUMNP,TOS,DOSE,NUSIZE
     2,NURAE,NUSEC,NUELE
      COMMON C11,C12,C13,C14,C15,C16,C17,C18,C19,C20,C21,C22,C23,C24,C25
     1,C26,C27,C28,C29,C30,C31,C32,C33,C34,C35,C36,C37,C38,C39,C40,C41
     2,C42,C43,C44,C45,C46,C47,C48,C49,C50,C51,C52,C53,C54,C55,C56,C57
      MULE=0
      XE=DOSE/10000.
      EWRA=((C29*XE+C28)*XE+C27)*XE+C26
      EWRD=((C33*XE+C32)*XE+C31)*XE+C30
      EWRB=EWRA+(EWRD-EWRA)*100./300.
      EWRC=EWRA+(EWRD-EWRA)*200./300.
      EWRE=((C37*XE+C36)*XE+C35)*XE+C34
      EWRF=((C41*XE+C40)*XE+C39)*XE+C38
      EWZA=((C45*XE+C44)*XE+C43)*XE+C42
      EWZD=((C49*XE+C48)*XE+C47)*XE+C46
      EWZB=EWZA+(EWZD-EWZA)*100./300.
      EWZC=EWZA+(EWZD-EWZA)*200./300.
      EWZE=((C53*XE+C52)*XE+C51)*XE+C50
      EWZF=((C57*XE+C56)*XE+C55)*XE+C54
C     DIFFERENCE TABLE
      OOTR=EWRB-EWRA
      ONER=OOTR
      TWOR=OOTR
      THRR=EWRE-EWRD
      FOUR=EWRF-EWRE
      OOTZ=EWRB-EWZA
      ONEZ=OOTZ
      TWOZ=OOTZ
      THRZ=EWZE-EWZD
      FOUZ=EWZF-EWZE
      SQNOTR=0.
      SQONER=0.
      SQTWOR=THRR-TWOR
      SQTHRR=FOUR-THRR
      SQNOTZ=0.
      SQONEZ=0.
      SQTWOZ=THRZ-TWOZ
      SQTHRZ=FOUZ-THRZ
      CUNOTR=0.
      CUONER=SQTWOR
      CUTWOR=SQTHRR-SQTWOR
      CUNOTZ=0.
      CUONEZ=SQTWOZ
      CUTWOZ=SQTHRZ-SQTWOZ
      DO 350 I=1,NUMEL
      IF(TAEL(I).GT.600.) GO TO 310
```

```
      EWX(I)=EWRA
      EWZ(I)=EWZA
      GO TO 319
  310 IF(MULE.GT.1) GO TO 312
C     LINEAR INTERPOLATION
      EWX(I)=EWRA+(EWRD-EWRA)*(TAEL(I)-600.)/300.
      EWZ(I)=EWZA+(EWZD-EWZA)*(TAEL(I)-600.)/300.
      GO TO 319
C     INTERPOLATION WITH NEWTON FORWARD DIFFERENCES
  312 IF(TAEL(I).GT.900.) GO TO 313
      SA=(TAEL(I)-800.)/100.
      SB=SA*(SA-1.)/2.
      SC=SA*(SA-1.)*(SA-2.)/6.
      EWX(I)=EWRC+SA*TWOR+SB*SQTWOR+SC*CUTWOR
      EWZ(I)=EWZC+SA*TWOZ+SB*SQTWOZ+SC*CUTWOZ
      GO TO 319
C    INTERPOLATION WITH NEWTON BACKWARD DIFFERENCES
  313 IF(TAEL(I).GT.1000.) GO TO 314
      SA=(TAEL(I)-1000.)/100.
      SB=SA*(SA+1.)/2.
      SC=SA*(SA+1.)*(SA+2.)/6.
      EWX(I)=EWRE+SA*THRR+SB*SQTWOR+SC*CUONER
      EWZ(I)=EWZE+SA*THRZ+SB*SQTWOZ+SC*CUONEZ
      GO TO 319
  314 SA=(TAEL(I)-1100.)/100.
      SB=SA*(SA+1.)/2.
      SC=SA*(SA+1.)*(SA+2.)/6.
      EWX(I)=EWRF+SA*FOUR+SB*SQTHRR+SC*CUTWOR
      EWZ(I)=EWZF+SA*FOUZ+SB*SQTHRZ+SC*CUTWOZ
  319 CONTINUE
      EWX(I)=EWX(I)/100.
      EWZ(I)=EWZ(I)/100.
  350 CONTINUE
      RETURN
      END
```

```
JOB(UMEM040,J12,CM40000,T500)                    JEZERNIK , STAG , DIRECT
FUN(S,,,,,,11554)
LGO.
'
      PROGRAM STAG (INPUT,OUTPUT,TAPE5=INPUT,TAPE6=OUTPUT,TAPE2,TAPE4)
      DIMENSION STX(500),STY(500),STZ(500),STXY(500),ST1(500),ST2(500),
     1ST3(500),ECX(500),ECY(500),ECZ(500),ECXY(500),COC(500),XE(3,2)
     2,STXR(500),STYR(500),STZR(500),STXYR(500)
     3,ECXP(500),ECYP(500),ECZP(500),ECXYP(500)
     4,PAA(500),NOW(50)
      COMMON C(6,6),DBA(3,6),DB(3,6),A(6,6),B(3,6),NSTART(30),NEND(30),
     1NFIRST(30),NLAST(30),NF(90),NB(90,2),BV(90,2),X(300,2),NOD(500,3),
     2ST(40,80),U(600,1),UF(600,1),TIEL(500),TAEL(500),EWX(500),EWZ(500)
     3,JO,QC,QG,NELEM,TOS,DOSE,NUSIZE,NURAE,NUSEC,NUELE
      COMMON C11,C12,C13,C14,C15,C16,C17,C18,C19,C20,C21,C22,C23,C24,C25
     1,C26,C27,C28,C29,C30,C31,C32,C33,C34,C35,C36,C37,C38,C39,C40,C41
     2,C42,C43,C44,C45,C46,C47,C48,C49,C50,C51,C52,C53,C54,C55,C56,C57
      READ(5,31) ARA,AZA,ARB,ARC
      QG=2.0
      NUSIZE=1
      NWRITE=2
    4 FORMAT(2(I4,3I3,6F7.1,2F6.0))
    5 FORMAT(4(I5,4F7.1))
   10 FORMAT(7I5)
   11 FORMAT(8F8.4)
   12 FORMAT(3I4,2E16.8)
   13 FORMAT(2F15.4)
   14 FORMAT(4E16.9)
   15 FORMAT(10F13.8)
   16 FORMAT(20I5)
   17 FORMAT(I10,3F10.2)
   21 FORMAT(5(I4,2F10.4))
   22 FORMAT(2(I4,2F11.3,2E16.8))
   23 FORMAT(I4,13F10.7)
   24 FORMAT(4I4,9F11.2)
   25 FORMAT(15F9.2)
      DO 750 LA=1,1
      READ(5,10) NPART,NPOIN,NELEM,NBOUN,NCOLN,NFREE,NCONC
      WRITE(6,10) NPART,NPOIN,NELEM,NBOUN,NCOLN,NFREE,NCONC
      DO 42 I=1,NBOUN
      READ(5,12) NF(I),NB(I,1),NB(I,2),BV(I,1),BV(I,2)
   42 WRITE(6,12)NF(I),NB(I,1),NB(I,2),BV(I,1),BV(I,2)
      NPART1=NPART+1
      DO 44 I=1,NPART1
      READ(5,10)NSTART(I),NEND(I),NFIRST(I),NLAST(I)
   44 WRITE(6,10) NSTART(I),NEND(I),NFIRST(I),NLAST(I)
      READ(5,13) E,PR
      WRITE(6,13) E,PR
      READ(5,36) CU
      READ(5,14)C11,C12,C13,C14,C15,C16,C17,C18,C19,C20,C21,C22,C23,C24,
     1C25
      READ(5,14)C26,C27,C28,C29,C30,C31,C32,C33,C34,C35,C36,C37,C38,
     1C39,C40,C41,C42,C43,C44,C45,C46,C47,C48,C49,C50,C51,C52,C53,
     2C54,C55,C56,C57
      DO 46 JO=1,50
   46 NOW(JO)=0.0
'     DO 47 JO=5,30,5
   47 NOW(JO)=JO
      CALL MESHR
```

```
      IDEM=0
      DO 700 MOVE=1,8
      READ(5,17) INC,POS,QC,TOS
      DO 700 JO=1,40
      ETX=1.
      MA=INC*(JO-1)
      DOSE=FLOAT(MA)
      STEP=FLOAT(INC)
      CALL TEMPR
      IF(JO.LE.1) GO TO 306
      CALL WIGN
      GO TO 312
  306 CONTINUE
      DO 310 I=1,NELEM
      EWX(I)=0.0
      EWZ(I)=0.0
      ECX(I)=0.0
      ECY(I)=0.0
      ECZ(I)=0.0
      ECXY(I)=0.0
  310 CONTINUE
  312 CONTINUE
      NPOIN2=NPOIN*2
      DO 313 I=1,NPOIN2
  313 U(I,1)=0.0
      IF(JO-1) 322,322,317
      IF(ETX.EQ.0.0) GO TO 322
  317 DO 320 I=1,NELEM
      CU=CV=FUNCT0(TAEL(I),DOSE)
      CW=4.*CU+2.*CV
      ECX(I)=FUNCT1(CU,CV,STXR(I),STYR(I),STZR(I),STEP,1)
      ECY(I)=FUNCT1(CU,CV,STXR(I),STYR(I),STZR(I),STEP,2)
      ECZ(I)=FUNCT1(CV,CV,STXR(I),STYR(I),STZR(I),STEP,3)
      ECXY(I)=FUNCT1(CW,0.,STXYR(I),0.,0.,STEP,4)
  320 CONTINUE
  322 CONTINUE
      SURF=0.0
  324 DO 330 N=1,NELEM
      IF(ETX.EQ.0.0) GO TO 326
      TADA=TAEL(N)-500.
      ARTO=ARA+ARB*TADA
      TADB=TAEL(N)-20.
      ETX=ARTO*TADB
  326 CONTINUE
      K=NOD(N,1)
      L=NOD(N,2)
      M=NOD(N,3)
      DO 325 I=1,3
      JJ=NOD(N,I)
      XE(I,1)=X(JJ,1)
      XE(I,2)=X(JJ,2)
  325 CONTINUE
      AI=XE(3,1)-XE(2,1)
      AJ=XE(2,1)-XE(1,1)
      AK=XE(3,1)-XE(1,1)
      BI=XE(2,2)-XE(3,2)
      BJ=XE(2,2)-XE(1,2)
      BK=XE(3,2)-XE(1,2)
      SUR=(AJ*BK-BJ*AK)/2.
```

```
      XLOAD(I)=FUNCT2(ETX,ETY,EWX(N),EWY(N),ECX(N),ECY(N),ECXY(N),
     1 XORD(I),YORD(I),XORD(J),YORD(J),XORD(K),YORD(K),E,PR,1)
      YLOAD(I)=FUNCT3(ETX,ETY,EWX(N),EWY(N),ECX(N),ECY(N),ECXY(N),
     1 XORD(I),YORD(I),XORD(J),YORD(J),XORD(K),YORD(K),E,PR,1)
      XLOAD(J)=FUNCT2(ETX,ETY,EWX(N),EWY(N),ECX(N),ECY(N),ECXY(N),
     1 XORD(I),YORD(I),0.,0.,XORD(K),YORD(K),E,PR,2)
      YLOAD(J)=FUNCT3(ETX,ETY,EWX(N),EWY(N),ECX(N),ECY(N),ECXY(N),
     1 XORD(I),YORD(I),0.,0.,XORD(K),YORD(K),E,PR,2)
      XLOAD(K)=FUNCT2(ETX,ETY,EWX(N),EWY(N),ECX(N),ECY(N),ECXY(N),
     1 XORD(I),YORD(I),XORD(J),YORD(J),0.,0.,E,PR,3)
      YLOAD(K)=FUNCT3(ETX,ETY,EWX(N),EWY(N),ECX(N),ECY(N),ECXY(N),
     1 XORD(I),YORD(I),XORD(J),YORD(J),0.,0.,E,PR,3)
      SURF=SURF+SUR
  330 CONTINUE
      WRITE(6,25) (U(I,1),I=1,NPOIN2)
      REWIND 4
      IF(IDEM.GT.1) GO TO 502
      INTER = 0
      DO 405 I=1,40
      DO 405 J=1,40
  405 ST(I,J)=0.
      DO 500 II=1,NPART
      NST=NSTART(II)
      NEN=NEND(II)
      K=NFIRST(II)
      L=NLAST(II)
      MINUS=K-1
      DO 445 LK=NST,NEN
      MM = LK - INTER
      DO 410 I=1,3
      JJ= NOD(LK,I)
      XE(I,1) = X(JJ,1)
  410 XE(I,2)=X(JJ,2)
      CALL FEM(XE,E,PR,MM,LK)
      DO 445 LL=1,3
      DO 445 KK=1,3
      IF(NOD(LK,KK)-K) 445,432,432
  432 IF(NOD(LK,KK)-L) 434,434,445
  434 M=NFREE*(NOD(LK,KK)-K)
      N = NFREE*(NOD(LK,LL) - K)
      I = NFREE*(KK - 1)
      J = NFREE*(LL - 1)
      IF(N) 445,436,436
  436 DO 440 NJ=1,NFREE
      DO 440 MI=1,NFREE
      MMI = M + MI
      NNJ = N + NJ
      IMI = I + MI
      JNJ = J + NJ
  440 ST(MMI,NNJ)=ST(MMI,NNJ) +C(IMI,JNJ)
  445 CONTINUE
      DO 460 I=1,NBOUN
      M=NF(I) - K
      MM = NF(I) - 1
      IF(M) 460,447,447
  447 M1=NF(I)-L
      IF(M1) 449,449,460
  449 DO 455 J=1,NFREE
      IF(NB(I,J)) 455,451,455
```

```
451 NMI=NFREE*M+J
    ST(NMI,NMI)=ST(NMI,NMI)*.1E+22
    JNJ = NFREE*MM + J
    U(JNJ,I)=ST(NMI,NMI)*BV(I,J)
455 CONTINUE
460 CONTINUE
    INTER = NEN
    M=NFREE*((NFIRST(II+1)-1)-(NFIRST(II)-1))
    WRITE(4)M,((ST(I,J),J=1,M),I=1,M)
    IF(NPART-II) 462,500,462
462 MM=M+1
    NN=NFREE*((NFIRST(II+2)-1)-(NFIRST(II)-1))
    N=NN-MM+1
    WRITE(4)M,N,((ST(I,J),J=MM,NN),I=1,M)
    LR=NFREE*(L-(NFIRST(II)-1))
    LRMM=LR-MM+1
    LRMMI=LRMM+1
    JXR=MM
    JIR=1
464 JXC=MM
    JIC=1
466 ST(JIR,JIC)=ST(JXR,JXC)
    JXC=JXC+1
    JIC=JIC+1
    IF(JXC-LR) 466,466,468
468 JXR=JXR+1
    JIR=JIR+1
    IF(JXR-LR) 464,464,472
472 CONTINUE
    DO 475 I=1,LRMM
    DO 475 J=LRMM1,40
475 ST(I,J)=0.0
    DO 480 I=LRMM1,40
    DO 480 J=1,40
480 ST(I,J)=0.0
500 CONTINUE
    IDEM=2
502 CONTINUE
    REWIND 2
    REWIND 4
    CALL SOLVE(NPART,NCOLN,NFREE,NBOUN)
    DO 615 N=1,NELEM
    IF(ETX.EQ.0.0) GO TO 607
    TADA=TAEL(N)-500.
    ARTO=ARA+ARB*TADA
    TADB=TAEL(N)-20.
    ETX=ARTO*TADB
607 CONTINUE
    K=NOD(N,1)
    L=NOD(N,2)
    M=NOD(N,3)
    DO 610 I=1,3
    JJ=NOD(N,I)
    XE(I,1)=X(JJ,1)
    XE(I,2)=X(JJ,2)
610 CONTINUE
    AI=XE(3,1)-XE(2,1)
    AJ=XE(2,1)-XE(1,1)
    AK=XE(3,1)-XE(1,1)
```

```
      BI=XE(2,2)-XE(3,2)
      BJ=XE(2,2)-XE(1,2)
      BK=XE(3,2)-XE(1,2)
      SUR=(AJ*BK-BJ*AK)/2.
      COC(N)=(SUR*NELEM)/SURF
      EPX=FUNCT4(YORD(I),YORD(J),YORD(K),DSX(I),DSX(J),DSX(K),1)
      EPY=FUNCT4(XORD(I),XORD(J),XORD(K),DSY(I),DSY(J),DSY(K),2)
      GAM=FUNCT5(XORD(I),XORD(J),XORD(K),YORD(I),YORD(J),YORD(K),DSX(I),
     1 DSX(I),DSY(I),DSX(J),DSY(J),DSX(K),DSY(K))
      X=FUNCT6(EPX,EPY,ETX,ETY,EWX(N),EWY(N),ECX(N),ECY(N),ECXY(N),E,PR,
     1 XORD(I),XORD(J),XORD(K),YORD(I),YORD(J),YORD(K),1)
      Y=FUNCT6(EPX,EPY,ETX,ETY,EWX(N),EWY(N),ECX(N),ECY(N),ECXY(N),E,PR,
     1 XORD(I),XORD(J),XORD(K),YORD(I),YORD(J),YORD(K),2)
      XY=FUNCT7(GAM,ECXY(N),E,PR,XORD(I),XORD(J),XORD(K),YORD(I),YORD(J)
     1,YORD(K))
      STX(I)=X
      STY(I)=Y
      STXY(I)=XY
  615 CONTINUE
      CZ=1330000.
  622 P=0.0
      DO 625 I=1,NELEM
      IF(ETX.LT.0.00001) GO TO 623
      TADA=TAEL(I)-500.
      AZTO=AZA+ARC*TADA
      TADB=TAEL(I)-20.
      ETZ=AZTO*TADB
  623 CONTINUE
      P=P+(ETZ+EWZ(I)+ECZ(I))*CZ*COC(I)
  625 CONTINUE
      DO 630 I=1,NELEM
      IF(ETX.LT.0.00001) GO TO 628
      TADA=TAEL(I)-500.
      AZTO=AZA+ARC*TADA
      TADB=TAEL(I)-20.
      ETZ=AZTO*TADB
  628 CONTINUE
      STZ(I)=P*COC(I)/NELEM-(ETZ+EWZ(I)+ECZ(I))*CZ*COC(I)
     1+PR*(STX(I)+STY(I))
      ST3(I)=STZ(I)
  630 CONTINUE
      DO 635 I=1,NELEM
      FIR=(STX(I)+STY(I))/2.
      SEC=SQRT(((STY(I)-STX(I))/2.0)**2+STXY(I)**2)
      XMAX=FIR+SEC
      XMIN=FIR-SEC
      PA=0.5*57.29578*ATAN(2.*STXY(I)/(STY(I)-STX(I)))
      IF(STX(I)-FIR) 631,634,634
  631 IF(PA) 632,634,633
  632 PA=PA+90.0
      GO TO 634
  633 PA=PA-90.
  634 PAA(I)=PA
      ST1(I)=XMAX
      ST2(I)=XMIN
  635 CONTINUE
      IF(ETX.LT.0.00001) GO TO 647
      DO 645 I=1,NELEM
      ECXP(I)=ECX(I)
```

```
      ECYP(I)=ECY(I)
      ECZP(I)=ECZ(I)
      ECXYP(I)=ECXY(I)
      STXR(I)=STX(I)
      STYR(I)=STY(I)
      STZR(I)=STZ(I)
      STXYR(I)=STXY(I)
  645 CONTINUE
      IF(TOS.GT.530.) GO TO 672
      POS=0.0
  672 IF(JO.GT.1) GO TO 676
      WRITE(6,673)POS
  673 FORMAT(1H0,18H CHANNEL POSITION ,F5.1,3H CM)
  676 WRITE(6,679) JO,DOSE
  679 FORMAT(17H0 INTERVAL NUMBER,I3,18H   EQUIVALENT DOSE,F8.1)
      NCASE=NWRITE/2
      GO TO (680,682,684) NCASE
  680 WRITE(6,681)
  681 FORMAT(2(67H ELEM NODE NO TEMP  X-, Y-, MAX-, MIN-, Z-, AND XY-, S
     1TRESSES ANGLE))
      GO TO 685
  682 WRITE(6,683)
  683 FORMAT(4(33H ELEM  PRINCIPAL STRESSES 1,2,3,  ))
      GO TO 685
  684 CONTINUE
  685 CONTINUE
      NW=NELEM+NWRITE
      DO 690 N=1,NW,NWRITE
      GO TO (686,687,688,689) NCASE
  686 I=N+1
      WRITE(6,4)  N,(NOD(N,J),J=1,3),TAEL(N),STXR(N),STYR(N),ST1(N),
     1ST2(N),STZR(N),STXYR(N),PAA(N),I,(NOD(I,J),J=1,3),TAEL(I),
     2STXR(I),STYR(I),ST1(I),ST2(I),STZR(I),STXYR(I),PAA(I)
      GO TO 690
  687 I=N+1
      J=N+2
      K=N+3
      WRITE(6,5) N,ST1(N),ST2(N),STZR(N),PAA(N),I,ST1(I),ST2(I),STZR(I),
     1PAA(I),J,ST1(J),ST2(J),STZR(J),PAA(J),K,ST1(K),ST2(K),STZR(K),
     3PAA(K)
      GO TO 690
  688 CONTINUE
  689 CONTINUE
  690 CONTINUE
      IF(JO.NE.NOW(JO)) GO TO 647
      ETX=0.0
      ETZ=0.0
      GO TO 312
  647 CONTINUE
  700 CONTINUE
  750 CONTINUE
      STOP
       END



      SUBROUTINE MESHR
```

```
      SUBROUTINE TEMPR

      SUBROUTINE WIGN

$IBFTC SUB1
      SUBROUTINE FEM(XE,E,PR,MM,LK)
      DIMENSION D(3,3),BTDBA(6,6),XE(3,2), ZX(3),ZY(3)
      COMMON C(6,6),DBA(3,6),DB(3,6),A(6,6),B(3,6),NSTART(30),NEND(30),
     1NFIRST(30),NLAST(30),NF(90),NB(90,2),BV(90,2),X(300,2),NOD(500,3),
     2ST(40,80),U(600,1),UF(600,1),TIEL(500),TAEL(500),EWX(500),EWZ(500)
     3,JO,QC,QG,NELEM,TOS,DOSE,NUSIZE,NURAE,NUSEC,NUELE
      COMMON C11,C12,C13,C14,C15,C16,C17,C18,C19,C20,C21,C22,C23,C24,C25
     1,C26,C27,C28,C29,C30,C31,C32,C33,C34,C35,C36,C37,C38,C39,C40,C41
     2,C42,C43,C44,C45,C46,C47,C48,C49,C50,C51,C52,C53,C54,C55,C56,C57
      DO 20 J=1,6
      DO 21 I=1,3
      B(I,J)=0.
      DB(I,J)=0.
   21 DBA(I,J)=0.
      DO 20 I=1,6
      A(I,J)=0.
      BTDBA(I,J)=0.
   20 C(I,J)=0.
      DO 22 J=1,3
      DO 22 I=1,3
   22 D(I,J)=0.
      ORX = (XE(1,1) + XE(2,1) + XE(3,1))*.333333
      ORY = (XE(1,2) + XE(2,2) + XE(3,2))*.333333
      DO 5 I = 1,3
      XE(I,1) = XE(I,1) - ORX
    5 XE(I,2) = XE(I,2) - ORY
      ZX(1) = XE(2,2) - XE(3,2)
      ZX(2) = XE(3,2) - XE(1,2)
      ZX(3) = XE(1,2) - XE(2,2)
      ZY(1) = XE(3,1) - XE(2,1)
      ZY(2) = XE(1,1) - XE(3,1)
      ZY(3) = XE(2,1) - XE(1,1)
      ZK = XE(2,1)*XE(3,2) - XE(3,1)*XE(2,2)
      Z=3.*ZK
      A(1,1)=ZK/Z
      A(2,1)=ZX(1)/Z
      A(3,1)=ZY(1)/Z
      A(4,2)=A(1,1)
      A(5,2)=A(2,1)
      A(6,2)=A(3,1)
      A(1,3)=ZK/Z
      A(2,3)=ZX(2)/Z
      A(3,3)=ZY(2)/Z
      A(4,4)=A(1,3)
      A(5,4)=A(2,3)
      A(6,4)=A(3,3)
      A(1,5)=ZK/Z
      A(2,5)=ZX(3)/Z
      A(3,5)=ZY(3)/Z
      A(4,6)=A(1,5)
      A(5,6)=A(2,5)
      A(6,6)=A(3,5)
      B(1,2)=1.
      B(3,3)=1.
```

```
      B(3,5)=1.
      B(2,6)=1.
      DEN=E*(1.-PR)/((1.+PR)*(1.-2.*PR))
      D(1,1)=DEN
      D(2,2)=DEN
      D(2,1)=DEN*PR/(1.-PR)
      D(1,2)=D(2,1)
      D(3,3)=DEN*(1.-2.*PR)/(2.*(1.-PR))
   72 DO 30 J=1,6
       DO 30 I=1,3
      DO 30 K=1,3
   30 DB(I,J)=DB(I,J) + D(I,K)*B(K,J)
      DO 40 J=1,6
      DO 40 I=1,3
      DO 40 K=1,6
   40 DBA(I,J)=DBA(I,J) + DB(I,K)*A(K,J)
      IF (MM) 126,126,127
  127 CONTINUE
  126 CONTINUE
      VOL=0.5*Z
      DO 50 J=1,6
      DO 50 I=1,6
      DO 50 K=1,3
   50 BTDBA(I,J)=BTDBA(I,J) + B(K,I)*DBA(K,J)*VOL
      DO 60 J=1,6
      DO 60 I=1,6
      DO 60 K=1,6
   60 C(I,J)=C(I,J) + A(K,I)*BTDBA(K,J)
      RETURN
       END


$IBFTC SUB2
      SUBROUTINE SOLVE(NPART,NCOLN,NFREE,NBOUN)
      DIMENSION AM(40,80),BM(40,40),YM(40,40),TF(40,1),RS(40,1),
     1DIS(40,1),F(40,1)
      COMMON C(6,6),DBA(3,6),DB(3,6),A(6,6),B(3,6),NSTART(30),NEND(30),
     1NFIRST(30),NLAST(30),NF(90),NB(90,2),BV(90,2),X(300,2),NOD(500,3),
     2ST(40,80),U(600,1),UF(600,1),TIEL(500),TAEL(500),EWX(500),EWZ(500)
     3,JO,QC,QG,NELEM,TOS,DOSE,NUSIZE,NURAE,NUSEC,NUELE
      COMMON C11,C12,C13,C14,C15,C16,C17,C18,C19,C20,C21,C22,C23,C24,C25
     1,C26,C27,C28,C29,C30,C31,C32,C33,C34,C35,C36,C37,C38,C39,C40,C41
     2,C42,C43,C44,C45,C46,C47,C48,C49,C50,C51,C52,C53,C54,C55,C56,C57
      EQUIVALENCE (AM(1,1),ST(1,1)),(BM(1,1),AM(1,41))
      DO 140 I=1,40
      TF(I,1)=0.0
      RS(I,1)=0.0
      DO 140 J=1,40
  140 YM(I,J)=0.0
      DO144LL=1,NPART
      READ(4)M,((AM(I,J),J=1,M),I=1,M)
      LS=NFREE*(NFIRST(LL))-1
      DO 424  I=1,M
      F(I,1)=U(LS,1)-TF(I,1)
      DIS(I,1)=F(I,1)
      LS=LS+1
      DO 424 J=1,M
```

```
424 AM(I,J)=AM(I,J)-YM(I,J)
    CALL SPNIST(AM,M,40,ISIG)
    IF(NPART-LL) 666,666,555
555 READ(4)M,N,((BM(I,J),J=1,N),I=1,M)
667 WRITE(2) M,N,((AM(I,J),I=1,M),J=1,M),((BM(I,J),I=I,M),J=1,N),
   1((F(I,J),I=1,M),J=1,NCOLN)
    GO TO 878
666 WRITE(2)M,((AM(I,J),I=1,M),J=1,M),((F(I,J),I=1,M),J=1,NCOLN)
878 DO 200 L=1,NCOLN
    DO 200 I=1,M
    DIS(I,L)=0.0
    DO 200 K=1,M
200 DIS(I,L)=DIS(I,L)+AM(I,K)*F(K,L)
    IF(NPART-LL) 437,437,303
303 DO 300J=1,NCOLN
    DO 300 L=1,N
     TF(L,J)=0.0
     DO 300 I=1,M
300 TF(L,J)=TF(L,J)+BM(I,L)*DIS(I,J)
    DO 110 J=1,N
    DO 110 I=1,M
    YM(I,J)=0.0
    DO 110 K=1,M
110 YM(I,J)=YM(I,J)+AM(I,K)*BM(K,J)
    DO 111 J=1,N
    DO 111 I=1,N
    AM(I,J)=0.0
    DO111 K=1,M
111 AM(I,J)=AM(I,J)+BM(K,I)*YM(K,J)
    DO 112 I=1,N
    DO 112 J=1,N
112 YM(I,J)=AM(I,J)
144 CONTINUE
437 REWIND 4
    JJ=NPART
    LS=NFREE*(NFIRST(JJ))-1
    DO 438 I=1,M
    UF(LS,1)=DIS(I,1)
    LS=LS+1
438 CONTINUE
    IF(NPART-1) 600,600,601
601 NA=NPART-1
    DO441 LL=1,NA
    II=LL+1
    JJ=NPART+1-II
    LS=NFREE*(NFIRST(JJ))-1
    BACKSPACE 2
    BACKSPACE 2
    READ(2)M,N,((AM(I,J),I=1,M),J=1,M),((BM(I,J),I=1,M),J=1,N),
   1((F(I,J),I=1,M),J=1,NCOLN)
    DO 462 L=1,NCOLN
    DO 462 I=1,M
    TF(I,L)=0.0
    DO462 J=1,N
462 TF(I,L)=TF(I,L)+BM(I,J)*DIS(J,L)
    DO 444 J=1,NCOLN
    DO 444 I=1,M
444 F(I,J)=F(I,J)-TF(I,J)
    DO 465 L=1,NCOLN
```

```
      DO 465 I=1,M
      DIS(I,L)=0.0
      DO 464J=1,M
  464 DIS(I,L)=DIS(I,L)+AM(I,J)*F(J,L)
      UF(LS,1)=DIS(I,L)
      LS=LS+1
  465 CONTINUE
  441 CONTINUE
      DO 500 LL=1,NPART
      II=(NPART+1)-LL
      IZ=NPART-LL
      READ(4)M,((ST(I,J),J=1,M),I=1,M)
       M2=M+1
      IF(NPART-LL) 656,657,656
  656  NN=NFREE*((NFIRST(LL+2)-1)-(NFIRST(LL)-1))
      READ(4)M,N,((ST(I,J),J=M2,NN),I=1,M)
  657 CONTINUE
      DO 290 I=1,NBOUN
       K=NFIRST(LL)
       L=NLAST(LL)
      M5=NF(I)-K
      MM = NF(I) - 1
      IF(M5) 290,242,242
  242  M1=NF(I)-L
      IF(M1) 243,243,290
  243 DO 230 J = 1,NFREE
      IF (NB(I,J)) 230,345,230
  345 NMI=NFREE*M5+J
      ST(NMI,NMI)=ST(NMI,NMI)*.1E-20
  230 CONTINUE
  290 CONTINUE
      IF(NPART-LL) 1004,1003,1004
 1004  DO 1001 I=1,M
       DO 1001J=M2,NN
       K=J-M
 1001 YM(I,K)=ST(I,J)
       DO 1002 I=1,M
       DO 1002J=1,N
 1002 BM(I,J)=YM(I,J)
 1003 CONTINUE
      DO 1000 I=1,M
      DO 1000J=1,M
 1000 AM(I,J)=ST(I,J)
      IF(NPART-LL) 659,658,659
  659 CONTINUE
  658 DO 510 J=1,NCOLN
      DO 510 I=1,M
      LS=NFREE*(NFIRST(II))-1
      LZ=NFREE*(NFIRST(IZ))-1
      F(I,J)=RS(I,J)
      DO 512 K=1,M
      F(I,J)=F(I,J)+AM(I,K)*UF(LS,J)
      LS=LS+1
  512 CONTINUE
      IF(NPART-LL) 662,510,662
  662 DO 520 L=1,N
      F(I,J)=F(I,J)+BM(I,L)*UF(LZ,J)
      LZ=LZ+1
  520 CONTINUE
```

```
  510 CONTINUE
      IF(NPART-LL) 663,500,663
  663 DO 700 I=1,N
      LS=NFREE*(NFIRST(II))-1
      RS(I,1)=0.0
      DO 700 K=1,M
      RS(I,1)=RS(I,1)+BM(K,I)*UF(LS,1)
      LS=LS+1
  700 CONTINUE
  500 CONTINUE
  600 CONTINUE
      RETURN
       END



$IBFTC INVIST  DECK
      SUBROUTINE  SPNIST(A,M,KK,ISIG)
      DIMENSION A(1)
      ISIG = 0
      N = M
      NN = KK
      N2 = N + N
      DO 10 J=1,N
      NJCOL = (N + J - 1) * NN
      DO 10 I=1,N
      KINJ = NJCOL + I
      IF(I-J)4,6,4
    4 A(KINJ) = 0.
      GO TO 10
    6 A(KINJ) = 1.
   10 CONTINUE
C  DETERMINE MAXIMUM ABS OF VARIABLE BEING ELIMINATED.  THIS BECOMES PIV
C    OTAL ROW
      L = 0
   12 L = L + 1
      LCOL = NN*L-NN
      KLL = LCOL + L
      IF(L - N)13,30,1000
C  FIND THE LARGEST ELEMENT IN THE LTH COLUMN.
   13 J1 = L
      C=ABS(A(KLL))
      L1 = L + 1
      DO 20 I = L1,N
      KIL = LCOL + I
      X=ABS(A(KIL))
      IF(C - X)14,20,20
C  RECORD THE NUMBER OF THE ROW HAVING THE GREATER ELEMENT.
   14 J1 = I
C  C BECOMES THE GREATER.
      C  = X
   20 CONTINUE
C  INTERCHANGE ROW J1 WITH ROW L. J1 IS THE ROW WITH THE LARGEST ELEMENT
C  TEST TO SEE IF INTERCHANGING IS NECESSARY.
      IF(J1 - L)22,30,22
   22 DO 24 J = L,N2
      JCOL = NN*J-NN
      KJIJ = JCOL + J1
```

```
      HOLD = A(KJIJ)
      KLJ = JCOL + L
      A(KJIJ) = A(KLJ)
      A(KLJ) = HOLD
   24 CONTINUE
C  IF  THE LARGEST ABSOLUTE ELEMENT IN A COLUMN IS ZERO WE HAVE A SINGUL
C    AR  MATRIX
   30 IF (ABS(A(KLL)) - .0000001)33,33,32
   33 WRITE(6,100)
      ISIG = 4
      GO TO 1000
C   ZERO ALL THE ELEMENTS IN THE LTH COLUMN BUT THE PIVOTAL ELEMENT.
   32 L1 = 1
      L2 = L - 1
      IF(L2)321,321,323
  321 IF(L-N)322,46,322
  322 L1 = L + 1
      L2 = N
  323 DO 324 I = L1,L2
      KIL = LCOL + I
      Z = -A(KIL)/A(KLL)
      DO 324 J = L,N2
      JCOL = NN*J - NN
      KIJ = JCOL + I
      KLJ = JCOL + L
  324 A(KIJ) = A(KIJ) + Z*A(KLJ)
      IF(N - L2)12,12,321
C  DIVIDE BY DIAGONAL ELEMENTS.
   46 DO 48 I = 1,N
      KKK = NN*I - NN + I
      ZZ = A(KKK)
      DO 48 J = 1,N2
      KKI = NN*J - NN + I
   48 A(KKI) = A(KKI)/ZZ
C   RETURN AFTER PUTTING A INVERSE INTO B
   49 DO 50 J = 1,N
      JCOL = NN*J - NN
      NJCOL = NN * N + JCOL
      DO 50 I = 1,N
      KIJ = JCOL + I
      KINJ = NJCOL + I
   50 A(KIJ) = A(KINJ)
  100 FORMAT(//20X,42H MATRIX IS SINGULAR, NO INVERSE OBTAINABLE///)
 1000 RETURN
      END
```